

Schlussbericht vom 15.10.2023

zu IGF-Vorhaben Nr. 291 EN (CORNET)

Thema

AndaCast - Substitute materials for Andalusite in castables

Berichtszeitraum

01.01.2021 – 28.02.2023

Forschungsvereinigung

Forschungsgemeinschaft Feuerfest e. V.

Forschungseinrichtungen

Forschungsgemeinschaft Feuerfest e. V.

Hochschule Koblenz, WesterWaldCampus, Fachrichtung Werkstofftechnik Glas und Keramik

Institut Interuniversitaire des Silicates, Sols et Matériaux (INISMa), Avenue Gouverneur Cornez
4, 7000 Mons, Belgien



Gefördert durch:



aufgrund eines Beschlusses
des Deutschen Bundestages

Vorwort

Das vorliegende Dokument stellt den gemeinsamen Schlussbericht für das IGF-Vorhaben 291 EN beziehungsweise für das CORNET-Gesamtprojekt aller drei beteiligter Forschungseinrichtungen dar.

Aus Deutschland wirkten die Forschungsgemeinschaft Feuerfest e. V. und die Hochschule Koblenz an dem CORNET-Gesamtprojekt mit. An dem CORNET-Gesamtprojekt war außerdem das Institut Interuniversitaire des Silicates, Sols et Matériaux (INISMa) in Belgien beteiligt, gefördert durch Service Public de Wallonie (SPW).

Table of Contents

1.	Introduction	6
1.1	<i>State of the Art</i>	6
1.2	<i>Scientific-technical and economic problem.....</i>	8
2.	Objective	8
3.	Approach and research strategy	10
4.	Materials and methods	11
4.1	<i>Andalusite raw material.....</i>	11
4.2	<i>Andalusite-based reference castables.....</i>	13
4.3	<i>Preparation of test-pieces</i>	14
4.3.1	Castable preparation, moulding and pre-firing at HSK	14
4.3.2	Castable preparation, moulding and pre-firing at INISMa	15
4.3.3	Ash preparation for the channel slag test at FGF	15
4.4	<i>Methods for analysis</i>	15
4.4.1	Thermal treatment of test pieces without dwell time	15
4.4.2	Thermal treatment of test-pieces with a dwell time of 8 hours	16
4.4.3	Mineralogical analysis	16
4.4.4	Microstructural analysis	16
4.4.5	Determination of bulk density and open porosity	16
4.4.6	CCS and MOR.....	17
4.4.7	Resonance frequency damping analysis (RFDA)	17
4.4.8	Thermal analysis (MMH)	17
4.4.9	Refractoriness under load (RUL, DIN EN ISO 1893).....	19
4.4.10	Wedge splitting test	19
4.4.11	Laser flash analysis (LFA).....	19
4.4.12	Creep under compression (CREEP; DIN EN 993-9).....	20
4.4.13	The channel slag test	20
4.4.13.1	Microstructural and chemical analysis after channel slag test	21
4.4.13.2	Temperature gradient in the channel slag test	21
5.	Results and discussion	23
5.1	<i>Thermal decomposition of andalusite raw materials.....</i>	23
5.2	<i>Nature of the reference castables.....</i>	30
5.3	<i>Thermal behaviour of the reference castables</i>	32
5.3.1	Thermal evolution of reference castables at a heating rate of 250 K/h with no dwell time ..	33

5.3.1.1	Reference castable RR	33
5.3.1.2	Reference castable RE	36
5.3.1.3	Reference castable RB	40
5.3.2	Comparison of RUL	40
5.3.3	Effect of firing temperature and holding time on the andalusite based castables	41
5.3.3.1	Mineral composition and microstructure after firing for 8 h at temperatures between 1000 and 1500 °C	41
5.3.3.2	Effect of holding time on the phase evolution in the reference castables	49
5.3.3.3	Macroscopic appearance of reference castables thermally altered	50
5.3.3.4	Evolution of bulk density and open porosity as a function of temperature and dwell times	51
5.3.3.5	Effect of heating on cold mechanical properties	53
5.3.3.6	Prograde evolution of normalized frequency derived from RFDA from room temperature up to 1400 °C	54
5.3.3.7	RFDA versus temperature of dried materials (first heating)	55
5.3.3.8	RFDA versus temperature of fired materials (24 h at 1350 and 1450 °C)	57
5.3.3.9	Creep under compression (EN 993-9)	59
5.3.3.10	Wedge splitting test	59
5.3.4	Corrosion resistance of the andalusite based reference castables	61
5.3.4.1	Macroscopic observations (polished section)	63
5.3.4.2	Microscopic observations - Corrosion by liquid slag	64
5.3.4.3	Microscopic observations - Corrosion by volatile components	74
5.4	<i>Development of andalusite-free castables</i>	74
5.4.1	Raw materials and recipes	77
5.4.2	Castable preparation and mixing design	78
5.4.3	Thermal and mechanical behaviour of andalusite-free model castables	79
5.4.3.1	Model refractory castable with luting sand addition (MRC-L)	80
5.4.3.2	Model refractory castable with SiC addition	83
5.4.3.3	Model refractory castable with kyanite addition MRC-K	86
5.4.4	Corrosion resistance of the andalusite-free model castables	88
5.4.4.1	Macroscopic observations	89
5.4.4.2	Slag interaction in the microstructure	92
5.4.5	Wedge Splitting Tests	102
5.5	<i>Conclusion</i>	103
6.	Literature	105

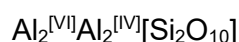
1. Introduction

1.1 State of the Art

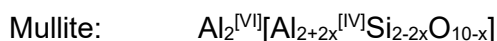
Andalusite, kyanite and sillimanite are natural minerals with the same chemical formula Al_2SiO_5 but different (polymorphic) crystal structures. Structurally, the minerals belong to the nesosilicates with anions foreign to the tetrahedron, which gives rise to the structural formula $\text{Al}_2[\text{O}|\text{SiO}_4]$. The polymorphic forms differ only in the coordination of the aluminium ions, one of which is always octahedrally coordinated. The second is also octahedrally coordinated in kyanite, trigonal di-pyramidal in andalusite and tetrahedral in sillimanite. Therefore, the polymorphs differ in packing density, with kyanite, andalusite and sillimanite being lower in order, which is also reflected in the density of the minerals. Kyanite is considered to be the high-pressure form, which causes the highest increase in volume during thermal decomposition and sillimanite the lowest. Ultimately, the structure of mullite can be derived from sillimanite:



We take twice the formula:



To reach the mullite, the SiO_2 content is systematically reduced by a factor of x (= number of oxygen vacancies):



If $x=0$ we obtain Sillimanite, if $x=0,25$ 3:2-Mullite is stable and finally if $x=0,4$, we obtain 2:1-Mullite. There is complete miscibility of both mullite end members.

All can be used as refractory raw materials, but andalusite is by far the most important due to its beneficial refractory properties. It is widespread in use for manufacturing industrial refractory unshaped products and fired brick materials. The usefulness of andalusite results mainly from the possibility of using andalusite in a raw state for ceramic mixes, both in fine and coarse fractions, as well as its relatively low prices (Wala et al 2024). Andalusite has unique properties that make it an essential component of refractory castables. Its superior high-temperature volume stability and high thermal shock resistance make it ideal for use in extreme temperature environments (Bowen et al. 2017, Poirier et al. 2009). The corrosion resistance makes it ideal for applications where alkali rich slags and atmospheres are present.

Due to its high content of alumina and silica, andalusite readily undergoes mullite formation when fired to high temperatures. The primary reaction responsible for this transformation can be described as follows: $3 (\text{Al}_2\text{SiO}_5) \rightarrow 3 \text{Al}_2\text{O}_3 + 2\text{SiO}_2 + \text{SiO}_2$, whereby SiO_2 is to be seen here as a chemical component and not as a mineral phase.

The process of transforming andalusite grains into mullite has been extensively investigated. This transformation occurs through a dissolution-precipitation mechanism that originates from the mineral inclusions (impurities) and grain boundaries. The mineral inclusions appear to facilitate local melting, which promotes the formation of mullite as this is no longer a pure solid body reaction. As the process progresses, mullite precipitates while excess silica, following the literature, gives rise to a liquid phase. However, it is not entirely clear what state of aggregation the SiO_2 is in. Assuming a fairly pure reaction, a glassy compound will probably precipitate even under the conversion conditions, which is more likely to be a segregation reaction. This is supported by the fact

that the reaction is kinetically hampered. When the temperature exceeds 1280°C, approximately 80% of the mineral transforms into the mullite phase, while the remaining 20% forms a silica glass phase. A portion of this liquid phase is expelled, but the majority (around 80%) becomes confined within an interconnected capillary network within the mullite structure. This glass phase is seen to act as both a shock absorber and a "healing agent" as it softens with increasing temperature. The presence of the silica-rich liquid at high temperatures allows microcracks to be deflected and consequently, andalusite-based refractories exhibit exceptional refractoriness under load (Poirier et al. 2009, Frulli et al. 2018).

Typical applications are biomass and waste incineration, permanent linings of vessels in the steel industry and the cement industry. However, there are only few andalusite deposits with economic feasibility.

Kyanite is also used in refractory materials. It is usually added as a minor component for controlling high-temperature shrinkage and therefore giving high-temperature volume stability. The natural resources of kyanite are also limited. Sillimanite is difficult to separate from the host rocks due to its acicular morphology and small size of the crystals which are complex intergrown in their host rocks. None of the three polymorphs of Al_2SiO_5 can be synthesized for refractory purposes.

High-temperature volume stability is required in all processes that involve high mechanical load on refractory structures, e.g. large linings. The superior high-temperature volume stability of andalusite based refractories is claimed to be the result of skeletal mullite crystals with interstitial amorphous silica, sometimes designated as "felted mullite" aggregates originated from slowly converting andalusite (Dubreuil 1999 McCracken 2014). These aggregates are claimed to be mechanically steadfast and still enable high volume stability of the refractory products. The conversion of andalusite is accompanied with 4-5% volume expansion which will itself also have another positive influence on the volume stability. The transformation of andalusite can take hours to months, depending on the temperature and the presence of impurities, which accelerate the conversion kinetics (Ildefonse et al. 1997, Liao et al. 2005). The "felted aggregates" of the mullite with interstitial, highly viscous silica in the refractory, in interaction with other components of an andalusite-based refractory, are believed to provide the resistance against deformation under external strains and thus the desired volume stability. The kinetics of the transformation process and thus the amount of mullite being formed depends on temperature & time, the presence of impurities (especially iron-rich, typically derived from biotite) and also the specific surface of the andalusite grain fractions, because the conversion typically starts from the surfaces. The kinetics of this formation process plays an important role in the use of andalusite-based refractories. The conversion of andalusite is believed to be an ongoing process during the service life of andalusite-based refractories.

This is particularly important as refractory linings are operated in a temperature gradient with only a few exceptions. Depending on the application temperature and thermal conductivity of the lining, only the first few centimetres of the lining are exposed to the application temperatures, after which there is at most a sintered material, which can still be in the green state up to the cold side. During operation, the usual wear exposes fresh, intact areas of the lining, with still unreacted andalusite, which in turn seals the structure to the hot side by expansion during decomposition. Even if the degree of melting on the hot side is high, which is often the case, as is also shown in this report, the lining retains the intended mechanical stability over its service life. The melt formation on the surface in turn leads to local ductile properties that counteract thermal stresses, giving the materials excellent thermal shock resistance. In addition, these areas are less susceptible to the infiltration of liquid and, above all, gaseous corrosion media, as the structure is sealed by the melting

phase. However, it must be taken into account that this foremost layer is susceptible to tribomechanical stress.

The highest corrosion resistance against alkaline rich slags or atmospheres of andalusite-based refractories is also believed to derive from the transformation reaction of andalusite, which provides an amorphous silica phase (Kakroudi et al. 2008, Nyoka et al. 2013, Ren et al. 2018). This is forming a highly viscous silica-rich melt phase together with other components of an andalusite-based refractory, acting as a coating at high temperature and protecting the structure of andalusite-based refractories from alkali attack. As silica-rich melt is continually being formed during the transformation reaction of andalusite, which may last over the entire lifetime of a lining made from andalusite-based castables, the protective silica-rich melt coating is maintained over the whole lifetime, too. As such a highly viscous silica-rich melt would not be formed from cristobalite (due to kinetic reasons), which is the decomposition product of kyanite, the abundantly available kyanite is unsuitable to replace andalusite as raw material.

1.2 Scientific-technical and economic problem

The refractory industry is suffering from unconfident supply of andalusite. On the global market, only a small number of companies supply relatively minor quantities of andalusite. Grain sizes and grades of impurities are very individual characteristics of each andalusite deposit. The andalusites from different deposits are thus not one-to-one exchangeable as raw materials for refractories. Increasing prizes and insecure future supply requires the refractory industry to develop substitution refractories that do not contain andalusite. It is quite sure that alternative grains will not be mined from natural deposits. They will be based on natural products that must be upgraded by thermal treatment, possibly after chemical purifying. This is a dilemma regarding environmental issues, because andalusite, after separation from the host rocks, can be used as it is. However, an advantage of andalusite substitutes could be a better homogeneity compared with natural andalusite from different deposits.

For the users of andalusite-based refractories, the superior high-temperature volume stability, high thermal shock resistance and corrosion resistance against alkali rich slags and atmospheres must be maintained in new refractory castables without andalusite. Therefore, it is first and foremost necessary to fully understand the role of andalusite in traditional andalusite-based castables. Herein, a key aspect is the prograde (at increasing temperatures) phase evolution in andalusite-based refractories in terms of structural and mineralogical changes and how these enable the unique high-temperature mechanical properties. Only if the mineralogical evolution of andalusite-based castables at increasing temperatures is understood, refractories without andalusite but similar high-temperature behaviour can be developed. This is one basic aspect of this work. The other basic aspect is the development of model refractory castables without andalusite, but other aggregates which have been identified as promising candidates for the basis of refractory castables without andalusite.

2. Objective

In recent years, there have been several challenges facing the use of andalusite as a raw material for refractory castables such as increase in price and inadequate supply of andalusite, which have significant impacts on the refractory industry and its users. These challenges can drive companies

to seek out alternative raw materials for their refractory castables. In the search for alternatives to andalusite in refractory castables, the key objective is to identify a substitute that possesses a similar microstructure to andalusite, thereby ensuring comparable behaviour and high thermo-mechanical properties in the castables. Finding a suitable replacement involves considering minerals or materials with similar characteristics, such as alumina and silica content, as well as the ability to undergo mullite formation at high temperatures. By selecting a substitute that closely resembles the microstructure of andalusite, it is possible to maintain the desired properties, such as defined thermal expansion, and good chemical stability, which are essential for optimal performance in refractory castables. Without wishing to prejudge the results of this work, the following raw materials have emerged as alternatives. Through diligent research and testing, the identification and integration of a suitable alternative can enable the production of refractory castables with similar behaviour and exceptional thermomechanical properties, without relying solely on andalusite as the primary raw material. In this research, kyanite, luting sand, silicon carbide (SiC), anorthite and kaolin were investigated as possible substituting materials. It is not possible to directly replace andalusite with these materials in refractory applications. However, studying the kinetics of thermal behaviour of each material with other components in high alumina low cement castable can provide valuable information about possibility of use this material as an alternative for andalusite in refractory castables.

Kyanite was selected due to its chemical similarity to andalusite. However, during its conversion to mullite and silica, the expansive effect is higher approximately by the factor 3 (volume expansion of kyanite $\approx 17\%$ and for andalusite is 4-5%) compared to the conversion of andalusite (Frulli et al. 2018, Namiranian & Kalantar 2011). The aluminium silicate minerals andalusite, sillimanite and kyanite form at moderate to high lithostatic pressures in the crust of the earth. At high temperatures and atmospheric pressure, they all convert following the reaction:



The molar volume of the newly formed phases (mullite and silica) is less compared with the precursor minerals, therefore the transformation results in a volume expansion. This is beneficial for the refractories because it compensates shrinkage during the sintering process. The transformation can help to improve the strength and volume stability of the castable. The addition of kyanite to the matrix can help to improve the thermomechanical properties such refractoriness under load and creep under compression through its transformation to mullite. Kyanite also more available than andalusite, making it an attractive alternative material for use in high alumina refractory castables.

The study also investigates the behaviour of "Luting sand" (Cölle 2013) a local type natural luting sand, as another potential component in a refractory castable without andalusite. It is a natural resource with a high content of quartz and clay minerals. It is already in use in manufacturing refractory products. This can be described as a quartz sand rich in clay minerals with binding properties and fire-resistant. The addition of luting sand to the refractory can help to improve thermomechanical properties of the refractory castable through its transformation to mullite in high-alumina castables. At high temperatures, "Luting sand" undergoes several thermal transformations, leading into an assemblage of mullite, christobalite and melt phase. The direct mullitization process of luting sand begins with the thermal decomposition of kaolinite (Cölle 2013). This effect may bear some resemblance to the behaviour of andalusite in high alumina castables.

SiC, a non-oxide ceramic, exhibits excellent refractory properties. Its addition to a refractory material is widely recognized for its significant contributions to improving high temperature strength, enhancing refractoriness under load and abrasion resistance, and even enhancing thermal shock

and corrosion/erosion resistance in challenging environments. However, the presence of SiC in refractory castables is constrained by some of oxidation problems (Mavahebi et al. 2019, Zawrah & Khalil 2005, Fangbao et al. 2004).

Mavahebia et al (Mavahebi et al. 2019) showed the addition of SiC fines in low cement bauxite refractory castable has been found to have a significant effect on the formation of mullite, leading to improvements in thermomechanical properties. Incorporating SiC up to 6 wt.-% enhances the refractoriness of the matrix, resulting in notable phase transformations in the exterior region of the test-pieces. This effect is primarily attributed to the passive oxidation of SiC and the subsequent reaction of its oxidation products, mainly SiO₂, with the alumina sources present in the matrix (reactive alumina and calcined alumina), leading to the formation of the mullite phase. Furthermore, the high temperature strength of the bauxite-based low cement castables shows an increase with the addition of SiC fines up to 6 wt.-%. This improvement can be attributed to the high refractoriness of SiC and the development of strong bonding within the matrix. The promotion of mullite phase formation and the reduction of the glassy phase in the interior zone of the specimens contribute to the enhancement of high temperature strength.

Kaolin, which primarily consists of kaolinite, Al₂[(OH)₄Si₂O₅], undergoes a series of structural and microstructural transformations during firing, somewhat resembling the mullitisation process observed in andalusite. The decomposition of kaolinite into meta-kaolinite occurs between temperatures of 400°C and 630°C. As metakaolin gradually collapses, it facilitates the formation of nanoscale mullite crystals, along with the generation of free amorphous silica. At 1200°C, the amorphous silica crystallizes to cristobalite, while a significant amount of mullite crystals is concurrently developed. The final transformation involves the formation of cristobalite, typically occurring at temperatures above 1400°C. The presence of impurities such as CaO, Na₂O, and K₂O in the initial kaolin promotes the vitrification of cristobalite at lower temperatures. To induce the formation of secondary mullite, the silica glass can be mullitised by adding alumina, aluminium hydroxides, or aluminium slag (Fouzia et al. 2018).

3. Approach and research strategy

This CORNET project was carried out by Forschungsgemeinschaft Feuerfest e. V. (Germany) = FGF, Hochschule Koblenz (Germany) = HSK, and Institut Interuniversitaire des Silicates, Sols et Matériaux (Belgium) = INISMa.

The main purpose of the project was to propose alternative solutions for castable compositions that perform like andalusite based castables in terms of thermomechanical and corrosive stability during service. HSK developed model castables with six different substitutes for andalusite, whereby the substitute raw materials were selected based on the knowledge gained from the reference castables. FGF investigated the corrosion resistance of andalusite free castables. Based to the results, all partners identified promising substitutes for further testing. The model castables were designed in such a way that the properties of the alternative raw materials used deliver significant results and are not yet considered ready for use but should provide a very good basis for developing future andalusite-free castables. It is not excluded that not only the identified alternative raw materials can also be cast in a suitable combination.

Firstly, the thermal behaviour of the different grades and grain sizes of andalusite raw materials were investigated. The focus here was on the influence of impurities in the andalusite raw material

and the grain size on the transformation temperature and transformation kinetics of andalusite. The chemical composition and the mineralogical composition as a function of the grain size distribution of the reference castable were investigated, to correlate them with the thermomechanical and thermochemical properties.

In a second step, the andalusite was bonded into a refractory castable and was investigated regarding the thermomechanical and technological properties as well as the corrosion resistance of andalusite. Three commercial castables provided by the Users Committee were first investigated. The castables were selected so that they differ in the binding phase. Two cemented systems were selected for this purpose, which differ in the amount of added calcium aluminate cement (CAC) and are specified as LCC and ULCC in accordance with DIN EN ISO 1927-1. As the presence of CAC significantly changes the matrix composition due to the presence of Ca, a cementless NC castable was also investigated. All reference castables are used where high thermal shock resistance is essential, such as for burner bricks, electric furnace lids, tundishes, induction furnaces in non-ferrous metallurgy and other discontinuously operating kiln units. The application temperature specified by the manufacturers is between 1200 and 1700 °C, whereby the application temperature increases with decreasing cement content.

The technological properties like porosity and density of the reference castables were investigated for test-pieces that were fired for 4 hours at 1000, 1250 and 1500 °C. The cold crushing strength (CCS, ISO 1927-6) and measurement of the bending resistance (modulus of rupture, MOR, DIN EN 993-6) were also determined for the same temperatures as well as porosity and density. The thermomechanical properties of three reference castables were determined by the standard methods, Refractoriness under load (RuL, DIN EN ISO 1893), Creep under compression (CREEP, DIN EN 993-9) and the wedge splitting test (WP 2). The corrosion resistance was tested for a time of 4 h in a thermal gradient from about 1550 to 100 °C, using a test setup developed in a previous CORNET project "SiCast" and optimized during the first half of the project duration. A macroscopic damage assessment and extensive microscopic investigation of the interaction between basic ash and reference castables and deposition of volatile elements as a function of temperature was carried out.

The thermal and kinetic evolution of andalusite based castables and its impact on the thermomechanical properties was investigated with the Method of monotonic heating (MMH), Laser flash analysis (LFA) and SEM. To identify the signal of the decomposition of andalusite to mullite and a SiO₂-rich melt in the MMH results, MMH analyses of the different grades and grain sizes of the pure andalusite raw materials were performed in advance. The MMH analyses were flanked by extensive microstructural analyses of test-pieces, which were tested after a thermal treatment at different maximum temperatures of 1000, 1200, 1300, 1400 and 1500 °C, all with a heating and cooling rate of 500 K/h (the same as applied in MMH) and without a dwell time.

4. Materials and methods

4.1 Andalusite raw material

Andalusite is a naturally occurring mineral, which is formed under pressures of less than 3.5kbar and temperatures between 200 and 800 °C from clayey sediments, so-called pelites, by contact metamorphism. Contact metamorphism is typically closely associated with magmatic intrusive bodies, which locally cause the country rock to overheat, resulting in the pressure and

temperature conditions mentioned. A prominent intrusive body is, for example, the Bushveldt craton in South Africa, which is also known for its associated andalusite deposits. However, these special formation conditions also mean that andalusite deposits are locally limited and andalusite is solely a component of metapelite, usually in association with muscovite, biotite quartz and feldspars. The minerals mentioned are therefore typical impurities in andalusite raw materials and are often closely intergrown with the andalusite. As will be shown later, these impurities play a significant role in the rate of decomposition when the raw material is subjected to temperature.

The aforementioned formation conditions are not technically feasible, meaning that andalusite cannot be produced synthetically.

On the global market, only a small number of companies supply relatively minor quantities of andalusite from deposits as summarized in Table 1. One of the main suppliers (IMERYS) was represented in the Users Committee of the CORNET project.

Table 1: Summarized table of andalusite suppliers and deposits as communicated by the suppliers.

Supplier	Deposit	Trading name	Grain size (mm)	Availability (t/a)
IMERYS	Glomel, Bretagne	Kerphalite	0,3-1,6	65.000
	Thabazimbi, South Africa	Purusite	0-4	90.000
	Segorong, South Africa	Randalusite/Durandal	0-8	30-40.000
Peru	Not available at the moment due to lack of infrastructure			
Andalusite Recourses	Thabazimbi, South Africa	Marlusite, same deposit as Purusite	0-4	65.000
Andalucia S.A.	Paita, Peru	Perusite	0-4	35-40.000

Grain sizes and grades of impurities are very individual characteristics of each andalusite deposit. The andalusites from different deposits are thus not exchangeable as raw materials for refractories. Increasing prizes and insecure supply requires the refractory industry to develop substitution materials for andalusite, which is the main objective of this project. Andalusite is available in France, South Africa (Durandal, Randalusite, Purusite) and Peru (Perusite). In Europe, the main supplier is IMERYS. Andalusite is available in different grades. They can be classified by their alumina content and particle size (Table 2).

Table 2: Andalusite grades as a function of alumina content and particle size.

	Fine (< 50 µm)	Medium (50-300 µm)	Large (300 µm-2 mm)	Very large (2-8 mm)
High alumina (>59.5 %)	Kerphalite KF (FR)	Durandal D60 (SA)	Durandal D60	
		Kerphalite KF	Randalusite (SA)	Randalusite
Medium Alumina (58-59.5)	Purusite (SA)	Durandal D59		Durandal D59
		Kerphalite KA	Kerphalite KA	Purusite
Low alumina (<58 %)		Kerphalite KB	Kerphalite KB	

Table 3 shows the mineralogical composition of different Kerphalite (andalusite) raw materials. Kerphalite KF is the purest andalusite quality with 96 wt.-% andalusite. Kerphalite KB has with an amount of andalusite of 87 % the lowest quality. Quartz and biotite are identified as the important impurities that can be reliably detected by mineral phase analysis. In further muscovite could be

present in minor concentrations. Andalusite and said impurities are syngenetic in metapelitic rocks.

Table 3: Mineralogical composition of Kerphalite in three different qualities (in wt.-%).

wt.-%	Kerphalite KA	Kerphalite KB	Kerphalite KF
Andalusite	90	87	96
Biotite	6	6	3
Quartz	4	8	1

4.2 Andalusite-based reference castables

Three andalusite-based reference castables were studied to investigate the high-temperature behaviour of andalusite in three different types of refractory castables. The high-temperature behaviour of andalusite, especially the decomposition of andalusite and the following mullitisation, in contact and interaction with the matrix of the refractory castables, were investigated and the resulting thermomechanical and thermochemical properties of the reference castables were studied. The results were used as a basis for the development of andalusite-free castables which is part II of the project.

The reference castables were commercial refractory castables that are optimized for different applications and operation conditions (Table 4). All have in common, that they are used in applications with massive thermal shock (TS) load. Two of the three are optimized for high temperature applications up to 1600 and 1700 °C, respectively, whereas one of them is installed in low temperature applications > 1200 °C (Table 4). To study the influence of the bonding system (represented by the fine fraction) to the high-temperature behaviour of andalusite, one silica sol bonded castable, one ultra-low cement castable and one low cement castable are chosen as reference materials (Table 9). The reference castables contain andalusite in various quantities, grades and crystal sizes but they have in common, that the coarse grain is mainly or exclusively composed of andalusite.

Table 4: Typical operation conditions and applications of the reference andalusite-based refractory castables.

	RR	RE	RB
Typical operating conditions	Massive TS load	TS-loaded wear lining, CO atmosphere, corrosive stress especially Fe and Cu smelting metallurgy (metal and slag phases)	Massive TS load
Applications	Burner bricks, electric furnace lids, covers of tunnel kiln cars, generally linings of discontinuously operated kiln units	Channel induction furnaces (holding, casting & continuous casting furnaces), crucible induction furnaces (preferably dry mixes), ladles of all types, channel systems, tundishes (steel melts), components (e.g. burner tubes in heat treatment plants, annealing furnaces)	Castables in front of heaters
Application temperatures	1000-1700 °C	1250-1600 °C	>1200 °C
Special material properties	Good thermal shock resistance, co-use of andalusite, cement-free bonding systems	Controlled elongation behaviour, controlled and controllable transformation behaviour according to mullite	Good thermal shock and mechanical resistance

4.3 Preparation of test-pieces

4.3.1 Castable preparation, moulding and pre-firing at HSK

A precise castable preparation was deemed essential for a smooth and reliable implementation of the research. To ensure a proper mixing, an intensive mixer (type R02, EIRICH) was used with a stick agitator and concurrent rotation for mixtures $\leq 4,5$ kg and star agitator and contrarious rotation for mixtures $\geq 4,5$ kg. The dry mixing stage lasted for 1 minute at the lowest speed. Subsequently, upon adding liquid binder No. 1 for the sol gel RR castable with 62.03 g per kilogram of the material, and 58.2 g and 65 g of water for the ultra-low cement RE and low cement RB castable respectively, the rotational speed was adjusted to 75 rpm for 1 min. during the dry mixing, with wet mixing subsequently continuing for an additional 3 minutes.

The specimens were shaped into different forms for various tests. Cylindrical test-pieces (50 mm in diameter, 50 mm in height, with an internal hole of 12-13 mm diameter) were used for conducting tests on creep under compression (Creep) and refractoriness under load (RUL). For the method of monotonic heating (MMH) test, a modified mould with thermocouples was employed to create cylindrical specimens (length = 100 mm, diameter = 46 mm) and disc samples with 11 mm high and 46 mm diameter were used for laser flash analysis (LFA) test.

For the investigation of the fracture behaviour, the investigated castable formulations were casted in 100 x 100 x 75 mm moulds and then machined with a precision saw to obtained, the wedge splitting test pieces (chapter 4.4.10). For the newly developed channel slag test (chapter 4.4.13), specimens were crafted using two moulds with a complex relief, featuring a groove and tongue system made up of two half shells, with overall dimensions of 260 x 300 x 80 mm (*Figure 1*). Subsequently, all test-pieces were placed in a climate cabinet at 20 °C and 95 % relative humidity for a period of 48 hours. After this, they were dried in a heating cabinet at 110 °C until a constant mass was achieved. Following the conditioning phase, the test specimens meant for RUL, Creep, and wedge splitting tests underwent a pre-firing process at 1000 °C for 1 hour, with a heating rate of 2 K/min. This pre-firing step was essential to prevent excessive shrinkage at lower temperatures, attributed to hydrate phase transformation and the early stages of sintering.

For the method of monotonic heating (MMH) and LFA test, the samples were pre-fired at 350 °C for 1 hour, employing a heating rate of 2 K/min. In the case of the channel slag test, the test pieces were pre-fired at 850 °C for 2 hours, using a heating rate of 2 K/min.

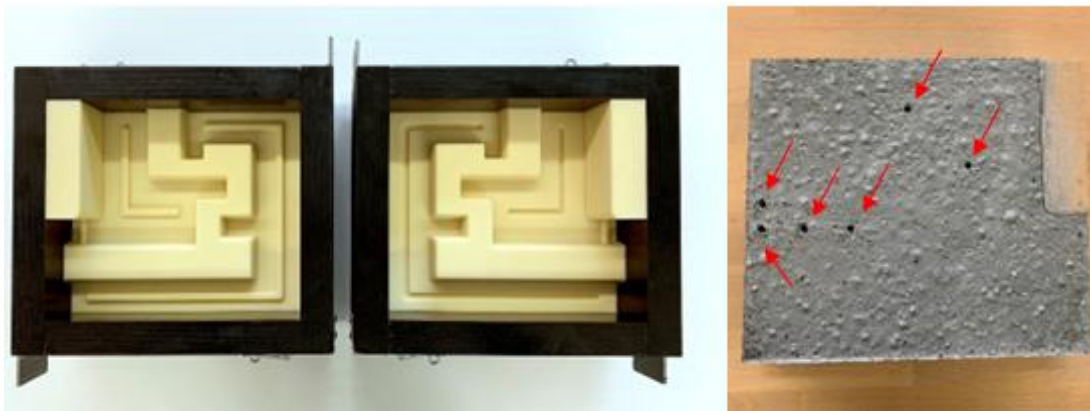


Figure 1: Two moulds with a complex relief with a groove and tongue system of two half shells and dimensions of 26 x 30 x 8 cm (left) and cast test-piece with holes after removing the placeholders for thermocouples (right).

4.3.2 Castable preparation, moulding and pre-firing at INISMa

The castables were prepared in an intensive (Eirich) mixer. The dry composition was mixed at 250 rpm for 1 minute before the necessary water was added. After that, the rotation speed was set up to 700 rpm for 4 minutes. The test-pieces were cast in 40 x 40 x 160 mm steel moulds with vibration on a table according to ISO 1927-5, maintained under a plastic cover for 24 h before to be demoulded and dried in stove at 100°C for 24 h.

4.3.3 Ash preparation for the channel slag test at FGF

In the novel channel slag test, a corrosive medium composed of a basic ash, containing components such as wollastonite, sodium carbonate, calcium phosphate, and potash, was introduced into the burner flame. The recipe for the synthetic slag, produced by ProKera GmbH, Montabaur, Germany, was based on the composition of average ashes of wood burning processes. A basic ash was chosen for the channel slag test because basic ashes are considered to be more aggressive than acid slags. The advantage was that measurable corrosion can already be expected in the short test period of 4 hours. The high number of alkalis is a good precondition to investigate the corrosion mechanism due to alkalis.

To obtain the ash, the raw materials were ground to a suitable grain size using a disc mill. This step aimed to enhance the reactivity and uniformity of the ash. The chemical composition of the ash is provided in [Table 5](#).

To ensure that the ash could flow smoothly through the designated channel of the test component, an intricate and time-consuming granulation process was employed. This process featured the utilization of a laboratory-intensive mixer, the EL01 from Eirich GmbH in Hardheim, Germany. A micro-granulation agitator, utilizing the eddy current method, operated at a rotational speed of 28.3 meters per second for 200 seconds. Polyethylene glycol 200 (PEG 200) served as the water-free binder for the granulation process of the ash.

Following the granulation process, the resulting granulate was dried at a temperature of 110 °C to eliminate any remaining moisture. Subsequently, the granulate underwent sieving to achieve a particle size of less than 1 mm, ensuring uniformity and consistency in the ashes used for corrosion testing.

Table 5: Chemical composition of the ash as determined by XRF.

	LOI	SiO ₂	Al ₂ O ₃	Na ₂ O	CaO	MgO wt.-%	Fe ₂ O ₃	K ₂ O	P ₂ O ₅	SO ₃	Mn ₂ O ₃
Ash	27.10	24.90	3.60	11.30	21.79	6.13	7.35	12.70	4.54	6.21	1.14

4.4 Methods for analysis

4.4.1 Thermal treatment of test pieces without dwell time

Test pieces of the reference and the model castables, all in the dimensions of the test-pieces used for MMH (100 mm in length and 46 mm in diameter), were thermally treated at different maximum temperatures of 1000, 1200, 1300, 1400 and 1500 °C, all with a heating and cooling rate of 500 K/h (the same as applied in MMH). The temperatures were measured in the centre of a test-piece that is equivalent to the test specimen and equipped with a thermocouple in the centre, as in MMH. After that, all test-pieces treated at different temperatures were investigated by

XRD and SEM for describing the prograde phase transformations and changes in their microstructures that occurred between each temperature step of 100 K. These prograde changes can be related to the results of MMH, because the phase composition and microstructures assessed after each temperature step can be directly correlated with the results of MMH (curve progression of a_{eff} and signals therein). This laborious procedure is very helpful for identifying the nature of the signals in the curve progressions of a_{eff} vs. test-piece temperature. The results also help to understand the mechanical behaviour of the castables during RUL.

4.4.2 Thermal treatment of test-pieces with a dwell time of 8 hours

Test pieces of the reference and model castables, in the dimensions of the test pieces used for MMH, were thermally treated at different temperatures of 1000, 1200, 1300, 1400 1500 °C in air, with heating and cooling rates of 500 K/h. The test pieces treated at different temperatures were investigated by XRD and SEM for describing the prograde phase transformations and changes in their microstructures that occurred between each temperature step.

4.4.3 Mineralogical analysis

Prior to analysis, the samples were finely powdered by crushing them in a WC-Co disc mill to a grain size < 63 µm. X-ray diffraction (XRD) was employed to measure the mineral phases. The analysis was conducted using a Philips X-PERT PRO instrument with a Cu K α tube. The slit length was 15 mm, the beam radius 240 mm and the measure time 24 minutes with a step size of 0,013 °. The mineral phase composition was calculated using the Profex 5.2.0 programme.

4.4.4 Microstructural analysis

To examine the prograde microstructural changes in the castables, SEM investigations were conducted using two different instruments. At HSK, a Jeol JSM 7200F microscope equipped with a Schottky field emission cathode was utilized. This instrument was used to investigate the raw material, reference castables and model castables after thermal treatment. Additionally, at FGF, a Zeiss Sigma 300 microscope with a similar cathode configuration was employed. The instrument was used for the investigation of the test-pieces following the thermal and chemical treatment within the channel slag test and the thermal treatment of test-pieces without dwell time. Both microscopes enabled high-resolution imaging. Polished sections of the fired castables were prepared for analysis. In the case of the Jeol JSM 7200F, a 0.5 nm iridium layer was applied using a BALTIC high vacuum CCU 010/HV sputter coater. As for the Zeiss Sigma 300, a 6 nm carbon layer was used for coating. Imaging of the specimens was performed using backscattered electron detectors, generating BSE-images, with an accelerating voltage of 15 kV. Chemical micro analysis was carried out using the installed Oxford Instruments Ultim Max40 (EDX-detector) and the associated AztecLive software.

4.4.5 Determination of bulk density and open porosity

The open porosity and bulk density of the reference materials and model castables were determined according to the standard EN 993-1 for shaped products for test-pieces that were dried for 24 h at 110 °C and for test-pieces that were fired for 4 h at 1000, 1250 and 1500 °C. The test-pieces with dimensions of 40 x 40 x 160 mm were dried, placed in a sealed vessel and maintained under vacuum for 30 minutes, and finally soaked with pure water.

4.4.6 CCS and MOR

The crushing strength was only measured at room temperature (cold crushing strength, CCS) according to ISO 1927-6. Load is applied (1 MPa/s) on tips of test-pieces with dimensions of 40 x 40 mm) perpendicular to the casting direction, up to rupture.

For the measurement of the bending resistance (modulus of rupture, MOR), samples with dimensions of 15 x 25 x 125 mm were cut and tooled. Three-point bending tests were realised according to EN 993-6.

Test were carried out in an electrical furnace under ambient atmosphere, at room temperature and at high temperature after heating (10 °C/min) and stabilisation (30 min) of targeted temperature. For every temperature, two test-pieces of each material were tested to determine a mean value.

4.4.7 Resonance frequency damping analysis (RFDA)

The Young's modulus was measured using the acoustic (RFDA) method. This method is based on the pulse excitation technique. The measurement principle is based on tapping the sample with a small hammer and recording the induced vibration signal with a microphone. The Young's modulus (E) is then calculated directly from: $E = 0.9465 \cdot (m f_2/w) \cdot (L_3/t_3)$ where m is the mass, f is the bending frequency, w is the width, l is the length and t is the thickness of the sample. In this work we only consider the frequency ratio: (f/f_0) , which allows the material transformation to be observed without any information about the change in sample size. In general, this method is sufficient to deduce the evolution of the material microstructure and/or phase transformations as a function of temperature during heating. The experiments were carried out from room temperature to 1400 °C, the frequency is measured at different temperatures during heating and cooling (10 °C/min).

4.4.8 Thermal analysis (MMH)

The Method of monotonic heating (MMH) was used to detect the phase transformations of the andalusite raw materials, the reference castables and the andalusite free castables during their first heating in the range between 300-1620 °C. Cylinders made of refractory castables with 100 mm in length and 46 mm in diameter were used.

A principal description of MMH is given in (Litowski 1982, Maglic et al. 1989). During the monotonic heating (i.e. with constant heating rate) of a cylindrical sample of the castables, a thermal gradient develops between the surface (T_x) and the centre of the sample (T_0) (*Figure 2*). The non-steady state temperature distribution is described by the Fouriers 2nd law:

$$\frac{\delta T}{\delta t} = a \frac{\delta^2 T}{\delta x^2} \left[\frac{K}{s} \right] \quad \text{Eq. 1}$$

The solution for a cylinder of infinite size that is symmetrically heated from the sides with a constant rate is given by:

$$a_{eff} = \frac{b \cdot x^2}{4 \cdot (T_x - T_0)} \quad \text{Eq. 2}$$

Where a_{eff} is the apparent thermal diffusivity, b is the heating rate in the centre of the sample, x is the distance between the thermocouples in the centre and close to the surface. The number 4 in the denominator is a geometric coefficient that applies to the cylinder shape geometry of the test specimen.

Should MMH being used with the purpose to determine the effective thermal diffusivities of ceramics, additional terms for correction are introduced in equation 1 that consider the temperature dependence of the thermo-physical properties of the sample materials as well as the non-linear heat flow in the samples. MMH can also be applied for thermal analysis. It provides valuable information on phase transformations in the test specimen like sintering, melting and others. This is based on two effects:

1. Sintering changes the microstructure of the sample and thus modifies the effective thermal diffusivity in an irreversible way. Because the effective thermal diffusivity is determined as continuous curve ("MMH-curve") above the sample temperature, the beginning of sintering is indicated by an accelerated increase of the effective thermal diffusivity. This effect is widely used for investigating the sintering behaviour of ceramics, but in general by applying the laser flash method (Dannert et al. 2000). Due to the large size of the test specimen, MMH is especially suited refractories because of their coarse grains.

2. The heat effects that accompany phase transformations (endothermal or exothermal) affect the heating rate at the centre of the sample as well as the temperature difference between the surface and the centre of a sample during MMH testing (equation 2). This causes deviations in MMH-curve in the form of peaks or steps, which are suitable to identify the temperatures of phase transformations (report AiF-No. 17764) Such effects can only be assessed by dynamic methods like MMH or STA and cannot be detected by static methods like the laser flash method.

Here, the key advantage of MMH is the large size of the test specimen (cylinder, $H = 100$ mm, $D = 46$ mm), that is sufficient to analyse coarse grained refractories. As in the case of the andalusite reference castables, grain sizes up to 6 mm prohibit the application of common thermal analytical methods (STA, DSC) that analyse test specimen with dimensions in the range of $5 \times 5 \times 5$ mm³.

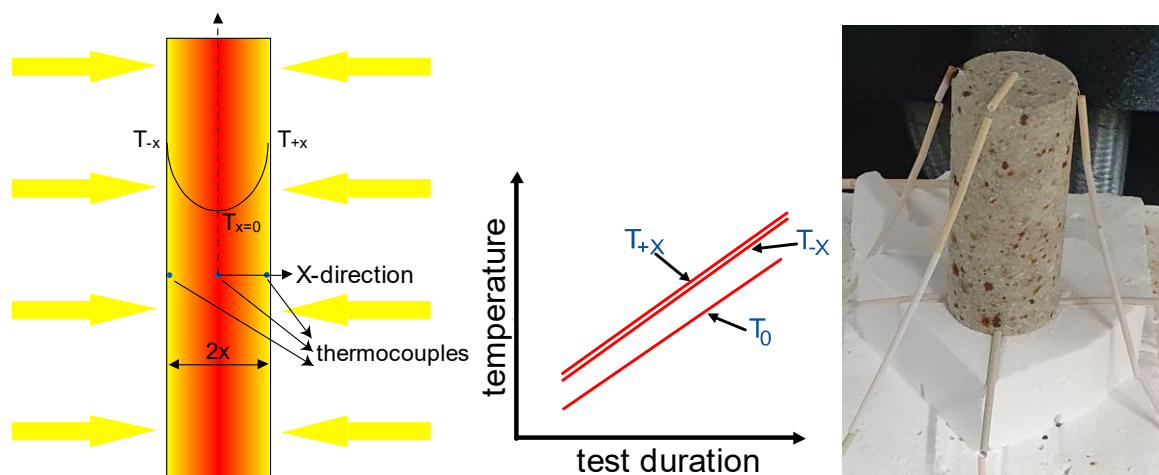


Figure 2: Schematic illustration of the MMH test set-up (left), representation of the temperature curve of the three thermocouples (middle) and a photograph of the assembled test piece in the furnace. At constant thermal diffusivity, the thermocouple, T_0 , remains at lower temperatures by the amount of the thermal diffusivity. As a rule, this changes when the rapid heating of the sample causes phase changes or melt formation/sintering to release energy (exothermic) or consume heat (endothermic).

4.4.9 Refractoriness under load (RUL, DIN EN ISO 1893)

The thermal expansion and high-temperature deformation of cylindrical test pieces under constant load and increasing temperature was measured by the method “Refractoriness under load (RUL)” following DIN EN ISO 1893. The results show the temperature of maximum expansion and subsequent compression at increasing temperature. The test is completed at 1700 °C or when the percentage change in height reaches 5 % (emergency shutdown of the system). Although the standardized, experimental conditions during RUL and Creep do differ from the various conditions during industrial application of the refractories, the results give, in combination with the experience of the operator, important information on the thermo-mechanical behaviour of refractory materials during application.

4.4.10 Wedge splitting test

The measurement was realised at FGF by applying an increasing traction stress on test pieces with a prefabricated notch and following the propagation of the crack in the test-piece (see Figure 3). The analysis of the loadcrack mouth opening displacement curve allows determining the specific fracture energy. The principle is therefore to measure the force required to initiate a crack in a refractory castable test piece and to determine the force required to propagate the crack within the test piece.

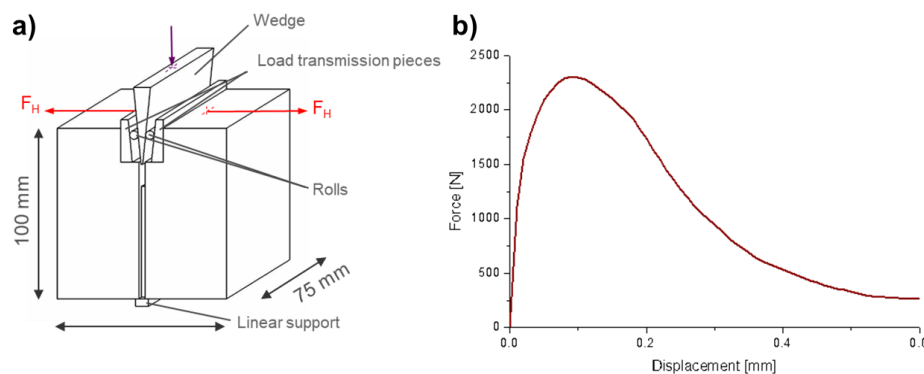


Figure 3: Schematic structure of the wedge splitting test (left) and a typical curve (right).

The wedge converts a small force over a long vertical displacement into way larger force over shorter horizontal displacement. This procedure allows a crack to be created in the test-piece which runs in a controlled manner through the specimen without causing sudden catastrophic failure. It is thus possible to determine the work-of-fracture by integrating the measured force over the measured displacement and the specific fracture energy by dividing the work-of-fracture by resulting fracture area.

4.4.11 Laser flash analysis (LFA)

Thermal diffusivity measurements were conducted with a high-temperature laser-flash apparatus at FGF that was specially designed and built for large refractory samples. The test-pieces are disc-shaped with a diameter of 45 mm and a height of 11 mm. The measurement is started by creating a laser pulse onto the front of a test-piece, which transfers heat into the test-piece. The time-dependant temperature increase at the far side of the disc is monitored by a pyrometer. Using an inverse FEM model, specially developed to simulate the time-dependant pyrometer signal, the thermal diffusivity of the sample is determined. Phase transformations like melt formation can be monitored by repeated measuring the thermal diffusivity of a material at constant

temperatures over long time, as the thermal diffusivity is being influenced by such structural and mineralogical changes. In the case of andalusite-based refractories, progressing formation of mullite and high viscous silica-rich melt (following andalusite transformation) gradually change the thermal diffusivity during prolonged exposure at a constant temperature. If LFA is carried out over a long time at constant temperatures, which are pre-selected from the temperatures of phase change events as determined by MMH, LFA should be suited to determine the kinetics of structural and mineralogical changes (andalusite transformation). Here, the actual efficiency of LFA in determining the kinetics of the transformation of andalusite in refractory castables was evaluated for the first time. The measurement temperatures were set between 1000 and 1500 °C.

4.4.12 Creep under compression (CREEP; DIN EN 993-9)

The experimental setup of the creep test is the same as for RUL. First, the specimen is heated under defined load with a constant rate of 5 K/min up to the test temperature, which is then maintained for 25 hours or until prescribed deformation occurs. Testing temperatures were selected at 1500 °C or 1450 °C, based on the results of RUL, that means about 50 K lower than the temperature of maximum expansion in RUL.

4.4.13 The channel slag test

The test setup at FGF consists of a gas burner that can inject corrosive media and fires into a specially prepared block made from two half shells and a chimney that are made of castables, which includes a firing channel through which the hot gas from the burner, together with corrosive media, travels through the block meandering (Figure 4 and Figure 5). A geometry like the post-combustion chamber of biomass combustion was created in a finite element method (FEM) simulation software and optimized regarding temperature gradient, gas flow and structural mechanics. With careful temperature control of the burner and dedicated cooling plates fixed to the block, the temperature gradient inside of the block (and thus inside of the two half shells made of different castables) can be controlled. The temperature of the gas burner is controlled by a thermocouple 2,5 cm inside of the block. The geometry of the block creates different areas of temperature in one block, so that both gaseous and liquid corrosion can be tested in simultaneously. This can be intensified by water cooling the block from the outside. Granulated slag can be constantly inserted by a vibration plate and compressed air via a tube that ends next to the gas burner (Figure 4).

The test-pieces for one corrosion test are two half shells of 30 x 26 x 8 cm (x, y, z) and a 50 x 11 cm two-piece chimney of refractory castables with a total weight of 50 kg (Figure 5). The construction with half shells allows to test two materials simultaneously. Put together, they form a block with a tortuous channel inside, allowing to create decreasing temperatures at the hot face of the channel from the inlet (burner torch) and the outlet (chimney). Three tongues were inserted into the half shell so that the corrosive media is retained longer in the component by a turbulent flow. The half shells include five bore holes each to insert thermocouples from the cold side into the half shell. They are positioned as depicted in *Figure 5*.

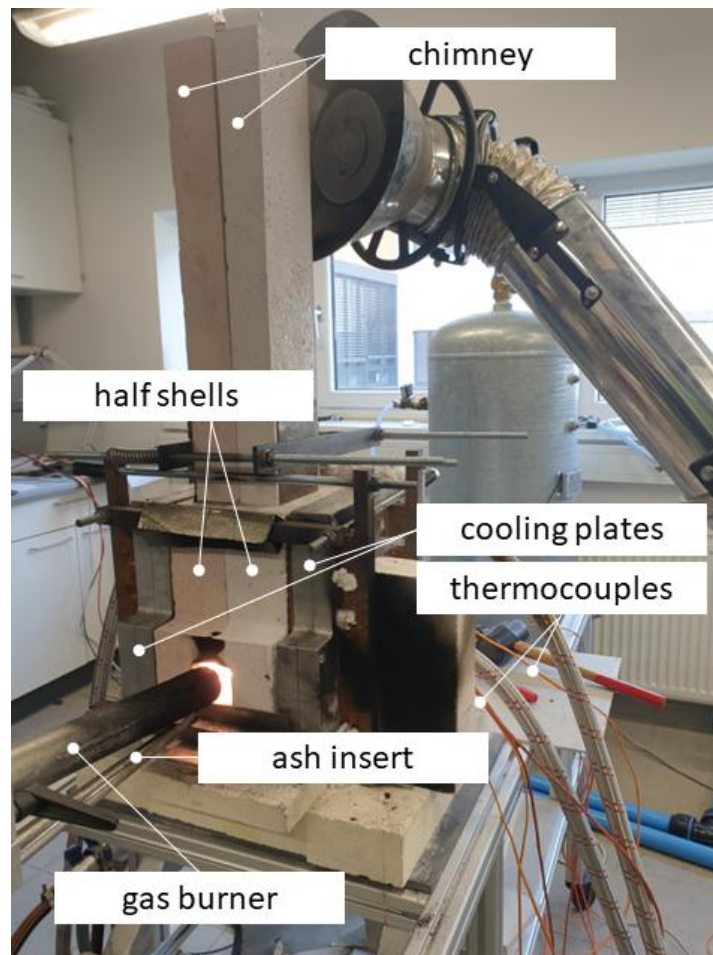


Figure 4: Corrosion test setup (channel slag test). The gas burner injects corrosive media and fires into a block of two half shells made from castables. Between the firing channel in the middle and the cooling plates at the outside a temperature gradient of several hundred degree occurs.

4.4.13.1 Microstructural and chemical analysis after channel slag test

For microstructural analysis of test-pieces from the channel slag test at positions 2 and 3 (*Figure 5*) were analysed using the field-emission scanning electron microscope Sigma 300 (Zeiss) at FGF. Chemical micro analysis was carried out using the installed Oxford Instruments Ultim Max40 (EDX-Detector) and the associated AztecLive software. Raman analyses were performed at HSK with an Apyron (WITec GmbH, Germany) equipped with a deep-depletion detector and a 532 nm laser.

4.4.13.2 Temperature gradient in the channel slag test

To determine the temperature gradient inside the castable during testing conditions, the temperatures were measured at 5 locations in each half shell (TC1-TC5 and TC7-TC11 in the corresponding other half shell) (*Figure 5*). At these locations 5 measurements were executed in different depths within the half shells (across the z-direction). For this test, a LCC model castable was used containing T60 in most of the grain fractions and anorthite (half shell 1, MRC-K) and anorthite plus kyanite (half shell 2, MRC-ANO/K) in the fine fraction.

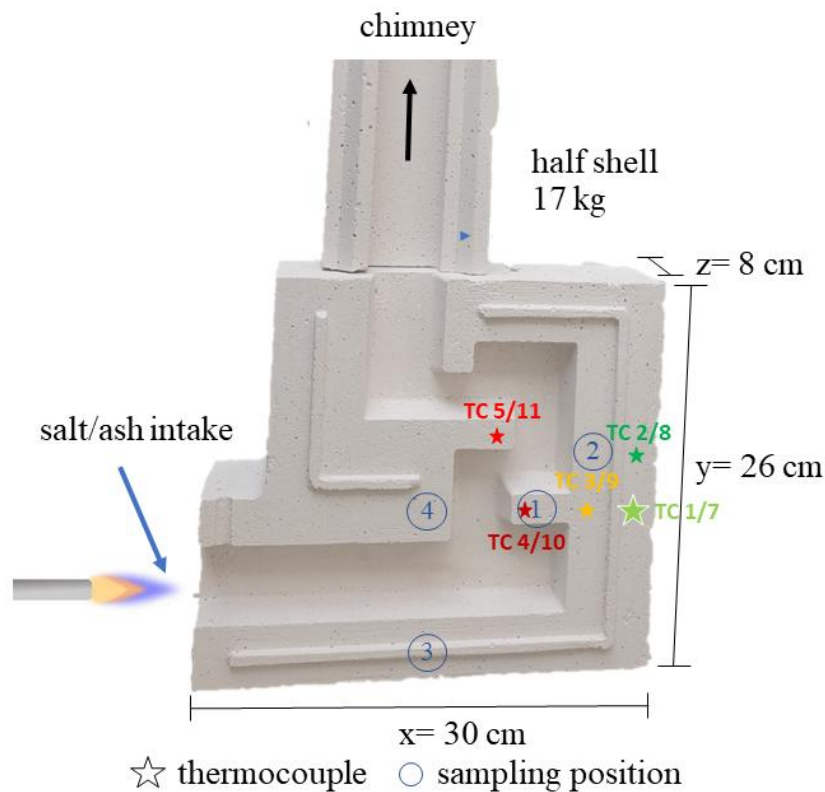


Figure 5: Cast half shell developed for the channel slag test with a chimney that is located on the top opening of the shells during the test. The corrosive media is injected at the bottom left with a gas burner. Four thermocouples and one control thermocouple (light green) measure the temperatures inside the castable. Sampling positions are marked in blue.

A thermal gradient develops within the firing channel with increasing distance from the gas flame in x-y direction and, in the direction of z within the castable, between the inner wall of the firing channel to the outside of the test-pieces where water-cooled metallic shells are installed. The temperature of the corrosion test device is adjusted to 1250 °C at the control thermocouple TC10 (Figure 5 position is marked with a dark red star) at z =2,5 cm inside the castable. The temperature is the highest where the gas flame hits the channel (up to 1520 °C at TC4/10) and decreases in all directions.

The temperature gradient of TC4/10 in z-direction is the highest and ranges from about 1520 °C to around 105 °C next to the cooling plates (Figure 6). The thermal gradient at the two outer thermocouples (TC2/8 and TC1/7) is the lowest, the temperature ranges from 530 to around 80 °C. The temperature in the chimney ranges from around 1000 to 500 °C at the hot face that decreases rapidly to the cold outer face. The positions of the thermocouples (TC4/10, TC3/9 and TC1/7) allow to determine the thermal gradient in x direction. The dependence of distance from the firing channel and temperature is clearly linear. As intended, the thermal gradient decreases with increasing depth (z value) of the thermocouple.

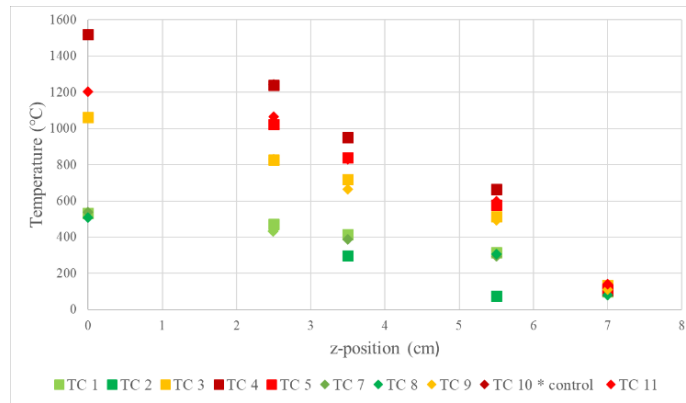


Figure 6: Thermal gradient occurring in z-direction (firing channel z=0 cooling plates z=8 cm) measured at five z-positions for each of the five x, y-positions (TC1-TC5 and TC7-TC11).

This preliminary test demonstrated that a large thermal gradient can be generated in the tested material with the channel slag test. It was found that the temperature gradient depends on the thermal conductivity of the tested material.

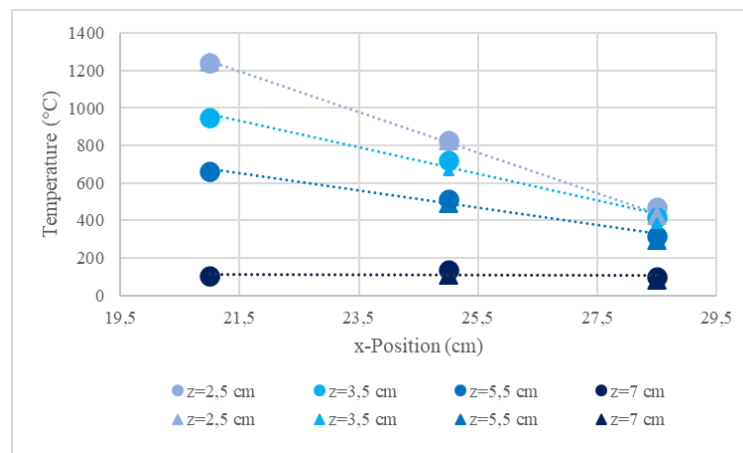


Figure 7: Thermal gradient occurring in x-direction measured at three x-positions (TC4/10, TC3/9 and TC1/7). The thermal gradient decreases with increasing depth (z-value) of the thermocouple.

5. Results and discussion

5.1 Thermal decomposition of andalusite raw materials

Andalusite is analytically proven to decompose to mullite and, as it is generally assumed, to amorphous SiO_2 from a temperature of about 1200 °C (Schneider and Majdic 1981). The aggregate state of the latter is generally debatable, with the frequently expressed opinion that it is a melting phase. However, this does not correlate with the purity of the SiO_2 formed and the assumed melting point of the pure phase. It can therefore be assumed that the decomposition of andalusite is a process controlled by solid-state diffusion, which is ultimately based on a segregation of the andalusite, in which SiO_2 segregates and mullite is formed as the main phase, which crystallizes oriented to the former andalusite lattice. Solid-state diffusively driven processes are generally

kinetically inhibited, so that andalusite, which is only thermochemically stable up to around 800 °C, can be significantly overheated.

To establish a fundamental understanding of this, coarse grain fractions were thermally treated at up to 1450 °C and different holding times. The resulting materials were investigated ex-situ in terms of mineral changes using X-ray phase analysis and microstructural methods.

Durandal D59 (Imerys) of a grain size between 3 and 5 mm was exposed to 1400 °C, at dwell times between 1 and 4 hours, as it could be assumed that at this temperature andalusite shall decompose at least to a degree of 50 % (Schneider and Majdic 1981). However, as envisaged in *Table 6*, the decomposition rate of andalusite remained low, so that even after a dwell time of 4 hours the residual andalusite was still at a level of 90 wt.-% and solely 10 wt.-% of mullite was formed. This clearly contradicts the data from Schneider and Majdic 1981, which is probably because the authors worked with fine-grained andalusite (not stated in the article). Furthermore, the andalusite analysed in the scope of this R&D project was of high purity, which further inhibits the kinetics of andalusite replacement. As will be explained in more detail below, the impurities play an important role as they form early melting phases, which means that there is no longer a pure solid-state reaction.

Table 6: Mineralogical composition of Durandal andalusite raw material annealed at 1400 °C as a function of time.

	1400 °C-0 h	1400 °C-1 h	1400 °C-2 h	1400 °C-3 h	1400 °C-4 h
	wt.-%				
Andalusite	99	92	93	87	90
Mullite	0	8	6	12	10
Quartz	1	Tr	Tr	Tr	Tr
Cristobalite	0	Tr	Tr	Tr	Tr

Tr=traces

If the dwell time was increased to 24 hours, it became clear that the Durandal (3-5 mm) transforms much more strongly. A treatment temperature of 1350 °C already leads to a decrease in the andalusite content from 99 to 84 wt.-% and a corresponding increase in the mullite yield. A 50 °C higher temperature results in a further decrease in the andalusite content (73 wt.-%). At 1450 °C, the andalusite content has more than halved, so that mullite is now the predominant phase. *Table 7* also shows cristobalite as a mineral phase, which increases in concentration with increasing holding time. This is basically plausible, as the decomposition of andalusite releases SiO₂, which in turn is converted over time to the cristobalite phase, which is stable at 1450 °C. In addition, the Durandal already contains α-quartz as an impurity.

Table 7: Mineralogical composition of Durandal D59 andalusite raw material annealed for 24 h, as a function of the temperature.

	1350 °C-24 h	1400 °C-24 h	1450 °C-24 h
	wt.-%		
Andalusite	84	73	42
Mullite	15	25	54
Cristobalite	1	2	4

In a further series of experiments, the Perusite was treated thematically in a comparable grain size to the Durandal. In contrast to Durandal, the andalusite content in Perusite is not 99 but only

93 wt.-% and, conversely, it contains significantly more impurities, with biotite and quartz being detectable by X-ray diffractometry. The aim of the investigation was to understand the incipient decomposition of the andalusite from a microstructural point of view. For this reason, the pre-treatment temperatures were deliberately kept low, and the dwell time was kept short at 1 hour. It was found that decomposition of the andalusite is only detectable by diffractometry from a temperature on of 1300 °C and that mullite is being formed in the process (*Table 8*). It should also be emphasized here from literature that biotite is no longer stable at 550 °C, so that hematite appears as a new phase instead of biotite after thermal treatment. This is because biotite decomposes to potassium feldspar and, at the prevailing p_{O2}, to hematite (see *Figure 12*). Potassium feldspar is not detectable because instead of this phase, a melt has most likely already been formed at 1100 °C, which solidifies into a glassy form during cooling. The reported proportion of quartz is based on the degree of impurity of the raw material and remains stable up to 1200 °C.

Table 8: Mineralogical composition of Perusite treated at different temperatures and dwell time of 1 h.

	room temperature	1100 °C	1200 °C wt.-%	1300 °C
Andalusite	93	93	93	91
Biotite	4			
Hematite		2	2	
Quartz	5	5	5	4
Mullite				5

The diffractometric investigations were accompanied by microstructural examinations of individual andalusite grains, which were aged at the respective temperatures (*Figure 8* to *Figure 13*). Even at a pre-treatment temperature of 1100 °C, the perusite exhibits first transformations to mullite and glass phase, but these are always linked to the impurities that occur. *Figure 8* shows an enlarged section on which euhedral mullite was formed along a crack-like impurified zone, which is associated with an iron-rich melt (glass at room temperature). According to this, the first mullitisation does not take place as a pure solid-state reaction, but in the presence of a melt phase that is already present at 1100 °C. The mullite also has a very high iron content, which can be easily recognized by the high contrast. After thermal pre-treatment at 1200 and 1300 °C, it is also noticeable that the coarse grains already exhibit expansion, which is evident in *Figure 10* and *Figure 11* as a clearly recognizable crack structure. All grains have areas that show a high contrast and basically represent ferrous impurities, which also promote mullitisation via a liquid phase.

However, pure andalusite decomposes at temperatures above ~1300 °C, resulting in the described “felted aggregates” composed of skeletal mullite with interstitial highly viscous silica phase. The nucleation of mullite crystals starts in relation on the andalusite crystal lattice. Therefore, the orientation of the skeletal mullite crystals in the “felted aggregates” is also oriented, inherited from the former andalusite lattice. The impurities (mainly Fe, Ti) formed hercynitic spinel as shown in *Figure 13*. Biotite and quartz were detected as typical impurities of the raw material at room temperature. During thermal treatment of 1200 °C for 1 hour, biotite transforms to potassium feldspar and hematite (see *Figure 12*), simplified for Annite:



It can therefore be concluded that impurities already cause melting phases inside of the materials at temperatures of 1100 °C, which may be regarded as a decomposition product of the biotite, whereby iron is partly involved in the potassium feldspar-rich melt formation but also crystallizes out in large quantities as hematite. The higher the proportion of impurities, the more mullite will

form, favoured by the formation of melt phases. However, a significant transformation of the andalusite can only be observed from 1300 °C if the firing time is extended from 1 to 3 hours. Only then can the typical orientation of the mullite crystals along the crystal lattice of andalusite be recognized. Whether this is a segregation reaction or topotactic growth cannot be said with absolute certainty. Since it is very likely that no melting phase plays a role in these areas and the decomposition reaction apparently takes place as a pure solid-state reaction, a segregation reaction would be preferable.

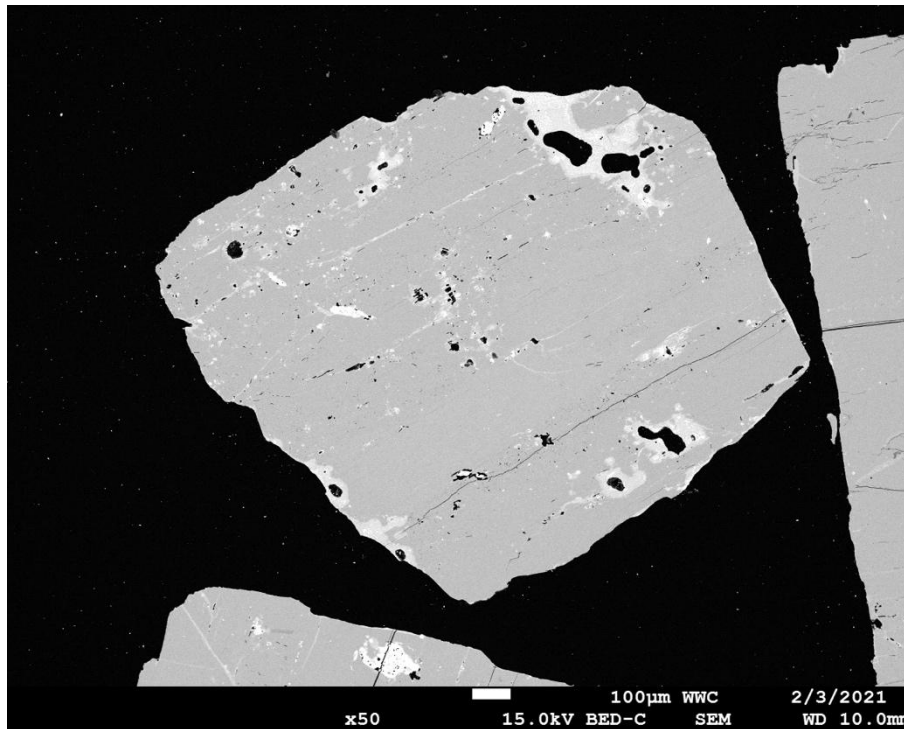


Figure 8: BSE image of Perusite pre-fired at 1100 °C for 1 h (magnification 50x): The micrograph shows a single crystal andalusite. Inside the grain high contrasting inclusions and veins (fissures) are visible that can be identified as hematite rich inclusions derived from the decomposition of biotite. The smooth surface of the grain indicates that the andalusite remains almost unchanged at 1100 °C.

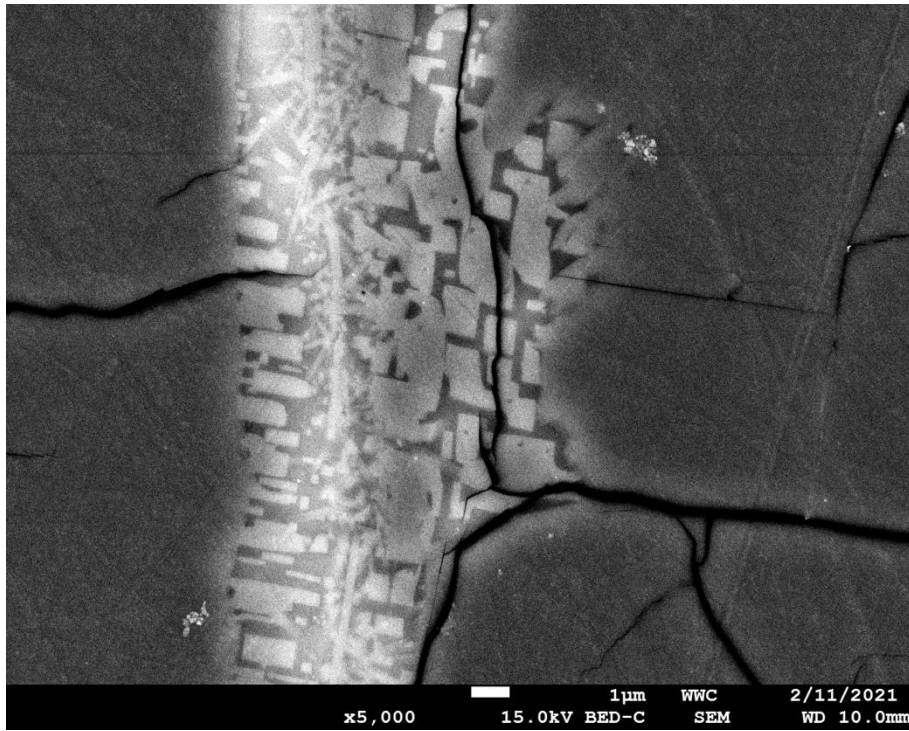


Figure 9: BSE image of Perusite pre-fired at 1100 °C for 1 h (magnification 5000x): The micrograph shows a section with higher magnification of Figure 8 and focus on a high contrasting vein. It becomes visible that in this vein a liquid phase was present at 1100 °C that allows an acceleration of the andalusite decomposition, because in here the andalusite decomposition is favored by the liquid phase. The high contrast of the euhedral mullite crystals is related to a significant incorporation of iron into the crystal lattice.

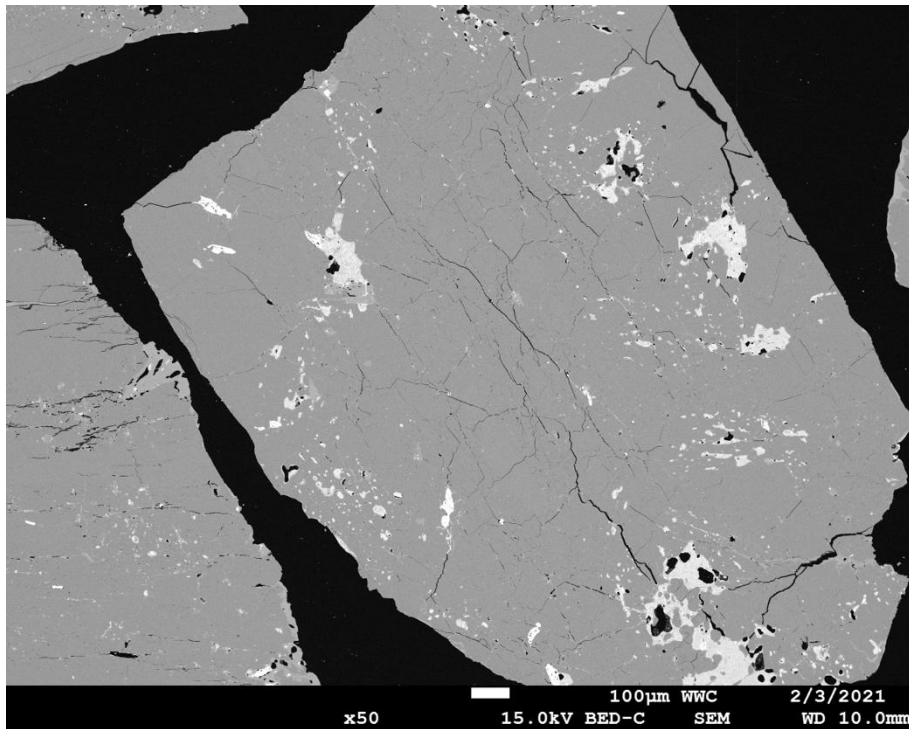


Figure 10: BSE image of Perusite pre-fired at 1200 °C for 1 h (magnification 50x): The micrograph shows a single crystal andalusite. In contrast to the grains that were pretreated at 1100 °C, the coarse grain shown here shows a clearly recognizable crack texture, which is due to thermal expansion. Inclusions with high contrast can be explained as in Figure 8.

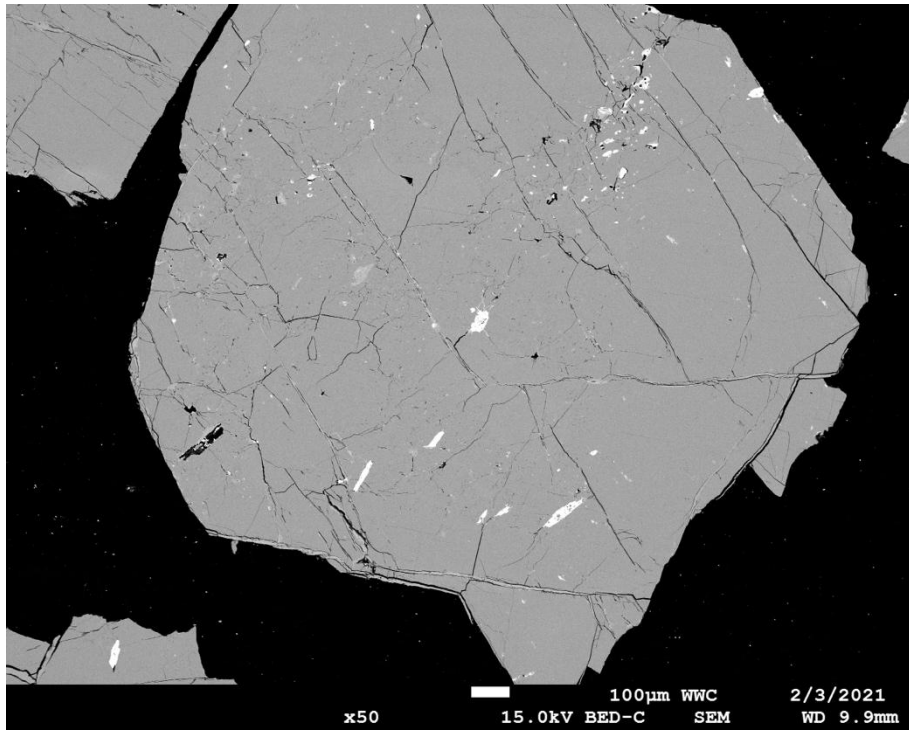


Figure 11: BSE image of Perusite pre-fired at 1300 °C for 1 h (magnification 50x): The micrograph shows a single crystal andalusite. The coarse grain shown here has a similar structure as in Figure 10.

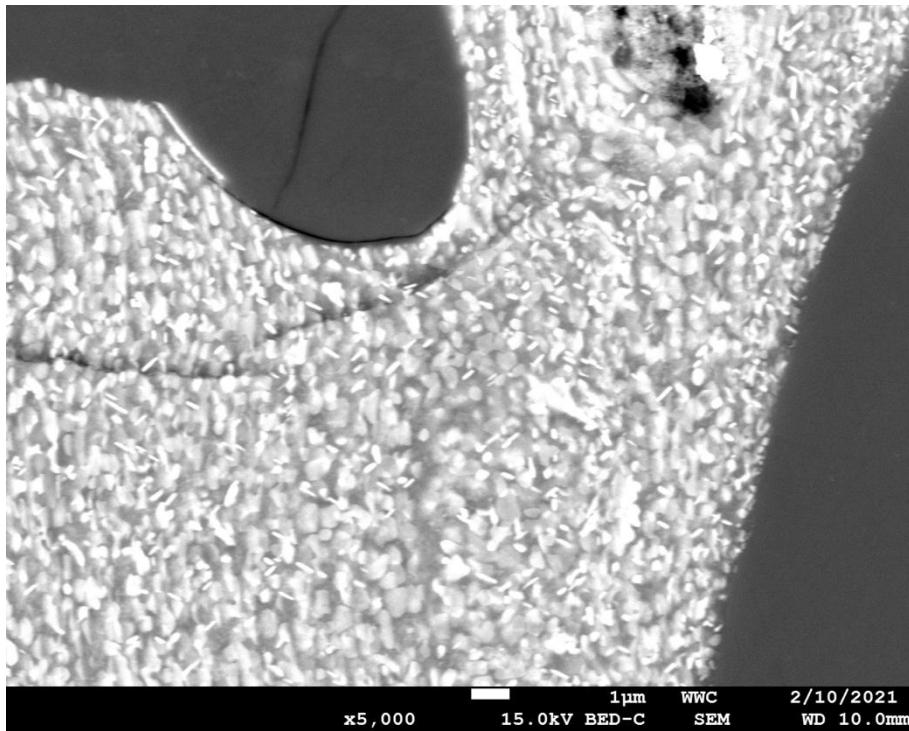


Figure 12: BSE image of Perusite pre-fired at 1300 °C for 1 h (magnification 5000x): The micrograph shows a high contrasting inclusion in a single crystal andalusite and shows a decomposed Biotite. Besides a glassy phase high reflecting euhedral hematite crystals are visible that obviously are orientated.

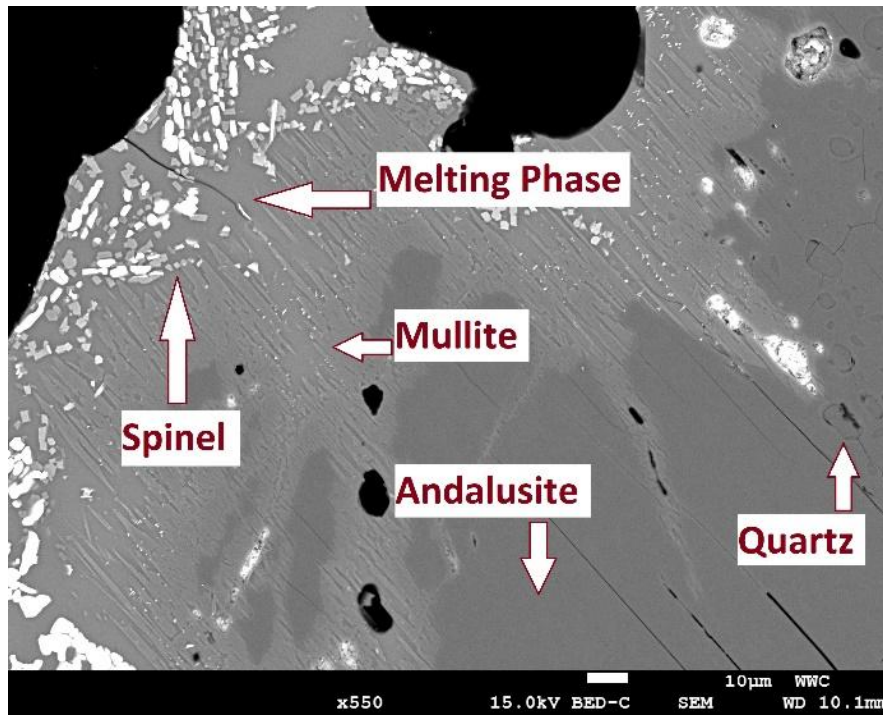


Figure 13: BSE image of Perusite pre-fired at 1300 °C for 3 h, magnification 550x: The decomposition of the andalusite coarse grain starts from the grain surface and the impurities in the grain. In addition to mullite and a fusion phase, a hercynitic spinel is formed on the surface, which indicates a high mobility of the aluminium, which combines with the hematite to form spinel.

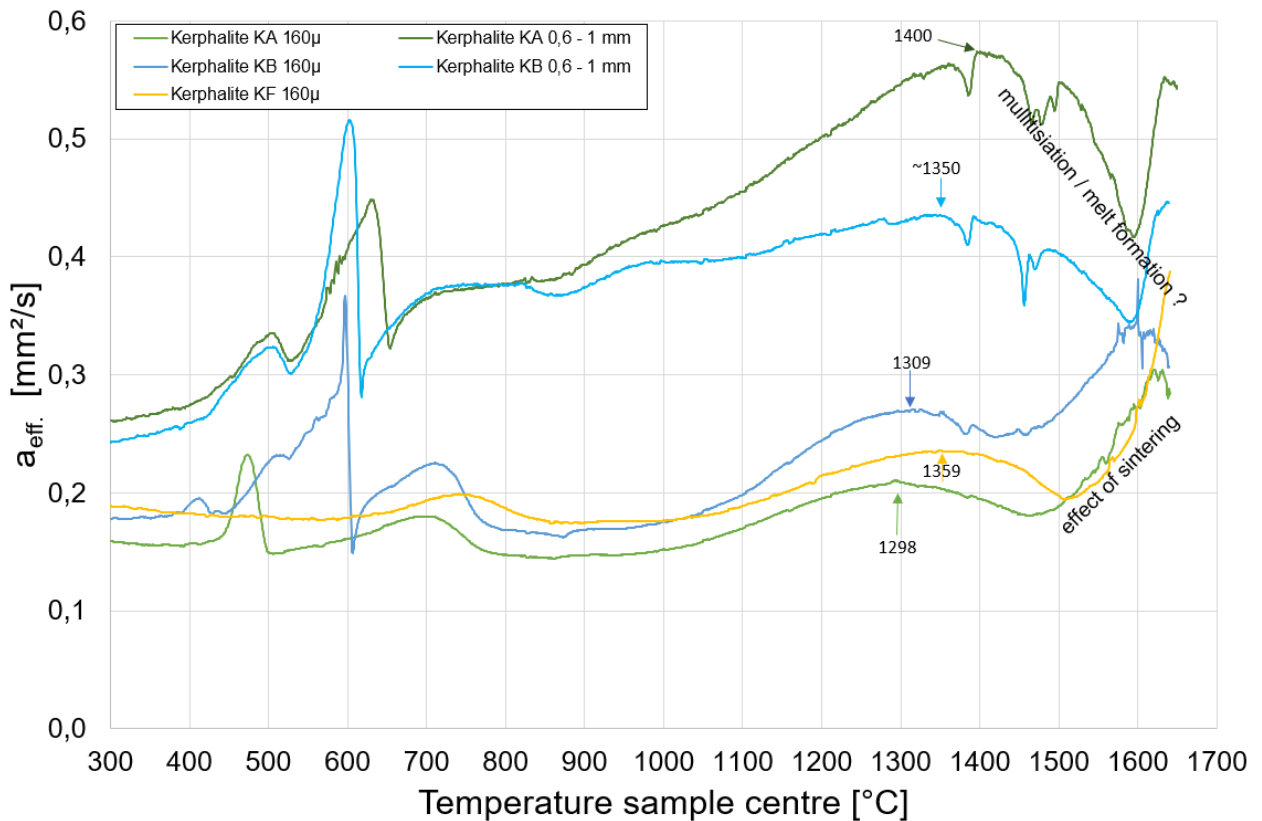


Figure 14: Heat up behaviour of Andalusite raw material determined by means of the method of monotonic heating (MMH). Exothermic peaks below 600 °C should be attributed to the dewatering of hydrate containing phases and their decomposition. Mainly biotite and muscovite, as natural occurring impurities, are involved in these reactions but also the formation of β -quartz at 573 °C.

To identify the characteristic signals in the MMH curves (effective thermal diffusivity vs. test piece temperature, *Figure 14*) referring to the andalusite decomposition, pure andalusite raw materials were investigated at first. Observed signals at temperatures below ~700 °C involve impurities (e.g. dehydration, quartz transformation) and give some information about side components in the raw materials. Maxima in the MMH-curves between ~1300 and ~1440 °C are attributed as the onset of the andalusite decomposition. The observed temperatures of the maxima increase with the level of purity of the andalusite raw materials as well the grain size. The downward slope following the peak corresponds with the ongoing andalusite transformation, as observed by SEM (*Figure 13*). SEM shows the beginning of andalusite decomposition in contact with impurities like biotite, commencing at grain boundaries in contact with the surrounding matrix and finally the cores of larger andalusite grains transform. SEM investigation reveals the begin of andalusite transformation in test pieces heated at 1300 °C for 1 hour.

In principle, the thermal decomposition of andalusite is kinetically hampered as long as no melting phase is present. Mullitisation therefore always begins at impurities typical of the raw material, such as biotite and muscovite, which lead to the formation of the first melts at temperatures of about 1100 °C. A higher proportion of impurities therefore also leads to earlier decomposition of the andalusite grain. The degree of impurities is deposit-specific and can be correlated with the respective particular (metamorphic) conditions of the deposit formation.

5.2 Nature of the reference castables

Refracast Nanobond A-72 C/TS (**RR**) is a silica sol castable (NCC), produced by Refatechnik in Bendorf, Germany and contains 36 wt.-% andalusite (Perusite and Durandal D-59) predominantly in the large fractions 1-2 mm and > 2 mm as coarse grain (Table 9 and Table 11). Andalusite is absent in the matrix, which is predominantly composed of alumina fines. Another component of RR is bauxite, which is also part of the coarse grain fraction.

EKW-Flow AU 75 (RE), manufactured by EKW GmbH in Eisenberg, Germany is an ultra-low cement castable (ULCC) containing 32 wt.-% Durandal D-59. Andalusite is beside bauxite part of the coarse grain (fractions 1-2 mm and > 2 mm) and also of the matrix (fine fraction 0.25-0.063 and > 0.063 mm). The matrix also contains corundum, kyanite, chamotte (mullite) and quartz (

Table 12). In the middle grain fractions between 0.25 and 1 mm RE contains corundum, kyanite and chamotte (mullite).

Belflow 605AF (**RB**), manufactured by Belref in Saint-Ghislain, Belgium is a low cement bonded castable (LCC) and has with 63 wt.-% the highest amount of andalusite (Perusite and Kerphalite) (Table 13). Andalusite is main component of all fractions. In the matrix alumina and quartz (impurity derived from andalusite) are also present. The coarse grain and the finest fraction > 0.063 mm also contain chamotte (mullite).

In the RB castable, the alumina content is low and the Al_2O_3/SiO_2 ratio is close to the one of andalusite, indicating a high level of andalusite in this composition (Table 9 and Table 10). RR and RE castable contain higher alumina level and their Al_2O_3/SiO_2 ratio are much higher than attributable to andalusite, indicating a high level of alumina addition in these compositions due to bauxite as a main side component. RR is sold as a non-cement castable (NCC), but also contains 0,30 wt.-% CaO. RE an ultra-low castable (ULCC) and RB is a low-cement castable (LCC), which is represented in the CaO content of the castables and the ignition loss (LOI). The alkali content for RB and RR castables is considerable high due to the presence of biotite and muscovite which is syngenetic to andalusite raw material metamorphic formation (contact metamorphosis of pelitic precursor materials). RE castable contains a high TiO_2 level (1.05 wt.-%) and even higher concentrations are measurable in RR (1.69 wt.-%). RB contains the lowest concentration (0.42 wt.-%). The TiO_2 concentration indicates that in RE and RR bauxite was a raw material compound in higher concentration. RB is supposed to be bauxite free. Here TiO_2 is derived from chamotte.

Hence, three castables were compared, which differ in the bonding phase, whereby RR is cement-free, RE is a ULCC and RB is an LC-castable. The thermal behaviour is significantly influenced by the CaO content in the matrix. RR and RB are comparable with regard to the decomposition behaviour of the andalusite, as the same raw material (Durandal 59) was used. In addition, both castables contain kyanite, which causes thermal expansion. In addition, bauxite is another important raw material in both, which is used in the medium and fine grains. RB, on the other hand, does not contain bauxite, which is replaced here by fireclay. In addition, RB uses Perusite, an andalusite raw material that is significantly less pure. Furthermore, RB contains significantly more cement. The selected castables therefore give a good, representative picture of andalusite castables as they are customary on the market.

Table 9: Properties of the reference andalusite-based refractory castables.

	Cement/non-cement bonded	Installation method	Type of andalusite	Amount of andalusite (wt.-%)	Main side component	Special additives
RR	NCC Silica sol (<0.2 wt.-% CaO)	Casting/vibration	Perusite/Durandal D-59	36	Bauxite	-
RE	ULCC (~1 wt.-% CaO)	Casting w/o vibration	Durandal D-59	32	Bauxite	-
RB	LCC (~ 1.5 wt.-% CaO)	Self flowing	Perusite/Kerphalite	63	-	Dispersant (sodium tripolyphosphate)

Table 10: Chemical composition of the reference andalusite-based refractory castables.

	LOI	SiO ₂	Al ₂ O ₃	Na ₂ O + K ₂ O	CaO	MgO	Fe ₂ O ₃	TiO ₂	P ₂ O ₅	Mn ₂ O ₃
	wt.-%									
RR	0.59	21.32	74.47	0.22	0.30	0.09	1.00	1.47	0.01	0.01
RE	1.00	23.87	72.00	0.10	1.03	0.00	0.72	1.07	0.05	0.01

RB | 2.03 35.67 58.53 0.34 1.73 0.06 0.93 0.42 0.09 0.02

Table 11: Mineral content of each fraction of RR.

RR	> 2	1-2	0.5-1	0.5-0.25	0.25-.063	>0,063	Sum
				mm			g
Mass in g	42.6	11.1	6.1	3.9	10.8	25.5	100
Andalusite	63	56	6	2	1	3	34.4
Corundum	29	33	81	86	91	67	51.2
Quartz	4	3	1	0	0	9	3.1
Kyanite	0	3	1	1	2	17	2.9
Mullite	4	7	11	11	6	4	8.6

Table 12: Mineral content of each fraction of RE.

RE	>2	1-2	0.5-1	0.5-0.25	0.25-0.063	>0,063	Sum
	mm						g
Mass in g	27.6	7.2	7.8	7.5	18.6	31.3	100
Andalusite	84	34	6	1	15	50	44.6
Corundum	10	55	58	51	54	29	34.2
Quartz	2	1	5	6	5	8	4.9
Kyanite	1	0	11	28	20	6	8.8
Mullite	2	10	20	14	5	7	7.0

Table 13: Mineral content of each fraction of RB.

RB	>2	1-2	0.5-1	0.5-0.25	0.25-0.063	>0,063	Sum
	mm						g
Mass in g	27.6	11.4	12.6	5.6	10.6	32.2	100
Andalusite	67	92	87	82	73	60	71.6
Corundum	1	1	1	1	6	4	2.5
Quartz	6	6	6	5	7	6	6.1
Kyanite	0	0	2	0	4	0	0.7
Mullite	25	1	4	11	10	30	18.9

5.3 Thermal behaviour of the reference castables

In order to understand how andalusite-containing castables accomplish their outstanding properties in later use, the reference castables as described in chapter 5.2 were pretreated at temperatures up to 1650 °C and examined mineralogically. The heating rates and holding times were varied in order to examine the decomposition kinetics of andalusite and kyanite. The method of monotonic heating (MMH, chapter 4.4.8), refractoriness under load (RUL, chapter 4.4.9) wedge splitting test (WSP, chapter 4.4.10) and Resonance frequency damping analysis (RFDA, chapter 4.4.7) were used for the description of the thermal behaviour.

The reference castables were pre-treated at 1000, 1200, 1300, 1400, and 1500 °C, (1600 °C) and experienced dwell time of 0 h, 8 h, and 24 h. Dwell time and heating rate are connected to the testing method, with the highest heating rates of 250 K/h obtained by MMH. As it is the nature of this method, no dwell time is foreseen. To better understand the MMH curves, samples were additionally heated up to break-off temperatures according to the MMH heating curves in order to subsequently carry out a mineral phase analysis. The break-off temperatures were based on significant changes in thermal diffusivity. The examinations were carried out as an alternative to the LFA examinations in order to support the interpretation of the MMH results. Unfortunately, LFA did not lead to significant results worthy of interpretation and were not considered further. Aging tests were carried out with holding times of 8 and 24 hours.

In addition, the reference castables were examined with regard to their mechanical properties, open porosity and bulk density.

5.3.1 Thermal evolution of reference castables at a heating rate of 250 K/h with no dwell time

The first investigations were related to the method of monotonic heating where a heating rate of 250 K/h are mandatory for the procedure to record the apparent thermal diffusivity that is changing according to the temperature and the microstructural and mineralogical changes in the material tested. It is in the nature of the method that no holding times are provided. In order to better understand the change in apparent thermal diffusivity as a function of temperature, the tests were accompanied by microstructural investigations, X-ray phase analysis and the determination of refractoriness under load. For the microstructure investigations and the development of the mineral phases, the conditions in the MMH furnace were simulated in a conventional furnace and the firings were stopped at temperature levels at which significant peaks could be recognized in the course of the MMH curve.

5.3.1.1 Reference castable RR

Up to temperatures of about 1350 °C, RR showed only minor deviations in the MMH curve (a_{eff} vs. sample temperature) (Figure 15). This indicated that only minor phase changes occur in this temperature range, in agreement with the results of XRD (Figure 16). However, the results of RUL showed the maximum of thermal expansion already at 1000 °C, the temperature of pre-firing.

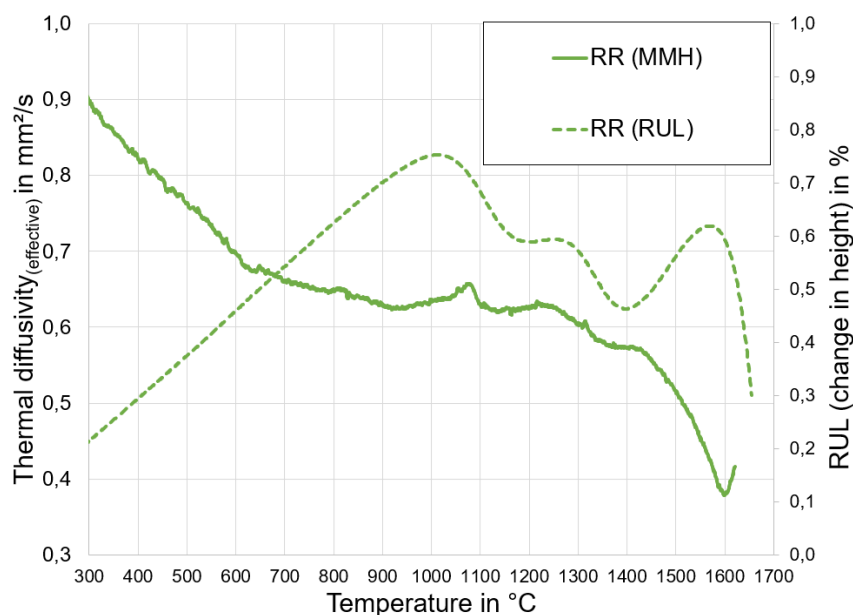


Figure 15 displays RUL (dashed line) and MMH of RR. RUL was performed on samples that were thermally pretreated at 1000 °C. This explains the linear elongation up to 1000 °C, after which an initial shrinkage becomes visible, which is caused by the onset of sintering of the matrix. It can also be seen that the test specimen slowly recovers from 1170 °C and reaches an intermediate peak at 1260 °C. This can be correlated to the decomposition of the kyanite associated with expansion. From around 1400 °C, the test body grows again, which can be explained by the expansion during the decomposition of the main proportion of andalusite. In principle, the MMH curve correlates with RUL, which is described in more detail in the text.

At 1000 °C cryptocrystalline phases and small spheres of the silica-sol still existed between the small, sub- μm particles of the matrix. The smallest grains started to vanish at 1100 °C, which can be observed in the micrographs (Figure 17).

A low intensive “peak” with a maximum at about 1130 °C (Figure 15) coincided with the first formation of mullite between 1100 and 1200 °C involving silica from the silica sol and reactive alumina in the matrix, as analysed by XRD (Figure 16). Fine particles already started to aggregate

due to some sintering, providing first ceramic bonding (Figure 17). Accompanied shrinkage in the matrix opened gaps between aggregated particles and larger grains.

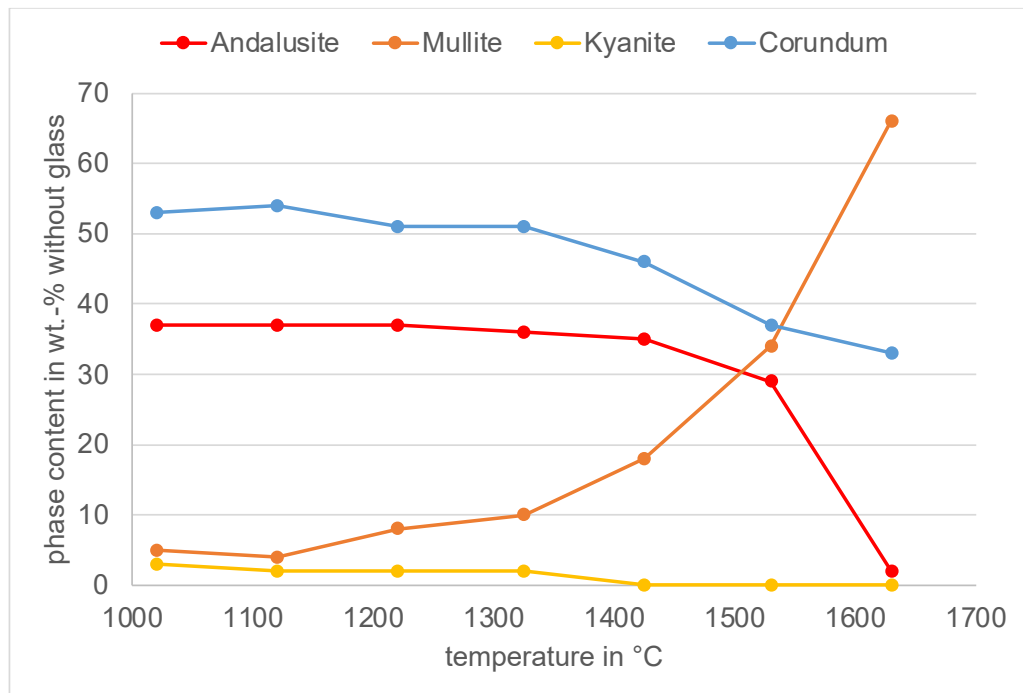


Figure 16: Rietveld analysis of phase content in reference castable, RR heated with 500 K/h. Firing without dwell time, simulating the MMH heating program. The results are given in wt.-% of the sum of 100 wt.-%, whereby the glass content was not considered.

At 1200 °C andalusite is stable. (RUL) at ~1260 °C also corresponds to a local maximum in the MMH-curve. This corresponds to intensive formation of mullite in the matrix (SEM/XRD after firing without dwell time). After firing to 1300 °C pure andalusite does not show a transformation. In contact with impurified melt phases the andalusite transformation has started, especially when the melt is rich in iron (as shown in Figure 9). Firing 100 °C higher leads to a transformation that slowly began in contact with the matrix (Figure 18) and ongoing where in contact with impurified melts. A slight increase of a_{eff} between 1350 °C and 1450 °C coincides with the beginning of intensive mullite formation in the matrix of the castable (Figure 17). The increase of a_{eff} could be due to heat of reaction (mullite formation) or by intensifying the thermal contacts of the components in the castable by the formation of ceramic (mullite) bonding. The major temperature interval of the andalusite transformation is between 1400 and 1500 °C, smaller grains are completely transformed. This clearly coincides with stabilization of RUL in this temperature interval. Extensive formation of mullite changed the microstructure of the matrix (Figure 17). The mullite crystals often enclosed small relict corundum grains. Solidified melt phase (darker grey) fills interstitial gaps between relict small corundum matrix grains and newly formed mullite. Pores became larger and more rounded, indicating an advanced degree of melting of the matrix. As expected, the kyanite already transforms at lower temperatures and is already transformed at 1300 °C at the edge. After reaching 1400 °C, the kyanite is already entirely transformed. At 1600 °C it is already absorbed into the matrix (Figure 19). The role of the kyanite is therefore to ensure sufficient expansion even at low temperatures in order to counteract sinter-related shrinkage cracks, so that infiltration of a process medium is avoided.

At higher temperatures, the MMH curve leads into a minimum at 1600 °C. This is the temperature interval in which andalusite transforms into mullite and silica, as proved from the results of XRD. The transformation was almost complete, some relicts in large (mm-sized) grains (Figure 18). The

results of XRD also show that silica from the andalusite transformation must be amorphous because cristobalite was not detected. Part of the amorphous silica derived from small andalusite in the matrix obviously formed mullite. Figure 17 shows at 1600 °C euhedral mullite crystals in a vitrified matrix.

As the transformation is an endothermic process, the heating rate inside the sample and thus a_{eff} decreases. When the andalusite transformation is complete, a_{eff} increases again at temperatures higher than 1600 °C. This also correlates with a third local maximum (RUL) at 1570 °C is due to highest rate of andalusite transformation in this temperature range (Figure 15 and Table 14). At higher temperatures, progressive weakening occurs.

RR thus already shows a significant transformation after aging between 1100 and 1200 °C, which is documented by the mineral phase analysis shown in Figure 16 by the formation of mullite, which is clearly visible in the microstructure here, crystallizing euhedral from a melt phase. Nevertheless, with a T_{05} of 1660 °C (Table 14), RR shows an extremely good refractoriness. However, this volume stability must be interpreted with a little caution, as the thermal behaviour cannot be correlated exclusively with the quantity of the melt phase that forms, as the thermal expansion, caused initially by the decomposition of the kyanite, followed by the mullitisation of the andalusite, counteracts shrinkage caused by melt formation. The apparent refractoriness under load is therefore based on the decomposition reaction of the Al_2SiO_5 polymorphs.

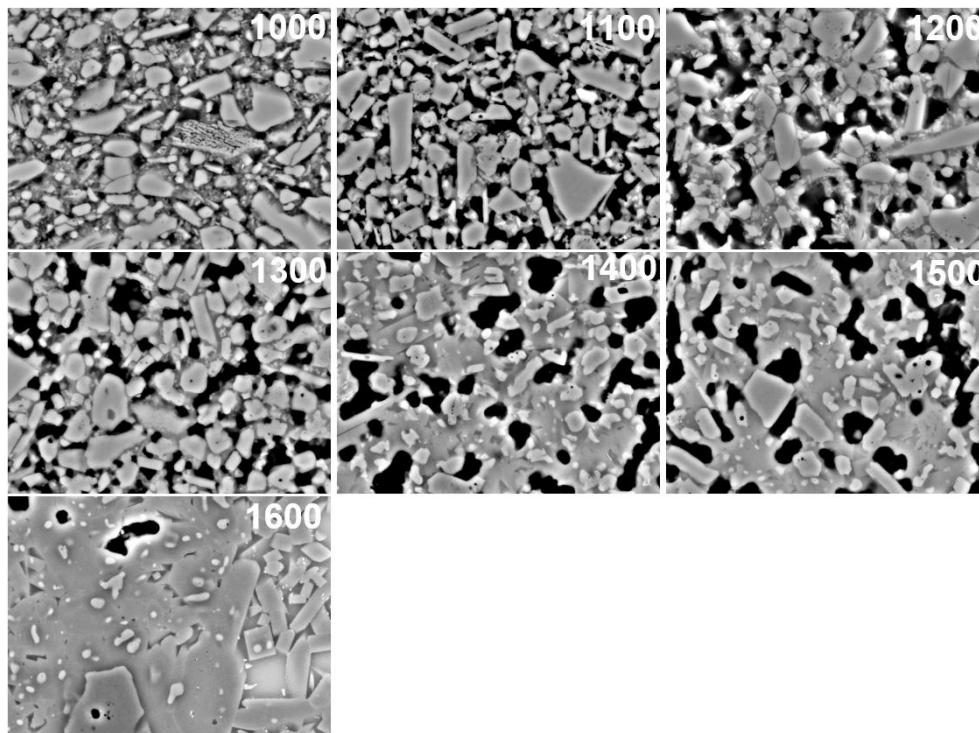


Figure 17: Evolution of the matrix of RR fired to 1200, 1300, 1400, 1500 and 1600 °C without dwell time (heating rate 500 K/h). As the temperature rises, the proportion of molten phase increases, which solidifies retrogradely to form glass and mullite. The latter is particularly visible after aging at 1600 °C. Here, euhedral mullite grains can be seen at the right edge of the image, indicating a high degree of melting.

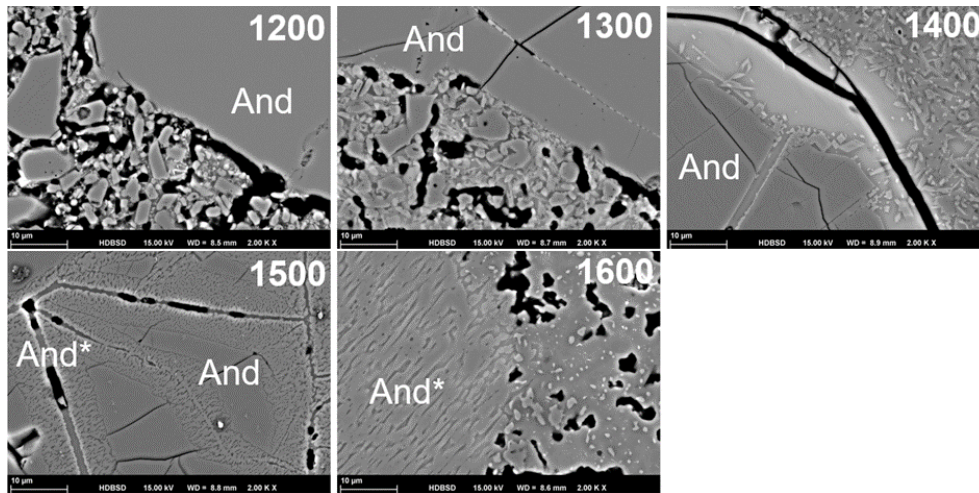


Figure 18: Transformation of Andalusite in RR fired to 1200, 1300, 1400, 1500 and 1600 °C without dwell time (heating rate 500 K/h). And = andalusite, And* = transformed andalusite. While aging at 1200 °C only leads to sintering of the highly reactive matrix caused by the silica gel, accompanied by the formation of shrinkage cracks, the andalusite coarse grain only shows the onset of transformation from 1300 °C, which is caused by the impurities in the raw material. The impurities already lead to larger melting in the matrix at 1400 °C, whereby euohedral mullite crystallizes out retrogradely and is clearly visible here at the contact with the coarse grain. The mullitisation of the andalusite is already well advanced after aging at 1500 °C, but not yet complete. The mullitisation progresses from the impurities in the andalusite into the coarse grain. After aging at 1600 °C, the andalusite is completely transformed.

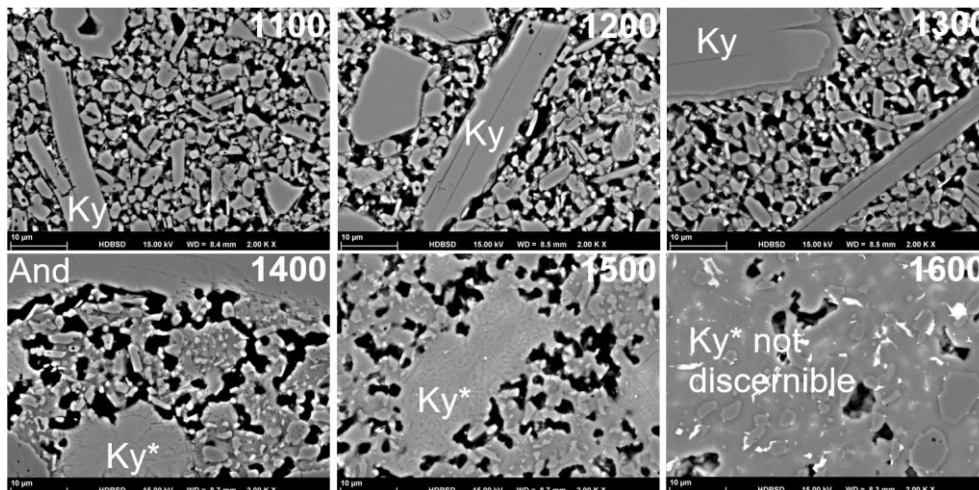


Figure 19: Prograde transformation of kyanite and the matrix of RR (heating rate 500 K/h). All images taken with backscattered electron detector, 2000x. And = andalusite, Ky = kyanite, Ky* = transformed kyanite. In contrast to andalusite, kyanite already shows a significant transformation after aging at 1300 °C, which progresses from the grain surface into the crystal. The kyanite is already completely decomposed after aging at 1400 °C.

5.3.1.2 Reference castable RE

In the reference castable RE, the first reaction observed by MMH took place between 1000 °C and 1100 °C (Figure 20). However, XRD gives no indication to any phase transformation in this temperature interval, while structural analysis (Figure 22 and Figure 23) shows beginning development of the ceramic bonding. The first local maximum (RUL) at 1000 °C coincides with a first increase in the MMH-curve, both effects indicating the beginning of sintering. Local maxima at about 1200 °C (RUL and MMH) coincide with formation of mullite in the matrix (Figure 21).

The finest particles in the matrix were extinct in this temperature interval between 1100 °C and 1300 °C and ceramic “bridges” among the other components became stronger. An increase of the pore sizes is caused by the consumption of the finest particles (Figure 22).

At 1200 °C, no andalusite transformation of the coarse grain can be recognized in the micrographs (Figure 23). Also, at 1300 °C, andalusite transformation of the coarse grain is not evident, while the transformation of kyanite is clearly in progress. At 1400 °C andalusite transformation can be recognized starting at the contact to the matrix.

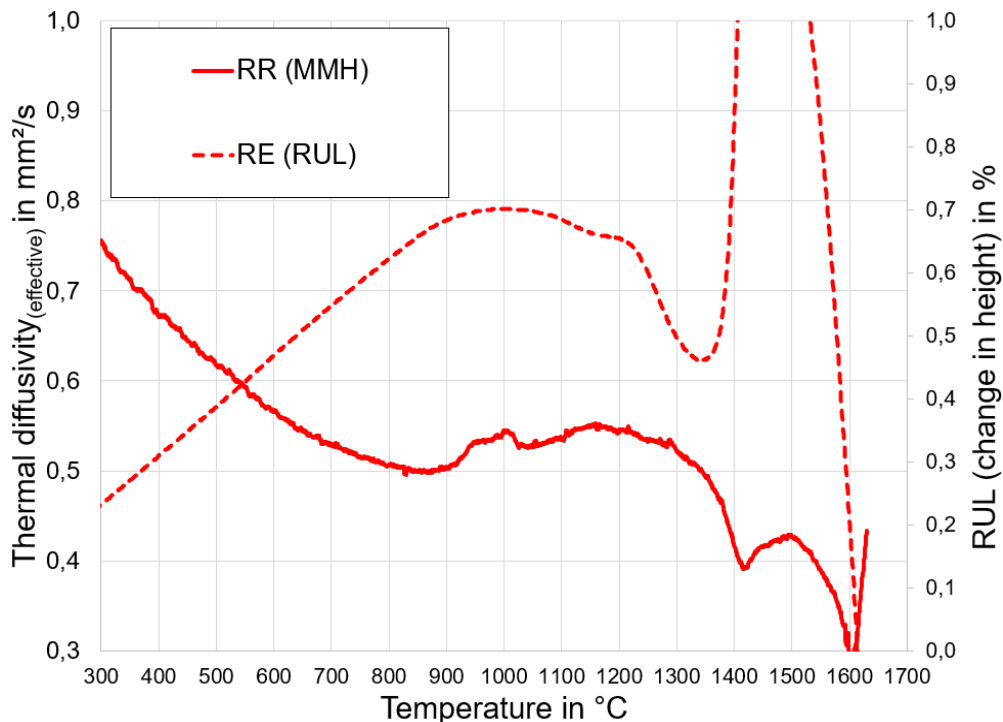


Figure 20: RUL and MMH of RE. Compared to RR, RE expands more significantly between 1400 and 1500 °C, which implies a faster decomposition of andalusite and the higher concentration of kyanite. The second maximum, which is clearly recognizable in the case of RR, is slightly lost in the case of RE, as the first maximum is less pronounced here.

Thermal expansion of the sample (RUL, Figure 20) is also in agreement and shows that the transformation due to kyanite transformation is very intensive at temperatures between 1370 and 1420 °C. From the series of photomicrographs can be derived that the transformation of kyanite significantly starts at 1300 °C and is (nearly) completed already at 1400 °C (Figure 24). From the test-pieces fired at 1400 °C on, the changes in the matrix become extensive. The formation of melt and mullite, involving the silica sol binder and corundum, is accompanied intensive local densification and the formation of a pore-network (Figure 22). At 1500 °C, the fines of the matrix are completely transformed to mullite and some solidified melt phase. Only corundum particles larger than about 1 µm survived the short time heating to 1500 °C. After 1600 °C, the matrix is completely recrystallized. Transformed kyanite grains cannot be discerned any more. Growth of mullite crystals continued. Smaller corundum grains are consumed, and larger grains show corroded rims. Pores smaller than a few µm have almost completely disappeared during the segregation of clusters consisting of mullite, melt phase and remnants of corundum matrix components.

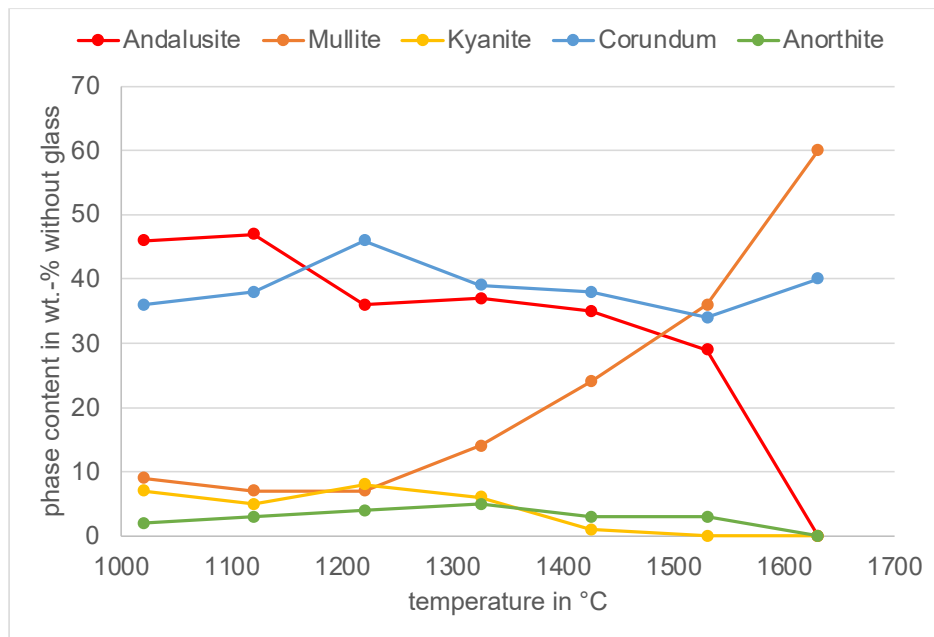


Figure 21: Rietveld analysis of phase content in reference castable heated with 500 K/h, RE. The results were calculated without considering the glass content, which increases considerably with temperature. Firing without dwell time. Already between 1100 and 1200 °C the andalusite content decreases significantly, which is due to the higher proportion of fine-grained andalusite compared to RR. Furthermore, anorthite forms in RE, which reduces the gain in mullite compared to RR, as the formation of anorthite is favoured in the presence of calcium derived from the cement phase. However, it must be considered that anorthite only crystallizes retrogradely from a liquid state.

Beside the early decomposition of fine graded Andalusite between 1100 and 1200 °C, the transformation of andalusite occurs at higher temperatures as observed for kyanite. However, andalusite in RE comprises much higher grain sizes up to 6 mm. SEM shows that large grains of andalusite need more time at higher temperatures to transform completely.

The following pronounced maximum (RUL) at 1420 °C is obviously based on the decomposition of andalusite. At the same temperature, MMH shows a prominent minimum. The thermal decomposition of kyanite obviously cause the MMH-curve to decrease, like the thermal decomposition of andalusite, that causes to decrease the effective thermal diffusivity at temperatures between 1500 and 1600 °C. In RUL, the andalusite decomposition obviously is overlain by the kyanite decomposition. At temperatures between 1500 °C and 1600 °C, the transformation of andalusite causes declining values of a_{eff} , similar as described for RR.

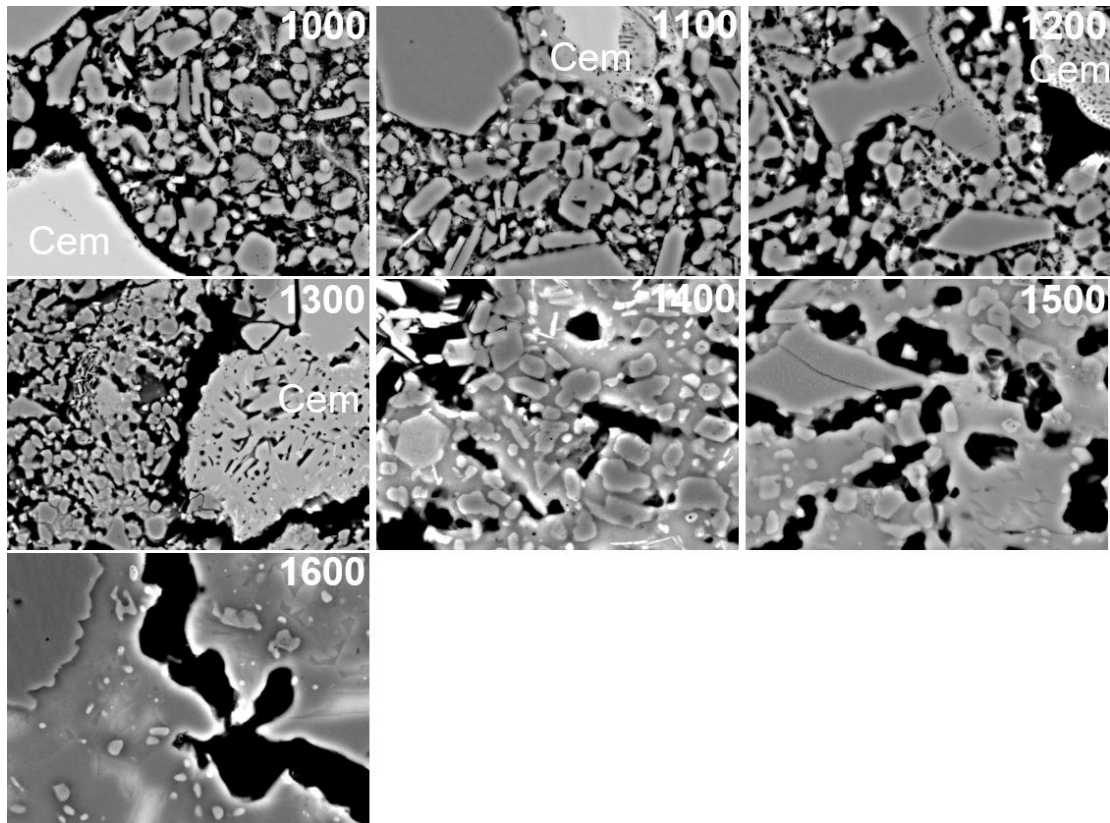


Figure 22: Evolution of the matrix of RE fired to 1200, 1300, 1400, 1500 and 1600 °C without dwell time (heating rate 500 K/h). An initial, sinter-related shrinkage of the matrix can already be seen at 1000 °C, causing cracks to form around the coarse grains. At 1400 °C, a large proportion of the matrix has already melted. Here, corundum is a stable phase, which is made clear by the euhedral grain shapes. This also correlates well with the increase in corundum concentration up to 1200 °C, which could be verified by X-ray diffractometry. The corundum is dissolved at higher temperatures so that at 1600 °C there is mainly melt in which retrograde euhedral mullite is precipitated.

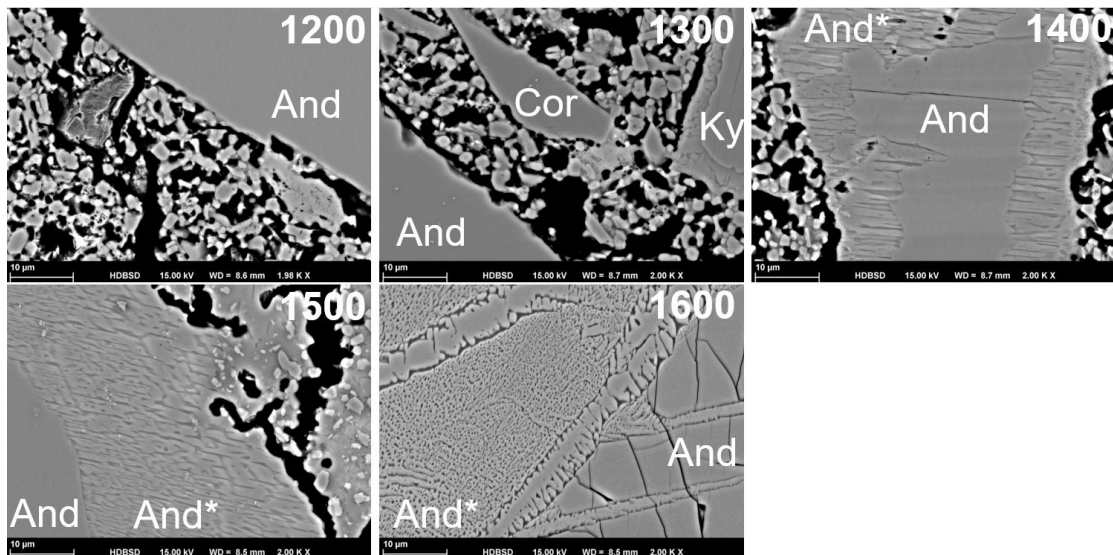


Figure 23: Transformation of Andalusite in RE fired to 1200, 1300, 1400, 1500 and 1600 °C without dwell time (heating rate 500 K/h). And = andalusite, And* = transformed andalusite. Although the same andalusite raw material was used in the RE, it decomposes more rapidly and already shows clear decomposition affecting the grain surface after aging at 1400 °C. Kyanite already begins to decompose significantly at 1300 °C. However, andalusite is still retained in RE even at 1600 °C, which is not the case in RR.

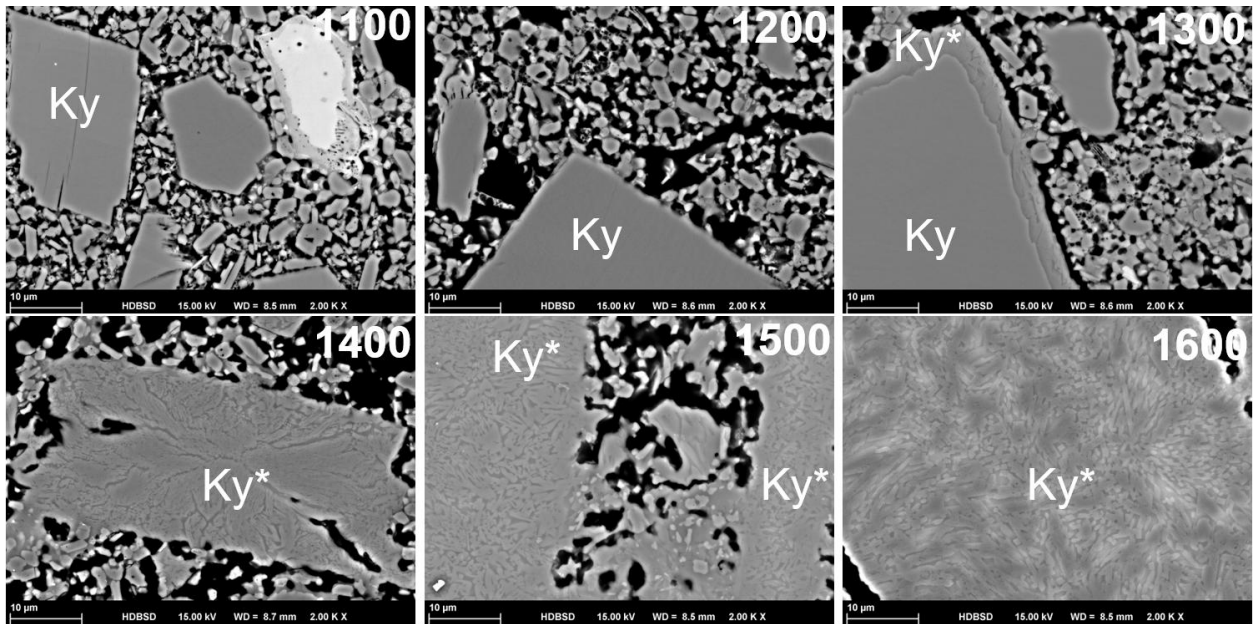


Figure 24: BSE-images showing the prograde transformation of kyanite and the matrix of RE (heating rate 500 K/h). All images scanned at 2000x. After aging at 1400 °C, kyanite is completely decomposed.

5.3.1.3 Reference castable RB

As observed for the castable RB, a first increase in the MMH curve occurs already at about 900 °C. The corresponding curve progression of RUL deviates from the linear expansion and starts to flatten, leading into the first maximum at about 1020 °C (Figure 25). The formation of mullite stabilizes RUL as well as the MMH-curve up to temperatures of 1200 and 1260 °C, respectively. The downward step in the MMH-curve at 1260 °C indicates rapid melt formation, obviously leading to the observed low strength (RUL) at higher temperatures. With lesser intensity than in RE, the MMH-curve of RB shows a minimum at about 1420 °C. Here, the effect of andalusite decomposition has less influence on the progression MMH-curve. Obviously, the effect is concealed by the influence of intensive melt formation on the effective thermal diffusivity.

No break-off sintering was carried out with material RB, as the manufacturer, Belref, discontinued production of this castable due to a shortage of raw materials and was therefore unable to provide samples.

5.3.2 Comparison of RUL

Figure 26 shows the results of RUL obtained for the three andalusite castables. With increasing temperatures, all experience nearly linear thermal expansion until the temperature of thermal pre-treatment (= 1000 °C) is reached. At higher temperatures, the local maximum at 1000 °C is followed by some compression due to sintering of the test specimen. This is attenuated around 1200 °C due to mullite formation in the matrix. At higher temperatures, sintering increases again until the thermal decomposition of andalusite decreases the rate of sintering (RB), leads to a local maximum at 1560 °C (RR). In RE, the thermal decomposition of kyanite superimposes the effect of expansion due to andalusite transformation and results in a pronounced maximum of expansion at ~1440 °C. At the highest temperatures, the RR is most stable, followed by RE and RB.

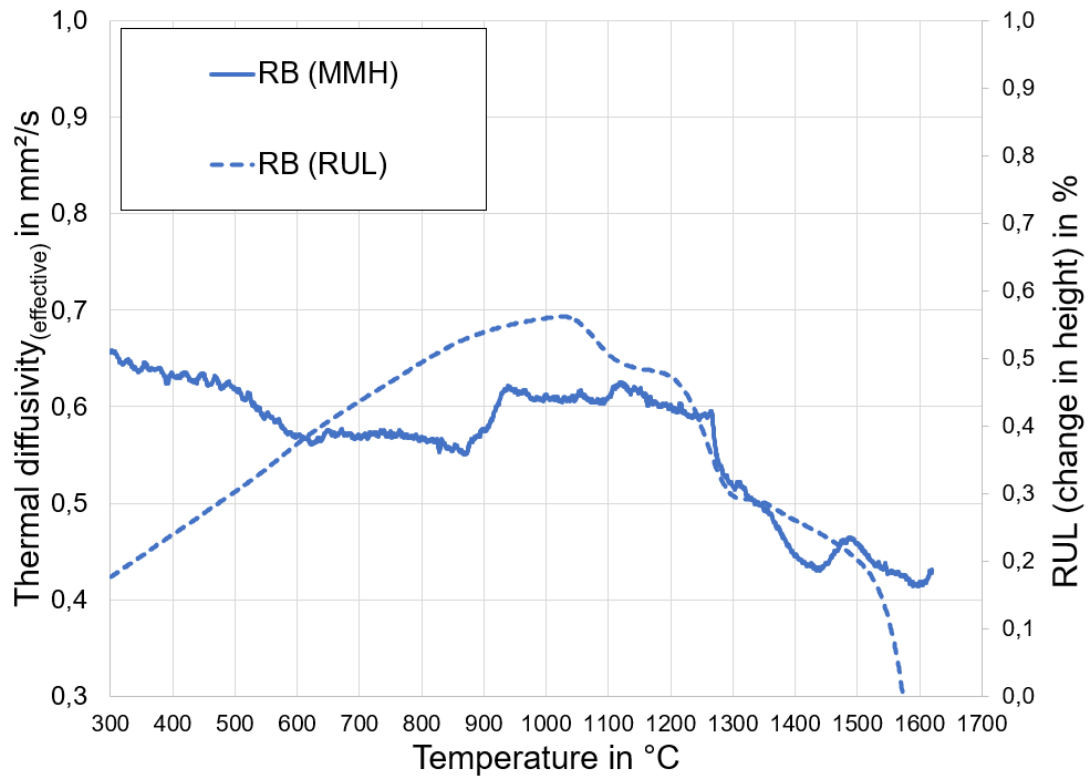


Figure 25: RUL and MMH of RB. Unlike RR and RE, RB does not stabilize at higher temperatures.

Table 14: Results of RUL of all reference castables.

Castable	T D _{max}	T ₀₅	°C		
			T ₁	T ₂	T ₅
RR	1013	1660	>1700	>1700	>1700
RE	1437	1545	1585	1645	>1700
RB	1025	1560	1615	1650	>1665

5.3.3 Effect of firing temperature and holding time on the andalusite based castables

5.3.3.1 Mineral composition and microstructure after firing for 8 h at temperatures between 1000 and 1500 °C

To understand the mineralogical and chemical changes, under the influence of time and temperature, cylindrical shaped samples (Diameter = 46 mm, height = 100 mm) were preheated at 1000, 1200, 1300, 1400, and 1500 °C for 8 h in air. The heating rate was 2 K per minute. After the heating process, the samples were cut into slices for polished sections and milled for XRD powder diffraction.

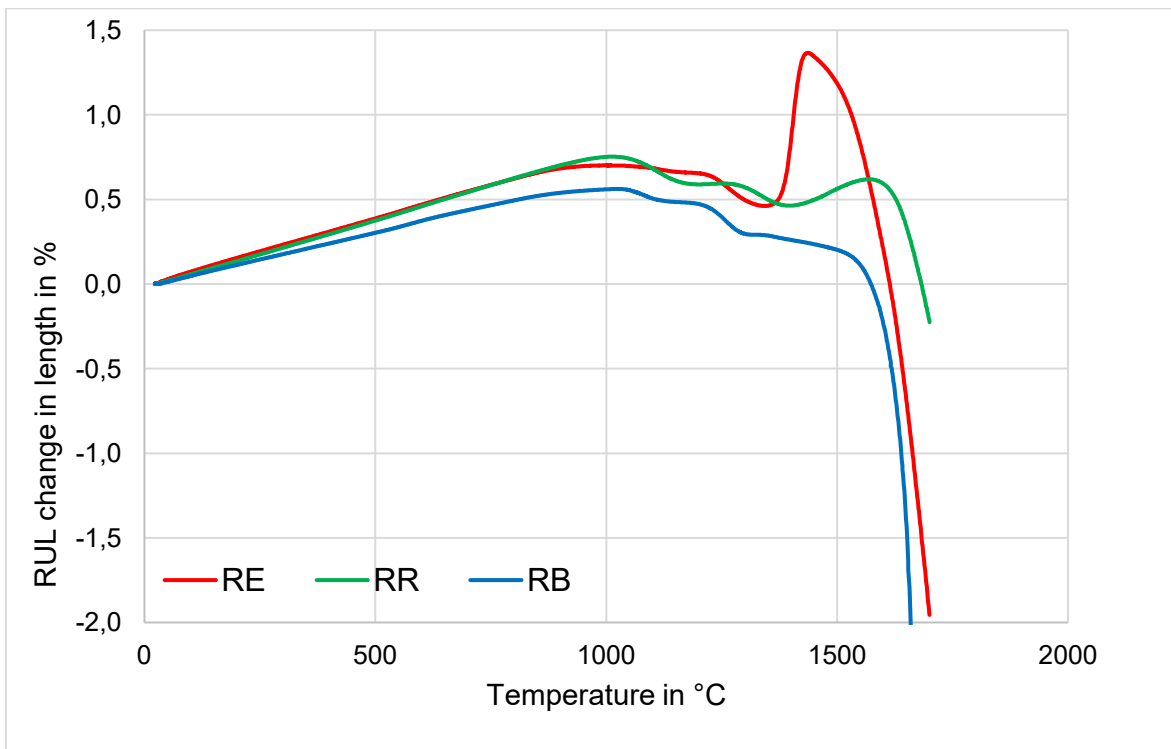


Figure 26: RUL of the reference castables.

Figure 27 envisages the phase evolution of castable RR that were thermally treated at 1000, 1200, 1300, 1400 and 1500 °C for 8 h in air. It should be noted that the phase analysis is calculated without glassy phase by means of Rietveld analysis. Predominantly corundum, andalusite and mullite were determined and minor amounts of quartz and kyanite were present at room temperature (see. Table 11). Quartz must be regarded as impurity that is syngenetic with the andalusite formation and kyanite is a minor component of the castables composition. The mullite starts to increase significantly at a temperature between 1200 and 1300 °C and consumes corundum. The degradation of corundum can certainly be explained by the presence of SiO₂ from the silica sol, whereby sufficient SiO₂ is available in the matrix to destabilize corundum. The decrease of andalusite is due to its awaited decomposition, the increase of mullite is higher than it could be explained by the corundum dissolution. The decomposition of kyanite also yields mullite and begins below 1200 °C, but hardly contributes to the formation of mullite due to the small amount. The cristobalite that is also formed during the decomposition of kyanite is not detectable, which is due to the expected low quantity.

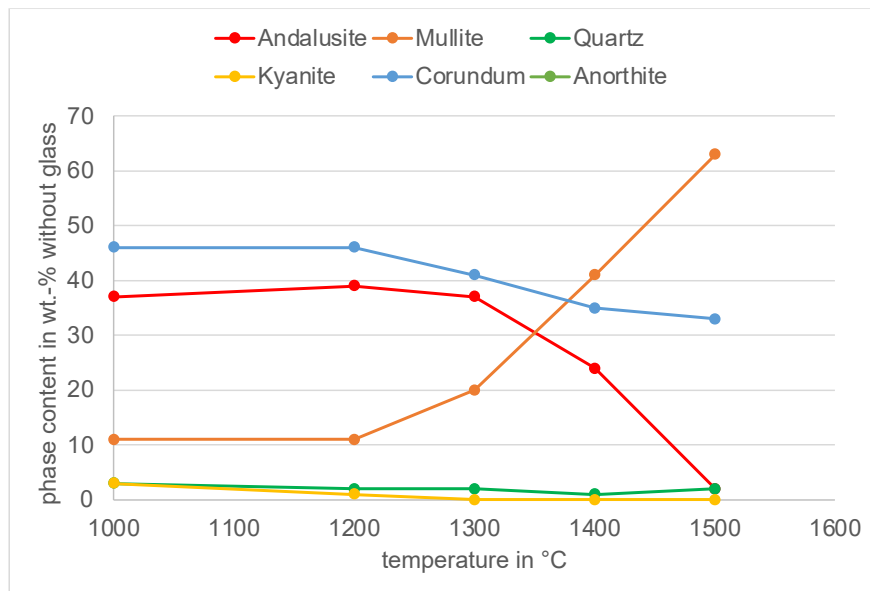


Figure 27: Rietveld analysis of phase content in reference castable, RR. The results were calculated without considering the glass content, which increases considerably with temperature. The diagram shows the results for RR castable treated for 8 hours at 1000, 1200, 1300, 1400 and 1500 °C. Between 1200 and 1300 °C the concentration of corundum decreases in favour of the mullite formation due to the presence of SiO₂ in the matrix (silica gel). In this temperature range andalusite begins to decompose noticeably to mullite.

Figure 28 envisages the phase evolution of castable RE that were thermally denoted for RR in the last paragraph. Again, it should be noted that the phase analysis is calculated without glassy phase by means of Rietveld analysis. Predominantly corundum, andalusite and mullite are determined and minor amounts of quartz and kyanite are present at room temperature (see. *Figure 12*).

Figure 28 depicts for RE a lower concentration for corundum which can easily be explained by the fact that RR, with around 51 wt.-% corundum, shows approx. 17 wt.-% more corundum in the XRD analysis, which in turn indicates the higher proportion of bauxite in RR. On the other hand, RR contains only 34 wt.-% andalusite instead of 44 (RE). However, both castables behave very similar in the thermal phase development. The decomposition of the andalusite starts between 1200 and 1300 °C, which is primarily documented in the increase in the proportion of mullite. After aging at 1500 °C, RE with 6 wt.-% andalusite still contains around 4 wt.-% more residual andalusite. Of greater significance in the comparison of the two reference castables, however, is the formation of anorthite in RE, which already appears between 1000 and 1200 °C at around 5 wt.-%. Anorthite is preferentially formed from the cement in the presence of the CA phase and should already lead to significant melting of the matrix at 1200 °C, which can ultimately be easily verified by microanalysis. Figure 35 shows this impressive. Primarily euhedral mullite can be seen, which has crystallized out of an anorthite-rich melt, presumably retrogradely.

Figure 29, left micrograph, shows the typical microstructure of RR castable with large andalusite grains, which are typically monocrystalline or twinned. The smooth surface indicates that these large grains have not yet undergone any transformation at 1000 °C. Brightly reflecting inclusions can be seen in the grains that are rich in iron and titanium, which can already be attributed to the decomposed biotite. Bauxite is significantly finer-grained and can be attributed to a medium grain fraction. Bauxite can be easily recognized by the dispersed fine-grained tialite. The picture on the right shows the matrix of the same castable. At 1000 °C, this matrix does not yet show any sintering, which is clearly recognizable by the sharp contours of the fine grains. With a little effort, the silica gel-based binder phase can still be seen between these grains. At a pre-treatment temperature of 1000 °C, the original microstructure has hardly changed.

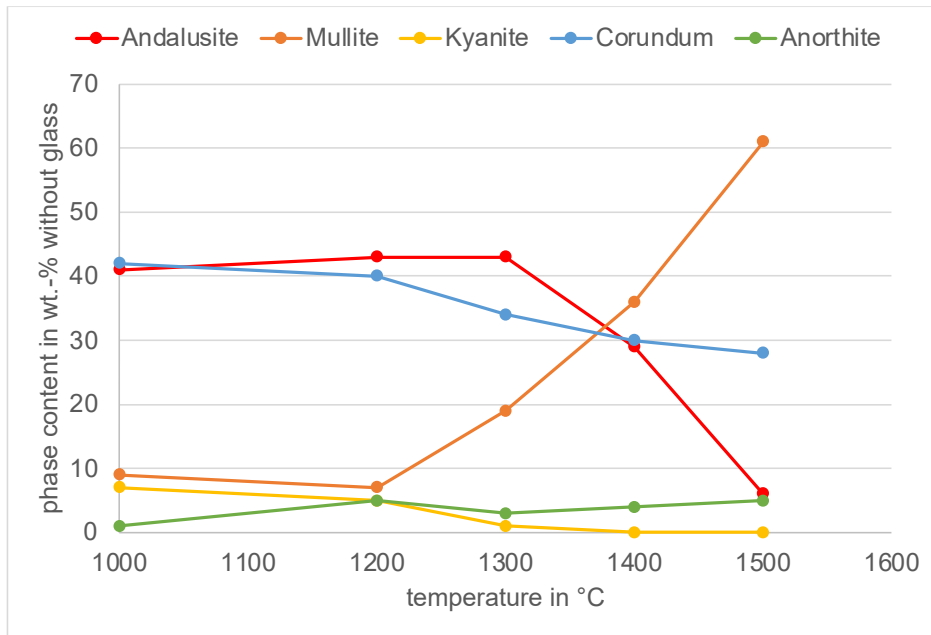


Figure 28: Rietveld analysis of phase content in reference castable, RE. The results were calculated without considering the glass content, which increases considerably with temperature. The diagram shows the results for RE castable treated for 8 hours at 1000, 1200, 1300, 1400 and 1500 °C.

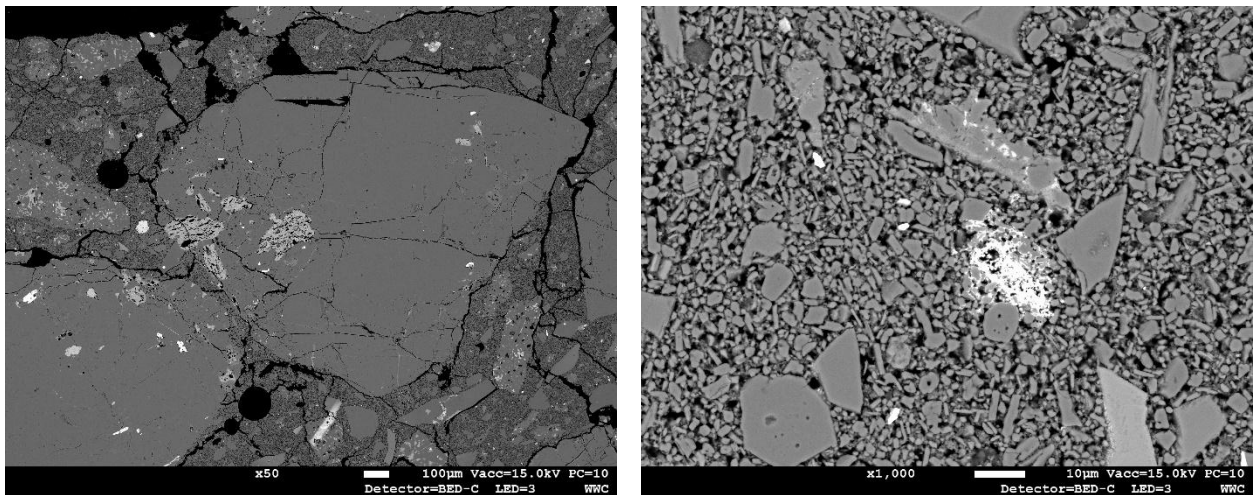


Figure 29: BSE micrographs of the RR castable, which was thermally pre-treated for 8 hours at 1000 °C. The image on the left shows an overview of the microstructure at a magnification of 50x and is dominated by two large andalusite grains that do not yet show any signs of decomposition. Inclusions with a bright contrast can be seen in the grains, which can be identified as decomposition products of the biotite. The bright contrast is due to the presence of iron. Biotite decomposes to hematite and sodium feldspar. The microstructure is interspersed with cracks, which are presumably caused by preparation and indicate the low strength typical of gel-bonded castables. The image on the right shows the microstructure of the matrix at a magnification of 1000x. The fine grains are splintery and show no sintering.

While thermal pre-treatment at 1000 °C resulted in hardly any effect on the microstructure, the microstructure showed significant thermal effects when the refractory material was pre-treated at 1300 °C for 8 hours. At this temperature, the added kyanite decomposed first, like andalusite, into mullite. Instead of a SiO₂-rich melt, cristobalite is formed, which is not detectable in detail as the decomposition products are closely intergrown. Figure 30 shows a micrograph of the RR castable. At the bottom centre (red circle) an approximately 3 mm large kyanite crystal can be seen, which has been almost completely transformed into mullite and cristobalite. Between the fine matrix grains, the formation of a bonding phase consisting of a SiO₂-rich glass is conspicuous. The locally high SiO₂ content also means that corundum is no longer a stable phase. At the bottom right

of the image, corundum crystals with a conspicuously sutured boundary can be seen, which indicates a decomposition reaction.

When the RR castable is thermally pre-treated for 8 hours at 1500 °C, massive decomposition of the andalusite sets in, as Figure 31 shows. In the micrograph on the left, which was taken at a magnification of 500x, you can see an andalusite grain filling the entire micrograph which only shows relict andalusite (smooth appearing, grey surfaces). Clearly textured areas exist that could be addressed as crystallized mullite grains that are topotactically oriented in the former andalusite lattice, which are surrounded by a SiO₂-rich melt. The image on the right illustrates this decomposition again at a magnification of 1500x. Areas with a bright contrast contain impurities typical of andalusite, which have already been completely melted. In general, it can always be observed that the decomposition of andalusite starts from the surface of the grains or begins at the impurities. It can therefore be assumed that the presence of a melt (impurities) favours the decomposition of the andalusite kinetically. Moreover, the melt dissolves the freshly formed mullite, so that it can be assumed that the former andalusite grain is already at an advanced stage of melting.

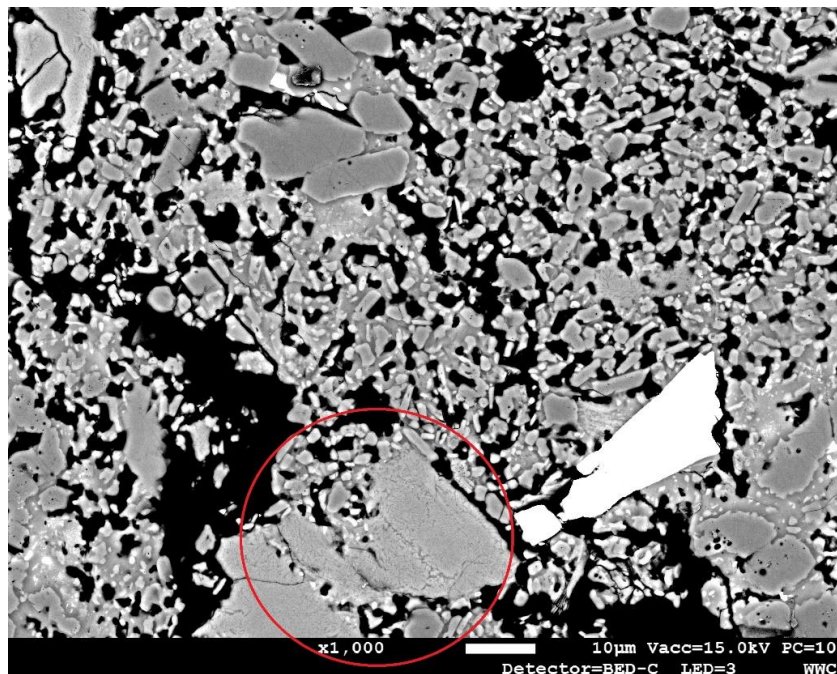


Figure 30: BSE image of castable RR treated at 1300°C for 8 h at a magnification of 1.000x: The micrograph envisages the matrix of RR. The grain marked with the red circle is a former kyanite grain identifiable by its rough surface. Between the fine matrix grains, the formation of a bonding phase consisting of a SiO₂-rich glass is conspicuous. The locally high SiO₂ content also means that corundum is no longer a stable phase. At the bottom right of the image, corundum crystals with a conspicuously sutured boundary can be seen, which indicates a decomposition reaction.

The presence of cement, as in the case of RE, leads to a massive melting of the matrix, which can be seen particularly well in Figure 35. Here euhedral mullite is present in a highly contrasted matrix, which is Ca-rich and chemically like anorthite. It must always be considered in this type of image that, on the one hand, the melt is vitrified and crystallizes retrogradely. The euhedral mullite that appears supports the assumption that it has crystallized from a melt.

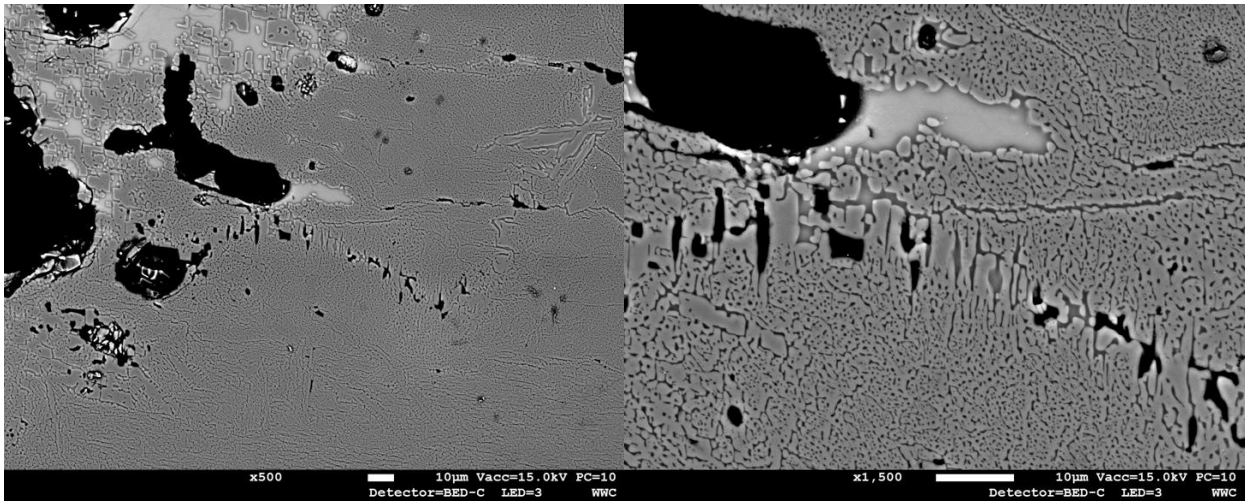


Figure 31: BSE image of castable RR treated at 1500°C for 8 h at a magnification of 500x (left) and 1500x (right): The micrographs envisage the coarse grains of former andalusite of RR. At given pre-treatment andalusite is entirely decomposed to mullite and SiO₂. Areas with a higher contrast contain iron and other typical impurities, which melt at temperatures of around 1100 °C and accelerate the reaction of andalusite to mullite.

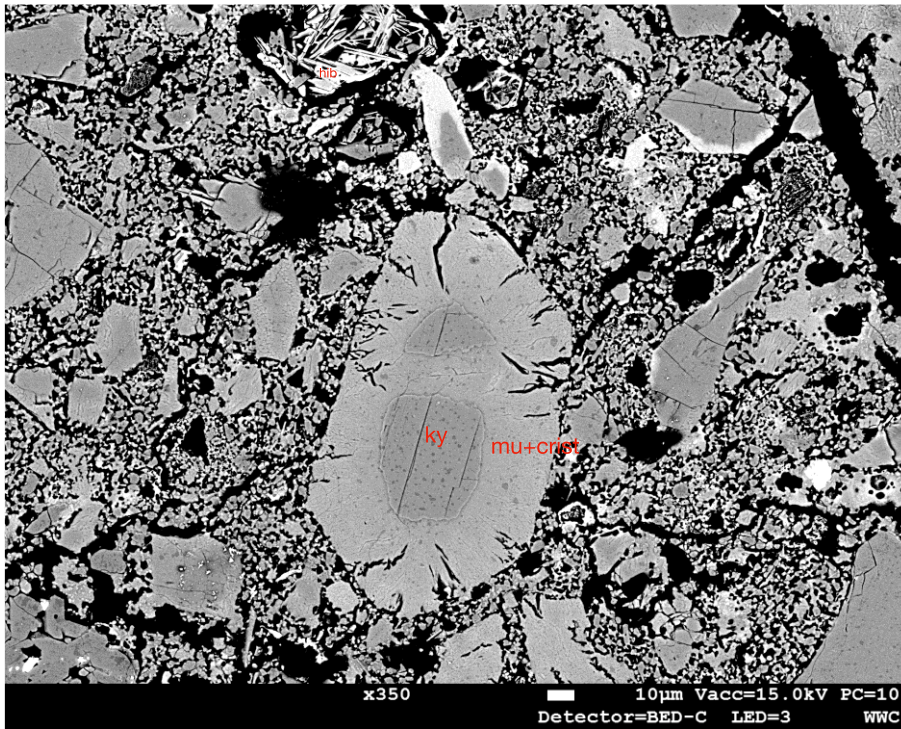


Figure 32: BSE image of castable RE treated at 1300°C for 8h at a magnification of 350x: The micrograph envisages a kyanite grain that shows a decomposed rim. The formation of mullite and cristobalite leads to significant expansion, which is clearly recognizable by the radially arranged cracks. A relict cement grain that has been completely hibanitized is visible at the upper edge of the image. The tabular habit of the hibanite grains and the bright contrast are typical features here.

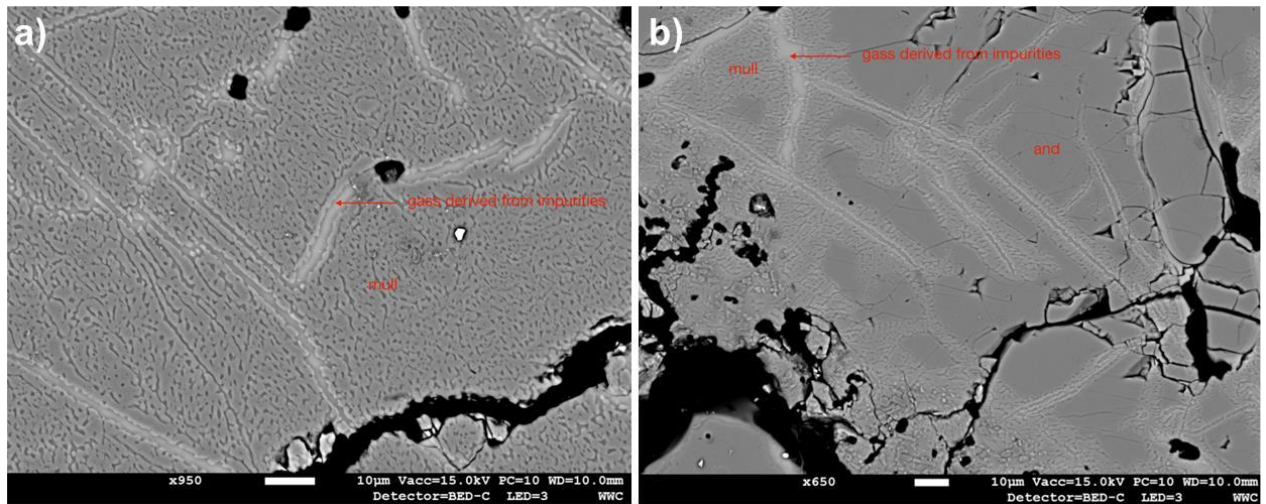


Figure 33: BSE image of castable RE treated at 1300 °C (right) and 1500 °C (left) for 8h: The pictures show the development of the decomposition reaction of andalusite which takes place between the temperature levels of 1300 and 1500 °C. While significant amounts of andalusite are still visible at 1300 °C, the transformation is complete at 1500 °C. Again, it is remarkable that the decomposition reaction starts from the impurities of the andalusite, which are already molten at the temperatures selected here. The reaction is kinetically favored by the presence of a melt. The forming crystal nuclei of the mullite subsequently promote complete mullitization. It should be noted that the image on the left was taken at a magnification of 650x and the one on the right at 950x. The apparent grain coarsening of the mullite is therefore an artefact of the magnification.

Figure 32 shows a kyanite coarse grain, which is converted to mullite from the surface after 8 h of aging at 1300 °C. Radial cracks can be seen starting from this grain, indicating the significant increase in volume of the kyanite during the transformation. However, this is also an indication that the matrix still exhibits brittle behaviour at 1300 °C. It is remarkable, however, that kyanite is still present in the core, even though the grain has been exposed to 1300 °C for 8 hours.

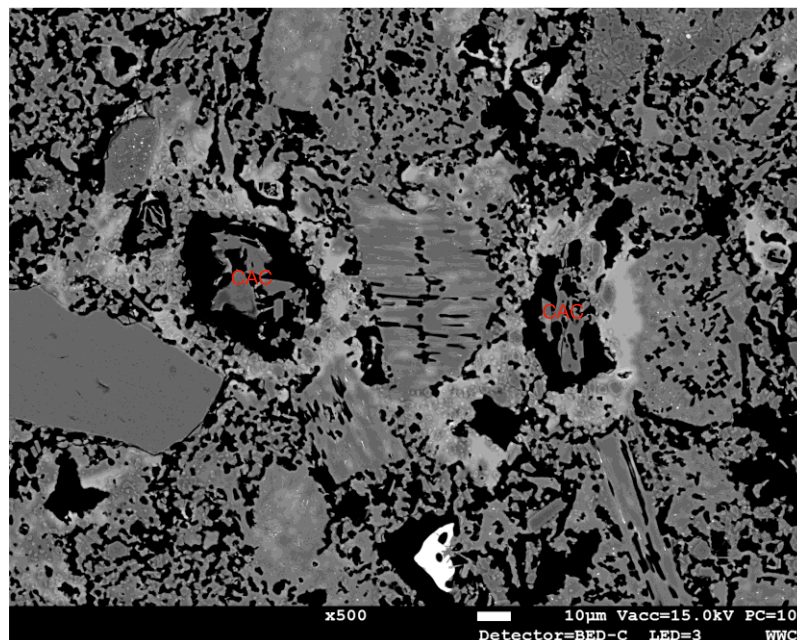


Figure 34: BSE image of castable RE treated at 1500°C for 8h: The micrograph shows a section of the matrix of the RE castable at a magnification of 500x. Two CAC grains can be seen prominently in the center, which contain relictic cement phase that has been partially converted to hibonite. The grains are surrounded by a bright-colored rim, which is Ca-rich and shows an anorthitic composition on closer inspection.

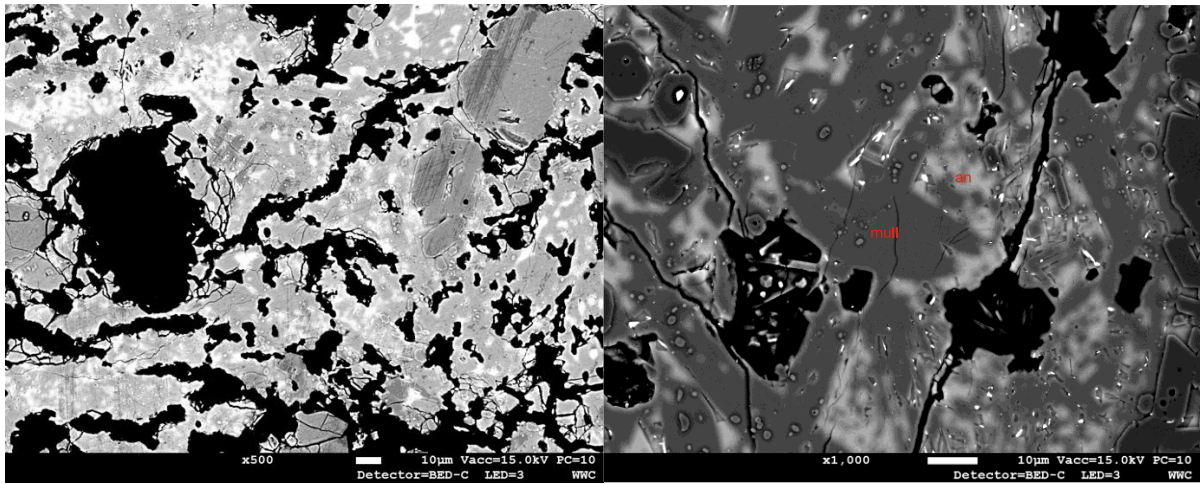


Figure 35: BSE images of castable RE treated at 1500 °C for 8 h: The micrograph shows the appearance of the matrix magnifications of 500 and 1000x. In this part of the matrix an almost entire dissolution of the Matrix is visible that leads to a high degree of melt formation. Large euhedral mullite grains are formed most probable during cooling. The matrix with the bright contrast has an anorthitic composition.

If one also compares the microstructures of the reference castable RB, it becomes clear that the use of less pure andalusite raw materials, perusite, leads to faster melt formation, which is already comprehensible from 1000 °C upwards. In addition, RB does not contain bauxite but fireclay as a further component and also contains significantly more cement. Overall, this significantly reduces the refractoriness, which is already clear from the RUL results (Figure 26). Basically, RB loses its volume stability after reaching 1050 °C. Figure 37 shows impressively that after ageing at 1500 °C, the matrix is almost completely melted.

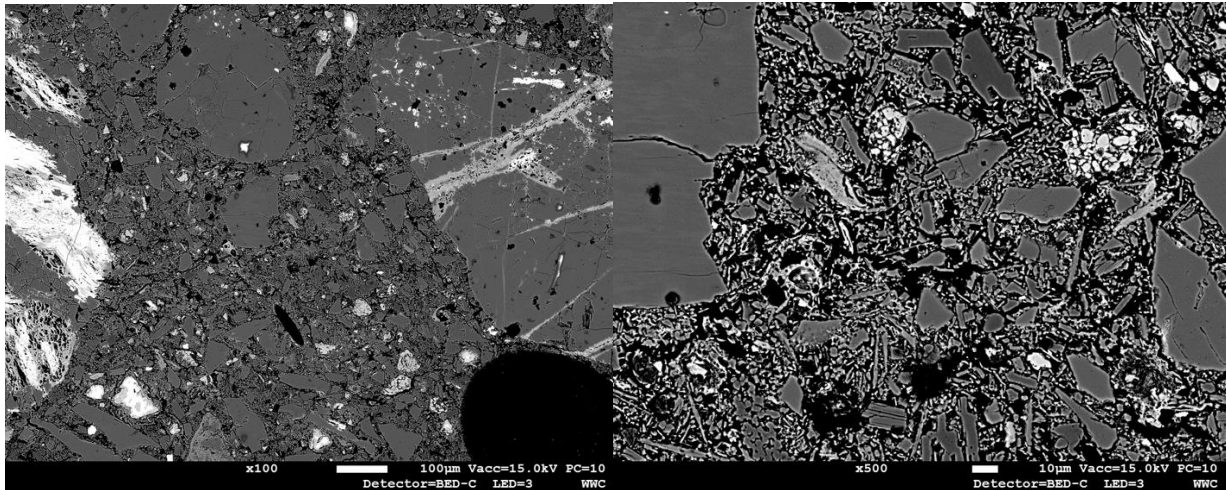


Figure 36: BSE images of castable RB treated at 1000 °C for 8 h: The micrograph shows the appearance of the matrix magnifications of 100 and 500x. Bigger andalusite grains depict their higher content of impurities compared to RR and RE that could be easily identified by the high contrast that is typical for higher atomic order number of iron. Higher contrasting smaller grains in the matrix indicate that cement has not reacted entirely during the setting of the castable.

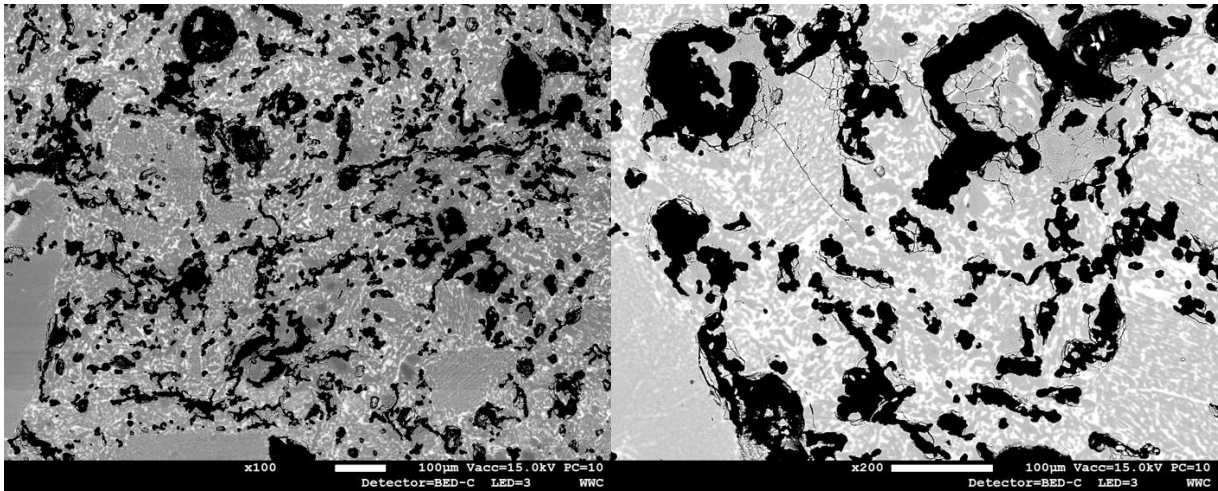


Figure 37: BSE images of castable RB treated at 1500 °C for 8 h: The micrograph shows the appearance of the matrix magnifications of 100 and 200x. The matrix shows a very high degree of melting, which is also evidenced by the formation of large spherical pores. Higher contrasting areas are of anorthitic nature, in which euhedral mullite is crystallized.

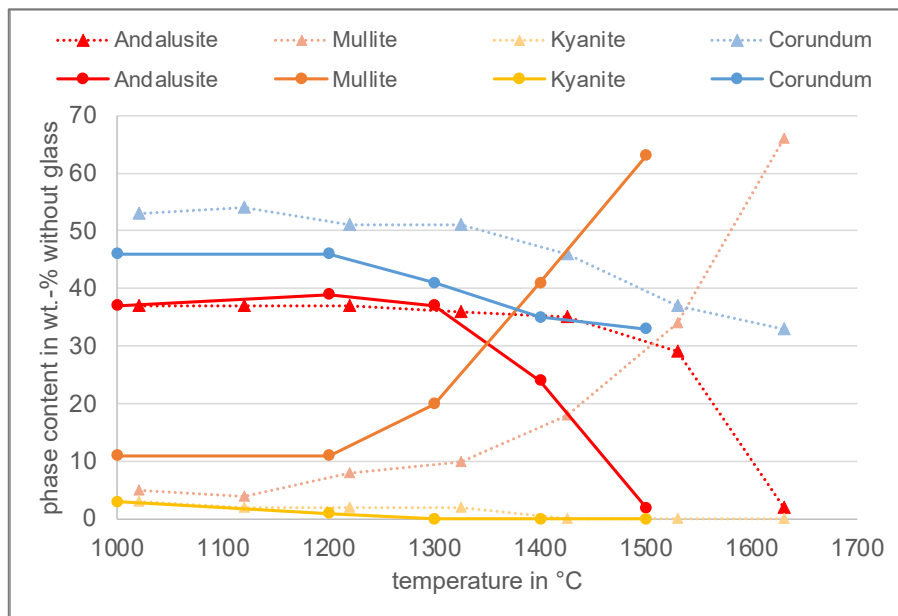


Figure 38: Rietveld analysis of phase content in reference castable, RR. The results were calculated without considering the glass content, which increases considerably with temperature. The diagram combines the results already presented in Figure 16 (firing without dwell time, dashed lines) and Figure 27 treated for 8 hours at 1000, 1200, 1300, 1400 and 1500 °C (solid lines).

5.3.3.2 Effect of holding time on the phase evolution in the reference castables

If the temperature-dependent mineral phase composition is now investigated as a function of time, it becomes clear that the introduction of a holding time of 8 hours leads to a higher mullite yield even at lower temperatures compared to pre-treatment with no holding time with a high heating rate of 500 K/h. This becomes particularly clear between 1200 and 1300 °C. At 1300 °C, an approximately 10 percentage points higher yield of mullite in the RR can be seen when the holding time is increased from 0 to 8 hours (Figure 38). However, it should be noted that RR and RE differ

systematically due to the cement content in RE. Primarily prograde anorthite is formed in the matrix instead of mullite. Between 1200 and 1300 °C, this leads to a smaller increase in the proportion of mullite by only 6 percentage points in the case of RE, however, it must be kept in mind, that RE contains significant higher amounts of melt that are now in a vitrified state at room temperature (Figure 39).

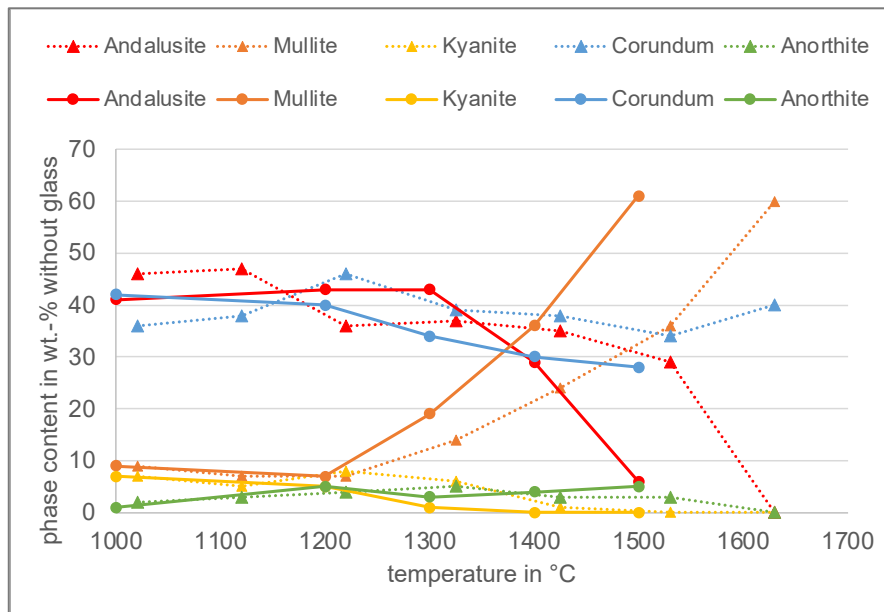


Figure 39: Rietveld analysis of phase content in reference castable, RE. The results were calculated without considering the glass content, which increases considerably with temperature. The diagram combines the results already presented in Figure 21 (firing without dwell time, dashed lines) and Figure 28 treated for 8 hours at 1000, 1200, 1300, 1400 and 1500 °C (solid lines).

5.3.3.3 Macroscopic appearance of reference castables thermally altered

The microstructure of the three commercial andalusite based castables RR, RE and RB fired for 24 h at 1450 °C exhibits differences of the sample surface structure visible with naked eyes (Figure 40). RB appears very compact with a homogenous structure, with few small defects that are mainly small spheric pores that are typical for materials that underwent a casting process. The matrix appears light beige with small white coarse grains (transformed andalusite) and larger grey coarse grains (chamotte). RE also exhibits a compact structure, with few small defects, that are predominantly spheric pores attributed to casting process. The matrix is light brown with large white coarse grains that have a grey core (relictic andalusite). Coarse grains with a brown appearance could be addressed as bauxite. The average particle size of the coarse grain is higher than average particle of RB and smaller than average particle size of RR. RB and RE show a typical dense structure of materials that contain a significant amount of glassy phase that is formed during the sintering process at 1450 °C. The microstructure of RR appears more brittle, indicating a lower amount of melting phase developed at 1450 °C. RR also contains of two (white/grey) of coarse grain of different nature that can be addressed as andalusite and bauxite. Average particle size also appears to be the highest in RR compared under the three castables selected for this study.

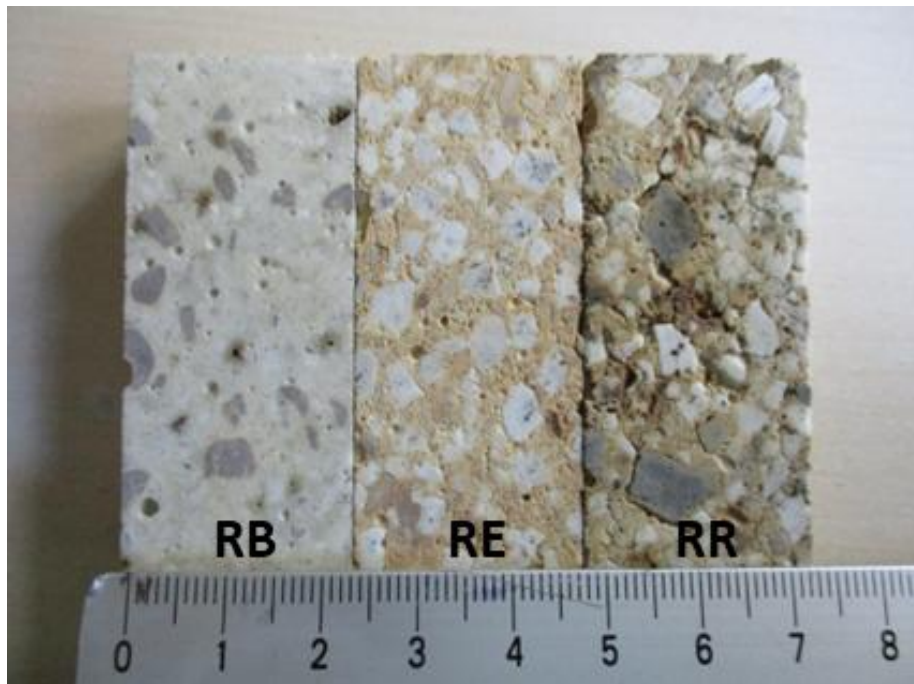


Figure 40: Microstructure of the three andalusite based castables (fired at 1450°C during 24h). From left to right, the proportion of glass phase, which was present in liquid form during aging, increases. RB therefore appears particularly smooth on the surface, which also applies to a lesser extent to RE. RR, on the other hand, shows a cracked texture, which clearly shows that the matrix was still brittle during the stretching of the andalusite during its decomposition.

It should always be noted that a high proportion of glassy phase, which increases systematically and significantly from RR to RE to RB, is present in the liquid state at the application temperature. On the one hand, this changes the volume stability, but the degree of compaction increases, which leads to a reduction in the open porosity.

5.3.3.4 Evolution of bulk density and open porosity as a function of temperature and dwell times

Figure 41 and Figure 42 present the bulk density and open porosity of the reference materials versus the firing temperature. With a bulk density of 2.94 g/cm³, the reference castable, RR, has the highest bulk density at room temperature, followed by RE (2.85) and RB, which only has a bulk density of 2.57 g/cm³. These differences are primarily due to the raw materials used. In addition to andalusite, RR and RE also contain bauxite to increase the refractoriness, whereby the difference in the bulk density of the two can be explained by the fact that RR contains slightly more bauxite, which is also used as a coarse grain. In RB, bauxite has been replaced by fireclay, which typically has a significantly lower apparent density. The apparent density of all reference castables decreases with increasing pre-treatment temperature, although this only becomes significant between 1250 and 1350 °C, i.e. in the temperature range in which the andalusite in particular is decomposed in the matrix. However, it can also be seen from Figure 41 that the measurements after an ageing time of 4 hours do not yet represent a stable state, as the measurements after ageing for 24 hours are significantly lower again. This is particularly clear for RR and RE and is significantly less pronounced for RB, which is due to the higher reactivity of the more impure andalusite raw material in RE and here even 4 hours leads to a far advanced decomposition of the andalusite. RR and RE are therefore significantly more reactive, as the decomposition of the andalusite progresses much more slowly.

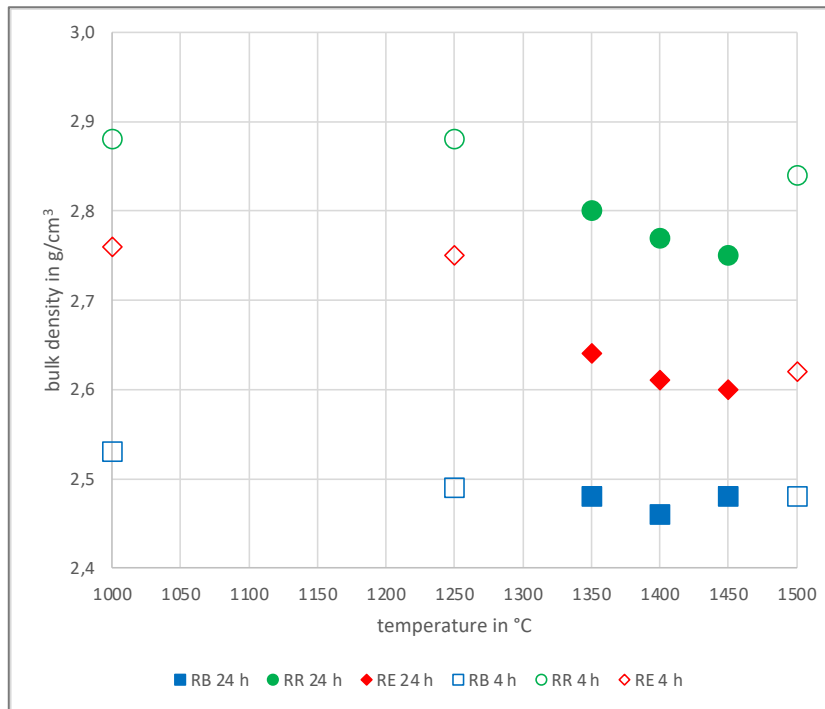


Figure 41: The bulk density as a function of the temperature. Open symbols indicate a dwell time of 4 hours and filled symbols indicate a dwell time of 24 hours.

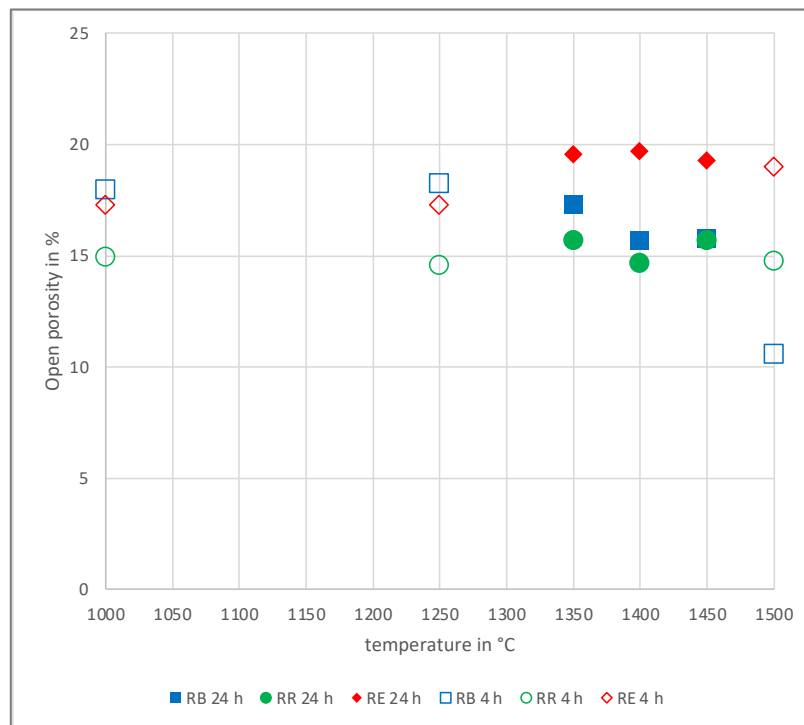


Figure 42: The open porosity as a function of the temperature. Open symbols indicate a dwell time of 4 hours and filled symbols indicate a dwell time of 24 hours.

RE shows the highest open porosity at room temperature with 14.4 vol.%, followed by RR (12.5 vol.-%) and RB (11.5 vol.-%), which does not change systematically and significantly up to aging temperatures of 1500 °C. RB is an exception here, as the lowest value of 10.6 vol.% is achieved with pre-treatment at 1500 °C. This is probably due to the high degree of melting of the castable,

which virtually vitrifies the surface of the test specimens and closes the porosity visible in Figure 37. Generally, the open porosities range between 15 and 20 vol.% (Figure 42).

5.3.3.5 Effect of heating on cold mechanical properties

The following figures (Figure 43 and Figure 44) depicts the evolution of cold crushing and cold bending strength as a function of the pre-treatment temperature and dwell times of 30 minutes and 24 hours.

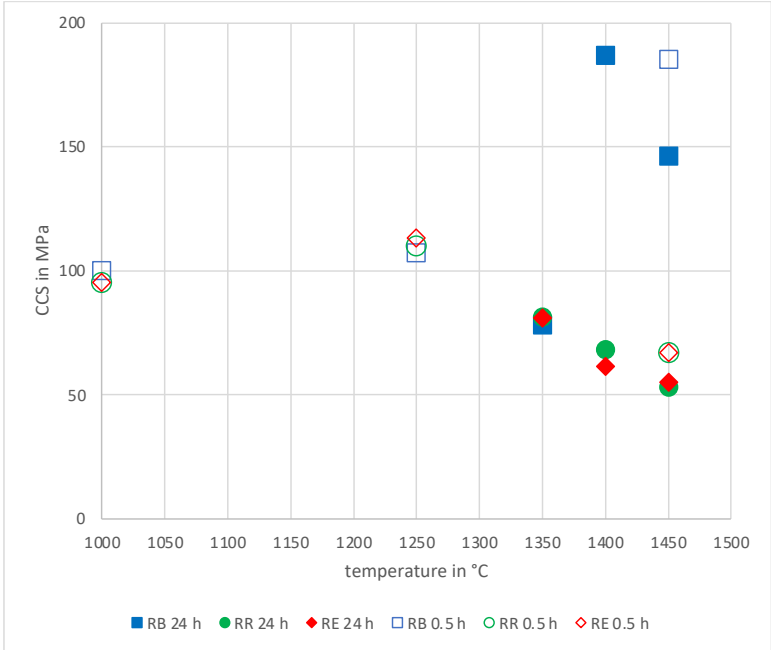


Figure 43: CCS of the reference castable as a function of the pre-treatment temperature and ageing time, 24 hours (closed symbols) and 0.5 hours (open symbols).

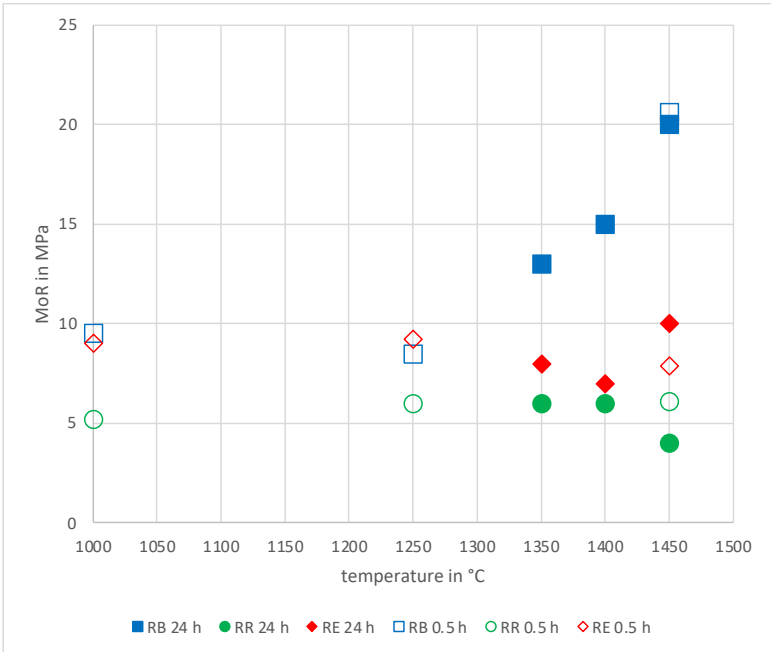


Figure 44: MoR of the reference castable as a function of the pre-treatment temperature and ageing time, 24 hours (closed symbols) and 0.5 hours (open symbols).

To record the temperature- and time-dependent development of the strength (CCS and MoR) of the reference castables, test specimens were pretreated at 110, 1000, 1250, 1350, 1400 and 1450 °C, whereby the holding time was also varied (0.5 and 24 hours) in order to be able to show the influence of the reaction kinetics of the andalusite decomposition on the strength development. As expected, the reference castable, RB, developed the highest strengths in MPa after drying at 110 °C (CCS, 73; MoR, 10.8) compared to RE (CCS, 45; MoR, 7.2) and RR (CCS, 24; MoR, 2.7). This is mainly due to the different cement addition, which is highest for RB. As an NCC, RR is cement-free, whereby the bond is based on the gelation of a silica sol. The measured strengths are typical for this product group. All reference castables show an increase in MoR and CCS up to 1250 °C and develop very similar strengths at this temperature of around 110 MPa (CCS), which also applies to MoR for RB and RE (approx. 9 MPa). RR is significantly lower at 6 MPa, but this can again be explained by the cement-free binder system. After a thermal pre-treatment at 1250 °C, no significant sintering of the microstructure has taken place here. Above 1250 °C, RR and RE show a reduction in strength, whereby this is monotonically decreasing for RR, but RE shows an increase in strength again after pre-treatment at 1450 °C. This is much more pronounced in the case of a longer pre-treatment of 24 hours than after 0.5 hours. RR continues to lose strength (MoR) if it is subjected to a longer holding time. The reference castable RB shows a completely different behaviour for CCS and MoR. At pre-treatment temperatures above 1350 °C, the strengths increase significantly and monotonically, which is particularly evident in the case of MoR. The highest strengths are achieved in comparison to the other reference castables. In principle, the prograde decrease in strength above 1250 °C can be explained by the increase in volume caused by the decomposition of the andalusite, provided the matrix behaves brittle. This applies in particular to the reference castable, RR, which is also well documented in Figure 40. Figure 29 also shows this brittle behaviour at 1000 °C, with cracks developing all around the large andalusite grains. RB, on the other hand, develops significant amounts of melt phase above 1250 °C, which prevents brittle behaviour and solidifies into a glassy phase retrogradely. As a result, the enormous strengths develop at room temperature. This also becomes clear at 1450 °C for RE, where significant melting can already be seen at these temperatures. The degree of melting at 1500 °C is shown very impressively in Figure 35.

To assess the gradual strength development, the decomposition reaction of the andalusite, which disturbs the microstructure through expansion, must therefore be considered on the one hand, but the degree of melting must also be taken into account, which makes the microstructure more ductile and thus more tolerant to expansion during the decomposition of andalusite. The glass phase, on the other hand, achieves very high strengths at room temperature (test temperature).

5.3.3.6 Prograde evolution of normalized frequency derived from RFDA from room temperature up to 1400 °C

The reference castables were examined up to 1400 °C with regard to the change in normalized frequency. The castables were heated at 10 K/min for this purpose. Measurements were carried out on samples that had only been dried (110 °C) and on samples that had been pre-treated at 1350 or 1450 °C for 24 hours. The observation of the heating behaviour of the only dried castables basically contains as a dynamic component the prograde change of the castables, from the point of view of the andalusite decomposition and the sintering or the vitrification of the matrix.

5.3.3.7 RFDA versus temperature of dried materials (first heating)

Figure 45 and Figure 46 present the prograde evolution of RFDA normalised frequency of solely dried castables. It was not possible to measure the RFDA curve of reference castable RR, because of its weak strength after drying and the resulting brittle structure.

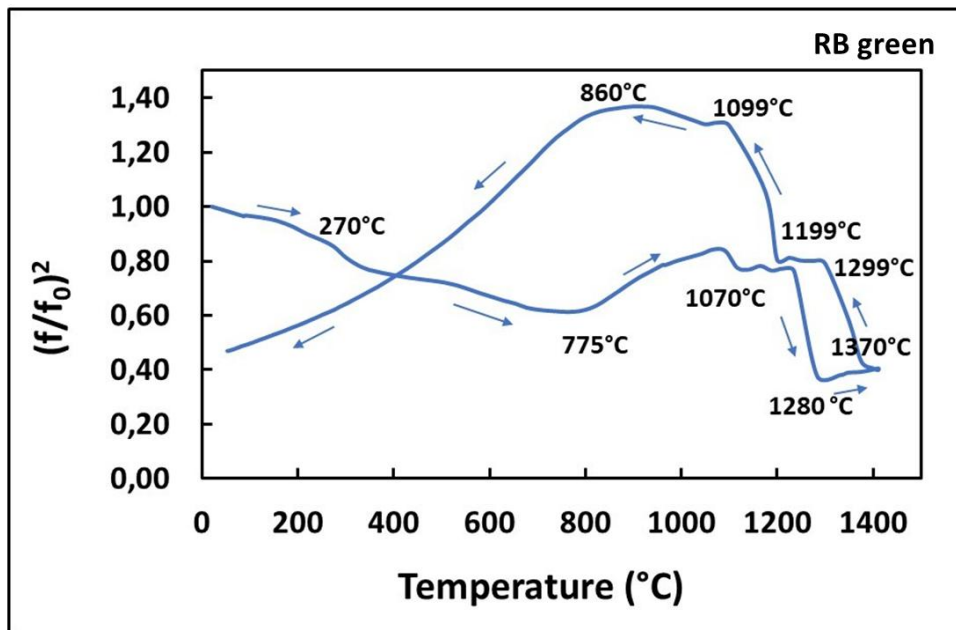


Figure 45: Prograde and retrograde evolution of the normalized frequency between room temperature and 1450 °C, derived from RFDA for reference castable, RB, dried at 110 °C.

For reference castable RB, the frequency (modulus of elasticity) decreases continuously from room temperature to about 775 °C. The decrease is due to thermal expansion and interatomic lengthening/weakening and to the dehydration of the cement bonding phases. The small knee in the curve at about 270 °C is due to the loss of still remaining free water and the beginning decomposition of cement hydrate phases (chemically bonded water). From about 775 °C, sintering starts and promotes bonding between matrix particles and strengthening of materials resulting in an increase of modulus of elasticity. From 1070 °C on, the frequency remains more or less constant due to competition between sintering and appearance of a liquid phase. The appearance of a liquid phase, even in small quantities, typically occurring at the grain boundaries, leads to decohesion and a significant decrease of frequency. A strong decrease at about 1280 °C, could be related to the appearance of a larger quantity of liquid phase. Stabilisation between 1280 and 1400 °C could be related to a stabilization between the appearance of a liquid phase and sintering. During cooling, an increase of the frequency between 1400 and 1299 °C can be explained by the beginning of the solidification of the liquid phase and may be related to the crystallization of euhedral mullite from the liquid phase. Almost constant values for the frequency between 1299 and 1199 °C is due to slow down of solidification. This is followed by a second increase (1199-1099 °C) that is obviously due to the ongoing solidification of the liquid phase causing a vitrified solid state. Between 1099 and 860 °C, frequency increases due to solidification of remaining liquid phase, to thermal shrinkage, and interatomic shortening/strengthening. Below 860 °C, up to room temperature, regular decrease is typical in this kind of material and is due to the appearance of defects/cracks which are generated by thermal induced stress between and aggregates and matrix which becomes more and more brittle with decreasing temperature. Mainly due to this crack formation, the final frequency is much lower than the initial modulus of elasticity.

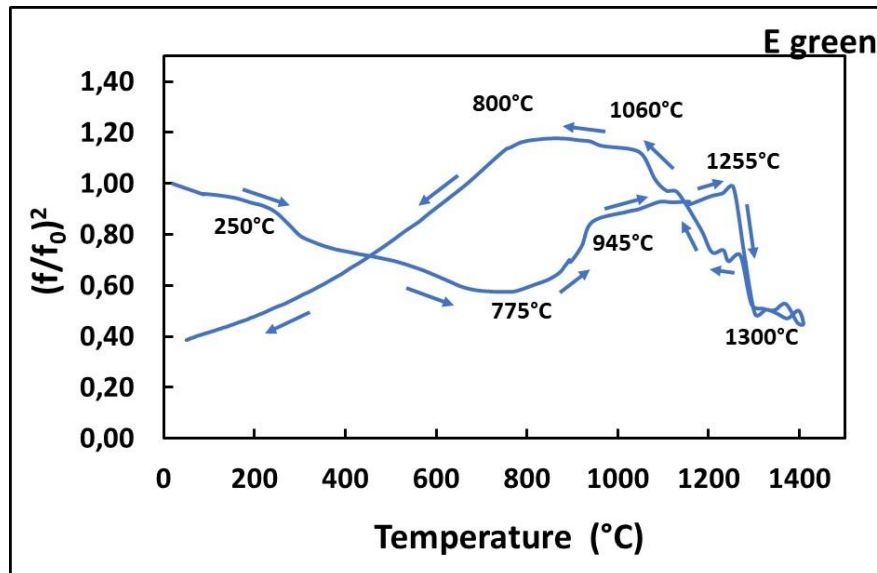


Figure 46: Prograde and retrograde evolution of the normalized frequency between room temperature and 1450 °C, derived from RFDA for reference castable, RE, dried at 110 °C.

The reference castable RE, showed a thermal evolution of the modulus of elasticity like that measured for RB. Between RT and 775 °C, a decrease of the normalized frequency could be correlated to the effect of thermal expansion and interatomic lengthening/weakening and to the dehydration of the cement phases. The small knee at about 250°C is indicating this water release. From about 775°C, sintering of the matrix compounds is initiated that promotes bonding and strengthening of the structure. At 945 °C, the frequency increases slow down due to competition between sintering and appearance of liquid phase. The appearance of liquid phase, even a small quantity, at the grain boundary, leads to decohesion and decrease of frequency. Sharp decrease at about 1255 °C, could be related to the formation of a larger quantities of liquid phase. Between 1300 and 1400 °C the modulus of elasticity stabilises and could be explained with a reduced formation of liquid phase and the appearance of intensified sintering. During the cooling, an increase of the frequency between 1300 and 1060 °C is due to the beginning solidification of the liquid phase. Between 1060 and 800 °C, frequency increases, slope of the curve is much lower, due to solidification of remaining liquid phase, to thermal shrinkage, and interatomic shortening/strengthening. Below 860 °C, up to room temperature, regular decrease is typical in this kind of material and is due to the appearance of defects/cracks which are generated by thermal induced stress between and aggregates and matrix which becomes more and more brittle with decreasing temperature. Mainly due to this crack formation, the final frequency is much lower than the initial modulus of elasticity.

As already mentioned, the reference castables which were only dried at 110 °C, show a similar sintering behaviour between room temperature and 1450 °C. The significant changes in frequency described above occur with RE shifted to about 70 °C higher temperatures, which is due to the higher refractoriness of RE compared to RB. In RB, the melting phase formations occur at lower temperatures, which can be associated with the higher cement content and the less refractory raw materials (impure andalusite and chamotte). However, it is also worth noting that in RE, solidification occurs at a temperature of 1255 °C, which does not occur in this form in RB. This can be attributed to the addition of kyanite in RE, which is decomposed at this temperature with high reaction kinetics and thereby prestresses the microstructure by increasing in volume.

5.3.3.8 RFDA versus temperature of fired materials (24 h at 1350 and 1450 °C)

In order to better classify the influence of the reaction kinetics of the inhibited decomposition of the andalusite, materials that were thermally pre-treated for 24 hours at 1350 and 1450 °C were also investigated in addition to the investigations on reference castables that were only pre-treated at 110 °C. The results of the previous chapters have already shown that considerable amounts of melting can be expected from 1350 °C onwards. The results of the previous chapters have already shown that considerable amounts of melt formation are to be expected from 1350 °C, whereby it turned out that the reference castables become more and more refractory from BR via RE to RR, which should result in significant differences in the determination of the moduli of elasticity per and retrograde depending on the amount of the melt phase. In addition, the proportion of residual andalusite decreases in the same sense from RB to RE to RR, as the formation of a melt phase leads to a kinetic favouring of the degradation reaction of the andalusite. The higher the degree of melting of the reference castable, the more the pro- and retrograde development of the Young's modulus should align. Figure 47 to Figure 49 show the standardised RFDA frequency versus temperature of the three castables thermally pre-treated at 1350°C and 1450°C.

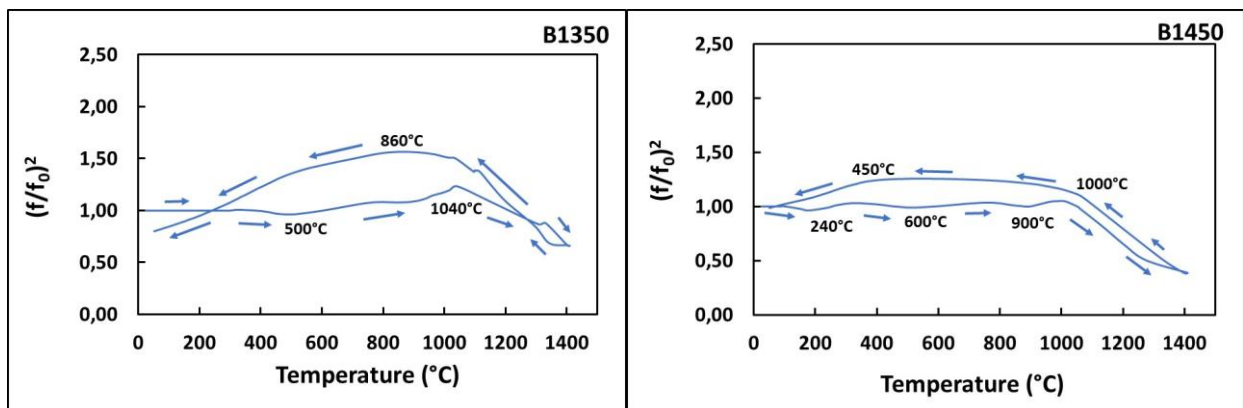


Figure 47: Prograde and retrograde evolution of the normalized frequency between room temperature and 1450 °C, derived from RFDA for reference castable, RB, pre-treated at 1350 (left) and 1450 °C (right) for 24 hours.

As shown in Figure 47, the shape of the curves is very similar for the reference castable RB, fired at 1350 and 1450 °C. From room temperature to about 1000 °C. The frequency shows a relatively stable value with small variations. In this temperature range there is a competition between expansion, which causes the modulus (frequency) to decrease, and closure of defects (cracks), which causes the modulus (frequency) to increase. Above 1000 °C the frequency (modulus) decreases continuously due to the presence of viscous phases and/or the appearance of a liquid phase at the grain boundaries, an increase in the amount of this liquid phase and/or a decrease in the viscosity of all these phases. The final value is close to the initial value. The phenomenon of crack closure-opening during heating-cooling of materials induces a whole curve with hysteresis. The size (area enclosed between the two curves) of the hysteresis is proportional to the size and/or number of defects. It is also clear that in the case of pre-treatment at 1450 °C, the prograde curve of the frequency adapts much more strongly to the retrograde curve, which also indicates a far advanced melting of the matrix. In addition, the decomposition of the coarse-grained andalusite is well advanced, as can also be seen in Figure 37.

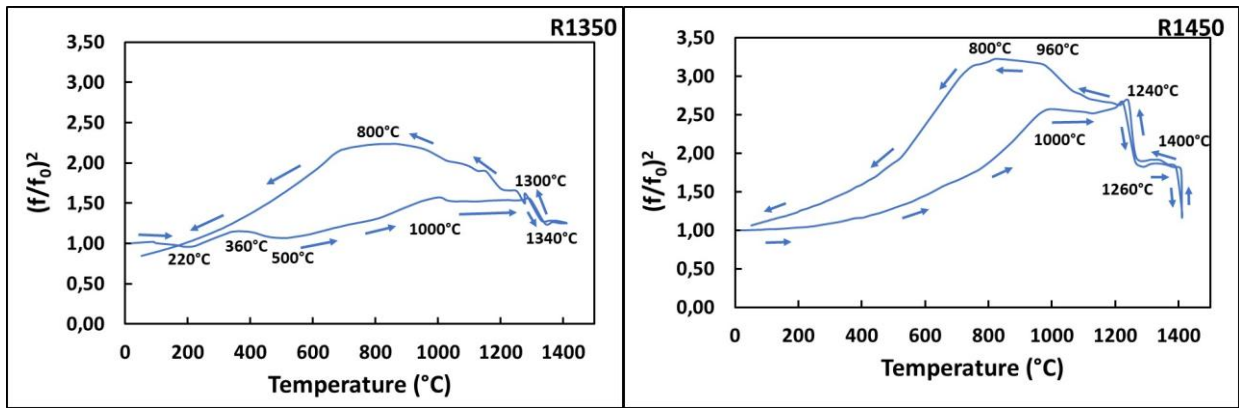


Figure 48: Prograde and retrograde evolution of the normalized frequency between room temperature and 1450 °C, derived from RFDA for reference castable, RR, pre-treated at 1350 (left) and 1450 °C (right) for 24 hours.

In case of reference castable RR, the frequency increases from room temperature to about 1000 °C. The variation is very high, mainly for material fired at 1450 °C, which indicates large defects and/or many defects closing. From about 1000 °C, there is a stabilisation of the frequency, due to the decrease of defects closing. At higher temperature (1300 °C for R1350 and 1240 °C for R1450, Figure 48), a pronounced decrease indicates the presence of viscous phases, appearance of liquid phases followed by a stabilisation and a second decrease (liquid phase) for the RB pre-treated at 1450 °C. During cooling an increase of the frequency is followed by a plateau (~950-800 °C) and then by a sharp decrease up to room temperature, corresponding to the opening of defects (cracks). In this case, the size (surface) of the hysteresis is much higher than for RB.

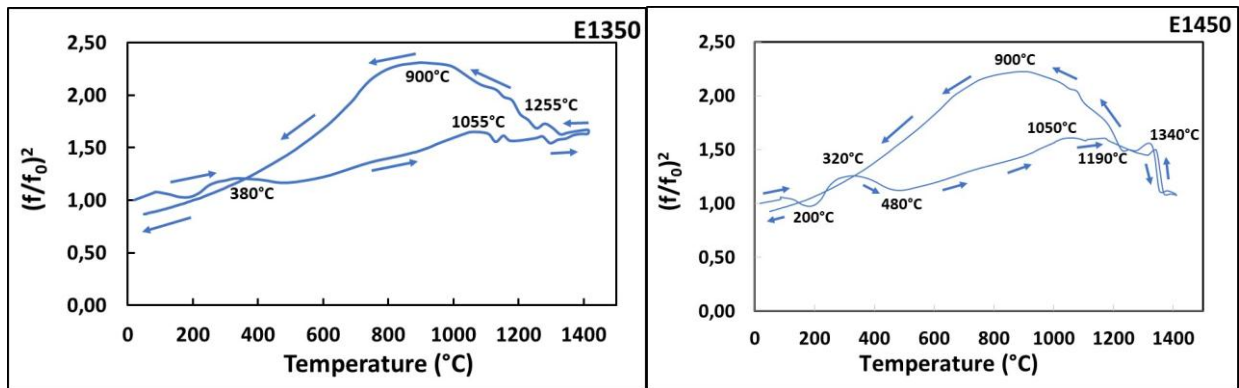


Figure 49: Prograde and retrograde evolution of the normalized frequency between room temperature and 1450 °C, derived from RFDA for reference castable, RE, pre-treated at 1350 (left) and 1450 °C (right) for 24 hours.

In the case of the reference castable RE, the frequency increases from room temperature to about 1000 °C. The variation is very high, especially for the reference castable fired at 1450°C, indicating large defects and/or many defect closings. Above about 1000 °C, there is a stabilisation of the frequency due to the decrease in defect closure. At higher temperatures (1340 °C, only for RE preheated at 1450 °C for 24 h), a sharp decrease indicates the presence of viscous phases and/or the appearance of liquid phases, followed by a stabilisation. On cooling, an increase in frequency is followed by a plateau (~950-800 °C) and then a sharp decrease down to room temperature, corresponding to the opening of defects (cracks). In this case, the size (area) of the hysteresis is much higher than for the reference castable, RB.

RE and RR therefore behave quite similar, which is due to the alike structure of the castables as far as the choice of raw materials is concerned and, in both cases, bauxite is taken into account,

which significantly increases the refractoriness. Heating up and cooling down show a clear difference in the course of the frequencies compared to RB, which also suggests that a sliding weight state has not yet been reached. RB, on the other hand, contains so much melt, even after pre-treatment at 1350 °C, that the system has almost approached equilibrium.

5.3.3.9 Creep under compression (EN 993-9)

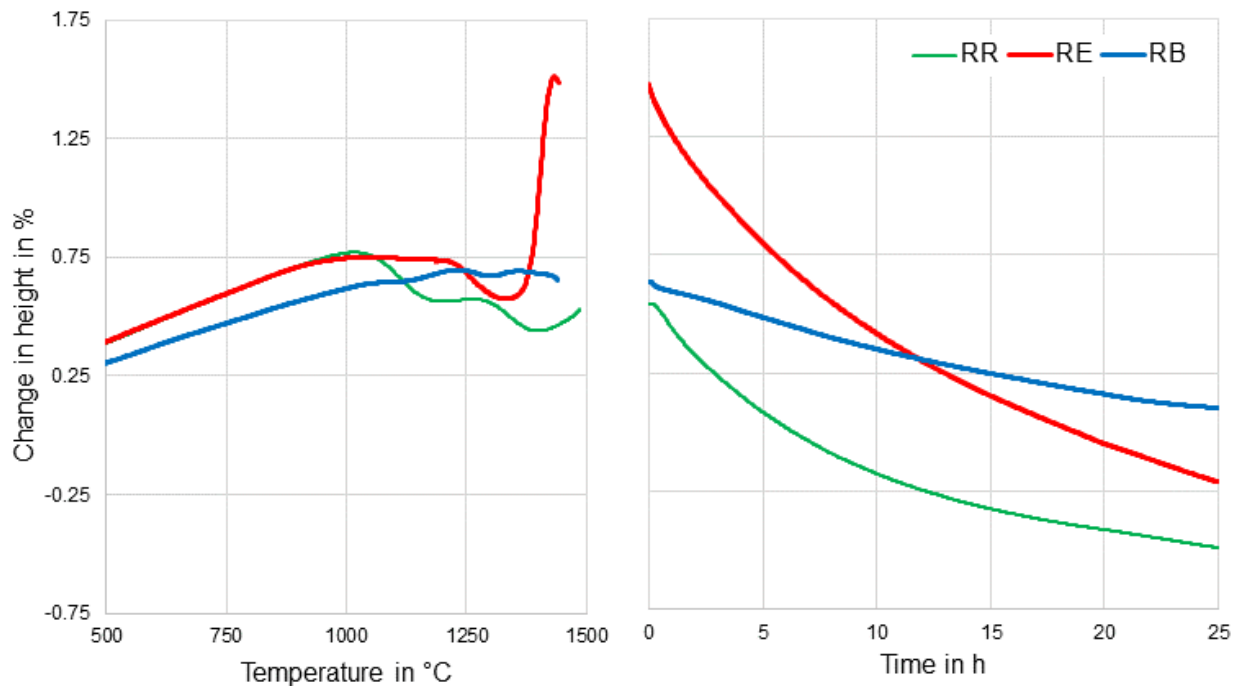
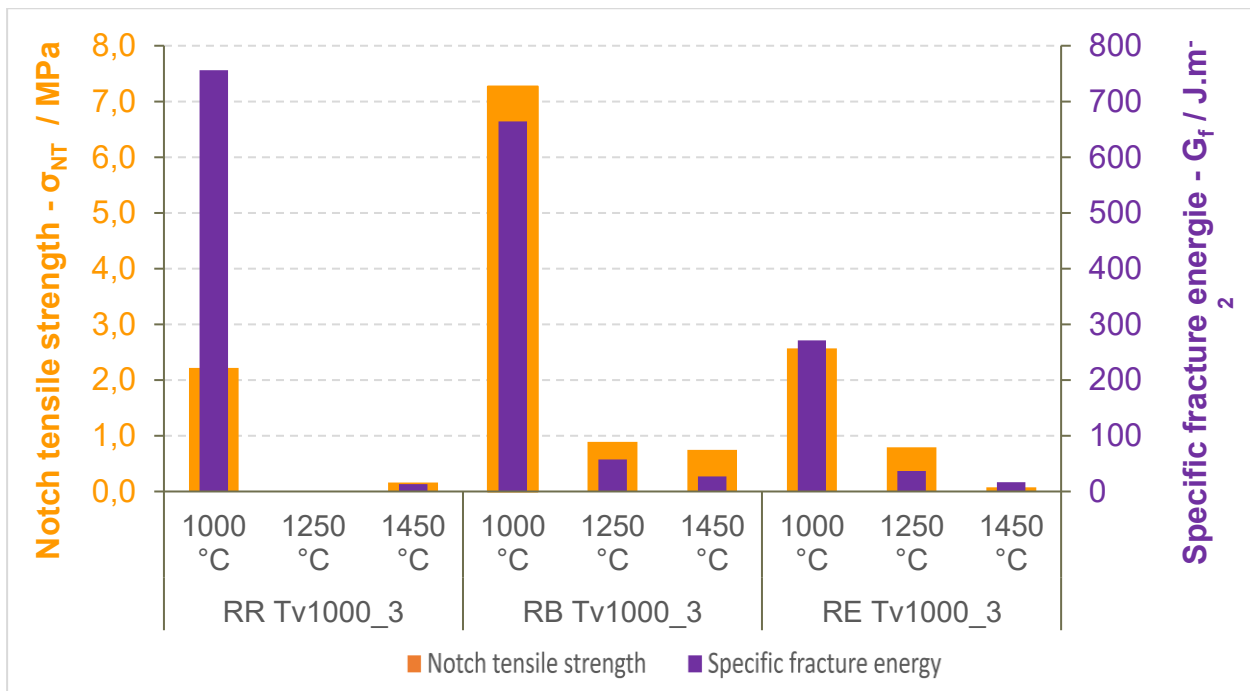


Figure 50: The test-pieces were pre-fired for 1 h at 1000 °C. CREEP tests were carried out on the three reference castables for 25 h at temperatures of 1450 °C (RE, RB) and 1500 °C (RR).

CREEP tests were carried out on the three reference castables for 25 h at temperatures of 1450 °C (RE, RB) and 1500 °C (RR) as envisaged Figure 50. The temperatures were selected based on the results of RUL. As RR attained a distinct higher temperature for T_{05} than RE and RB, CREEP was carried out at 1500 °C instead of 1450 °C (what is more realistic considering temperatures of application intended by the producers (see Table 4)). The observed creep rates decrease with time but did not reach stable deformation after 25 h. At the predefined temperatures, none of the reference castables achieved satisfactory refractory stability and are unlikely to have sufficient volume stability at the specified temperatures. This becomes particularly clear for the reference castable RE, which only reached its test temperature after the very high-volume increase, mainly triggered by the kyanite decomposition. The curves serve as benchmark when evaluating the creep behaviour of the andalusite free model castables.

5.3.3.10 Wedge splitting test

The results of wedge splitting tests provide valuable information on the fracture behaviour of the castables at high temperatures. Measurements were carried out on reference castables RE, RB and RR at 1000, 1250, and 1450 °C (



). The behaviour of the castables is being driven on the one hand by the castables bonding system that usually dictates the strength (ability to resist fracture initiation) after the setting of the castable and up to moderate temperatures, as well as the tendency of the system to form melts at higher temperatures, which usually weaken the system. On the other hand, the castables microstructure and especially the presence of defects (e.g. networks of cracks, gap in the particle size distribution, etc) tend to be warranted for the ability of the castables to resist fracture propagation, which is reflected by high specific fracture energy, after the setting of the castable and up to moderate temperatures, while thermal expansion mismatch, the reactivity of the castables matrix and the formation of new phases strongly modulate the ability of the castables to resist fracture propagation at higher temperatures.

The ULCC castable RE showed a moderate notch tensile strength and specific fracture energy by 1000 °C, both decreasing with increasing temperature likely because of the progressive formation of melts in the castable. However, the ratio specific fracture energy to notch tensile strength, which reflect the ductility of the castable, stayed at a decent level, indicating a rather ductile behaviour despite the losses in strength and specific fracture energy. In comparison, the LCC castable RB, displayed at 1000 °C a quite high notch tensile strength granted by the comparably high amount of calcium aluminate (CA) bonding phase, but also a quite high specific fracture energy. In spite of a massive decrease of both of these with increasing temperature, again likely as results of melt's formation, they remained at a level higher than observed for the ULCC castable RE. The higher content of andalusite in the castable initial mix, which lead to the formation of almost continuous network of mullite crystals within the former andalusite aggregates and the castables matrix, might explained this observation. However, the ratio specific fracture energy to notch tensile strength is also slightly lower than for the ULCC castable RE and accordingly should present a slightly more brittle behaviour. In contrast, the sol-gel bonded castable RR displayed the lowest notch tensile strength at 1000 °C, which is typical for sol-gel bonded castables, but the higher high specific fracture energy, resulting in an impressive the ratio specific fracture energy to notch tensile strength, indicating a very ductile behaviour. Yet, probably because of the presence of amorphous silica (bonding phase) relatively homogeneously distributed in the matrix and keen to form liquid phases at elevated temperature, the mechanical strength of the sol-gel bonded castable RR vanished at 1250 °C and no notch tensile strength and

accordingly neither high specific fracture energy could be assessed. At 1450 °C the formation of mullite inside the test piece might have provide enough strength so that a measurement was possible.

It is worth noting that because of the specific testing configuration of the wedge splitting test, tensile stresses are generated to which refractory materials are notoriously vulnerable (in comparison to compressive stresses). It is therefore quite usual, by high temperature measurements, to assess very low values of strength, or strength lying under threshold of the acquisition system, well before the typical service temperature of the castable are reached. However, low or no measurable strength and accordingly specific fracture energy (without measurable strength, no load-displacement curves to calculate the specific fracture energy) does not mean that the castable will automatically fails since 1) most of the stresses arising at the hot face under typical refractory service conditions are compressive stresses and 2) refractory linings experience a temperature gradient and the colder part of the lining bear the mechanical load and ensure the structural stability of the linings.

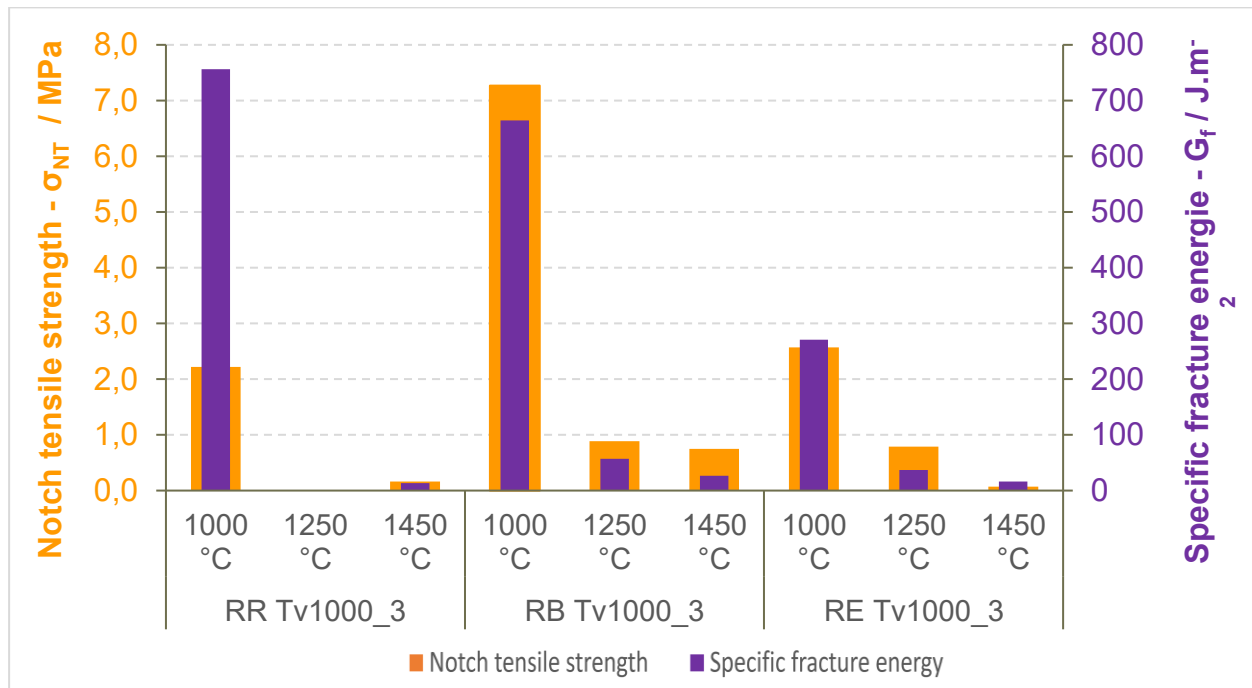


Figure 51: Results of the wedge splitting tests on the castables RR, RB and RE performed at 1000 °C, 1250 °C and 1450 °C.

5.3.4 Corrosion resistance of the andalusite based reference castables

The corrosion resistance of the three reference materials RE, RR and RB was investigated by using the channel slag test. The refractory castables were mixed and casted into moulds to form half shells as necessary for the testing device (chapter 4.3.1). As mentioned before, RR is a silica sol gel bonded andalusite based castable with bauxite as main side component which was developed for good resistance to thermal shock and application temperatures between 1000 and 1700 °C. RE is a cement bonded ULC castable with bauxite as main side component, also. RE is designed for thermal shock loaded wear lining and corrosive stress due to especially Fe and Cu smelting metallurgy (metal & slag phases) in a typical temperature interval between 1250-1600

°C. The andalusite content of RB is almost twice that of the other two reference castables. RB is developed for lower application temperatures and is designed for a good thermal shock, - and mechanical resistance, also. It should be noted, that the three reference castables are designed for different applications and not optimized for corrosion resistance of alkalis.

In each experiment a set of two half shells (T1 RR and RB, T2 RE and RB) was fired with a heating rate of 300 K/h to the maximum testing temperature of 1250 °C at the control thermocouple in one of the half shells (Figure 5). The maximum temperature in the test setup was around 1520 °C, measured in a preliminary test above the entry of the gas flame into the block. The lowest temperature measured was around 70 °C next to the cooling plates TC2/TC8 (Figure 6). With this setup, the corrosion resistance could be measured in a temperature gradient of around 1450 °C. 300 g of an alkali-rich granulated slag (chemical composition see Table 5) were continuously injected by a vibration plate into the firing channel during a testing time of four hours. In the area where the flame entered the half shells, the castables were in direct contact with the slag. A layer of slag was rapidly assembled on the hot face that had a thermal insulating effect for the half shells. Other areas only encountered the volatile elements of the slag and were exposed to significantly lower temperatures (Figure 53).

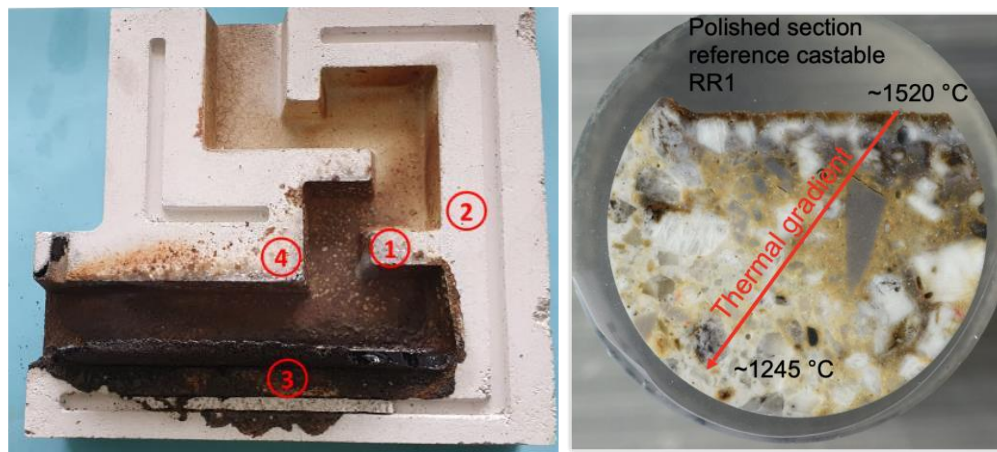


Figure 52: The coloration of the test-pieces (here RR is shown) after the corrosion test already showed that the test-pieces were exposed to the corrosive material to different degrees. The flame entry area of the half shells was covered by a black layer of solidified glassy slag. The rest of the channel was brownish in colour, with the degree of coloration decreasing as the distance from the flame entry area increased. On the right a polished section of RR is shown that was taken from position 1. The photograph also shows the thermal gradient under corrosion condition.

The coloration of the test pieces (half shells and chimneys) after the corrosion test already showed that the test-pieces were exposed to the corrosive material to different degrees (Figure 52). The flame entry area of the half shells was covered by a black layer of solidified glassy slag. The rest of the channel was brownish in colour, with the degree of coloration decreasing as the distance from the flame entry area increased. At P1 the castable is in contact with very hot gases carrying slag and volatiles and the temperatures are the highest (about 1520-1250 °C). For all other positions the absolute temperatures are unknown, but the grade of andalusite decomposition can be used as a temperature indicator. At P2 the temperatures are probably the lowest of the four positions. The castable is in contact with hot gases transporting slag and volatiles. At P3 the castable is in contact with a liquid slag basin. The temperatures are lower than P1, due to the isolating liquid slag. P4 is in contact with very hot gases transporting slag and volatiles. The temperatures are high, but no absolute temperature information is available.

The lower third of the chimneys was covered by a brownish layer (Figure 53). In the upper part, the layer turned from white to light blue. Therefore, the test-piece is exposed to two different

corrosion phenomena; corrosion by a liquid slag and corrosion by volatiles which left the slag due to the high temperatures.

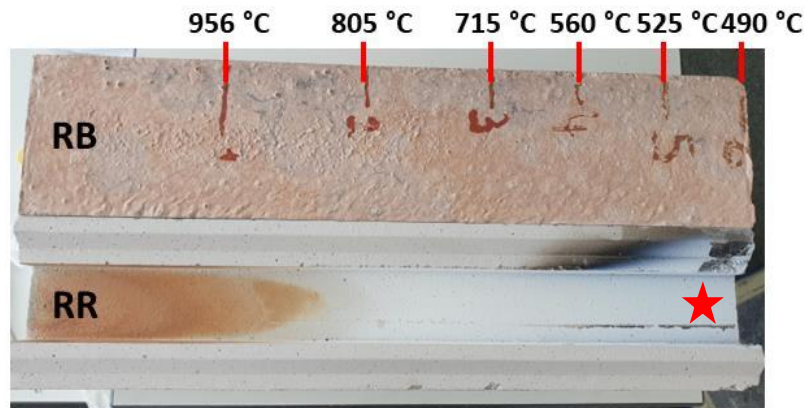


Figure 53: The lower third of the chimneys (here RR and RB) was covered by a brownish layer. In the upper part, the layer turned from white to light blue.

5.3.4.1 Macroscopic observations (polished section)

A thick layer of brownish slag adhered on the surface on the test pieces of the refractory castables RR, RE, and RB at position 3 (slag pool, Figure 54). Within the castable, changes in the colour of the matrix and the degree of visible andalusite transformation visualize the direction of a thermal gradient that developed during the test in position 3 (indicated by a red arrow). At the contact to the slag pool, within a layer of about 2 mm in thickness, the matrix appears greyish and only here, andalusite grains are opaque-whitish indicating they are transformed (A* in Figure 56). Andalusite grains in the other parts of the polished section are transparent-greyish, indicating they are not transformed (A in Figure 56). Beyond the thin layer, but still close to the slag pool and especially in the upper left sector of the polished section, the matrix is more yellow. In the cooler parts of the polished section from position 3, the matrix is predominantly whitish and only here it contains dark “dots” of small bluish corundum grains.

Coarse grains protruding into the adhering slag indicate anticipating dissolution of the matrix by the slag as the predominant corrosion mechanism. Intensive infiltration of slag into the castable, as indicated by dark brown discoloration within the castable, seems restricted to local domains very close to the contact. This corrosion mechanism is particularly evident in RR. In RB, on the other hand, there appears to be little infiltration into the matrix Figure 54.

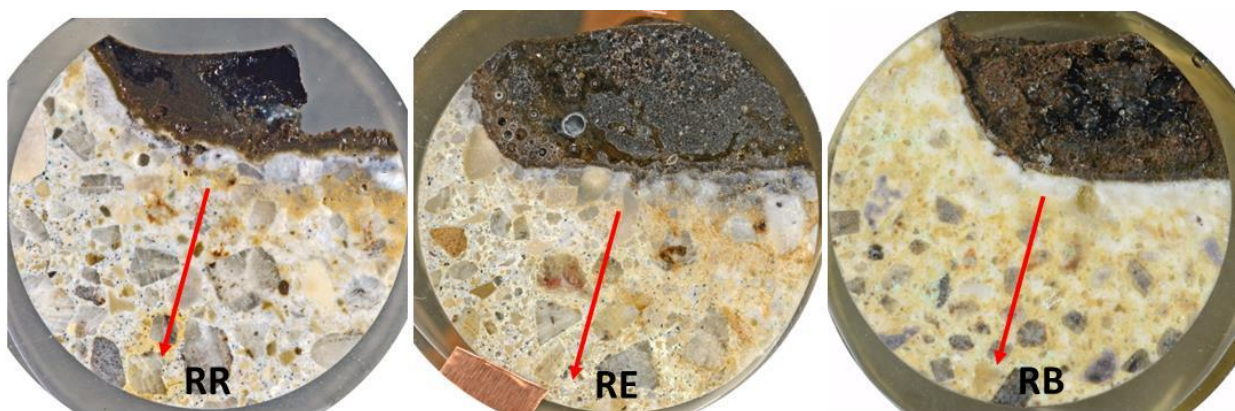


Figure 54: A thick layer of brownish slag adheres on the surface on the test specimen of the refractory castables RR, RE, and RB (Position 3). Within the castable, changes in the colour of the matrix and the degree of visible andalusite transformation visualize the direction of a thermal gradient that developed during the test in position 3. The decreasing

temperature (thermal gradient from the channel to the outer surface of the castable) is indicated by a red arrow. Size of the polished section 30 mm.

The temperature is the highest at position 1. The temperature gradient ranges from approximately 1520 °C to 1240 °C. The thermal gradient is indicated by a red arrow. Similar to position 3, the coarse grains in RR protruding into the adherent slag are an indication of anticipating dissolution of the matrix by the slag.

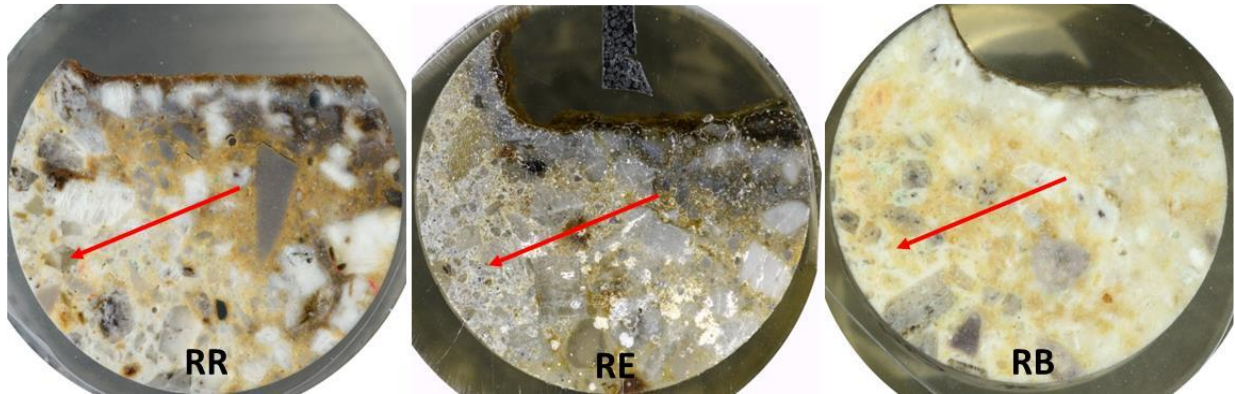


Figure 55: A thin layer of brownish slag adheres on the surface on the test specimen of the refractory castables RR, RE, and RB (Position 1). The temperature gradient ranges from approximately 1520 °C to 1240 °C and is indicated by a red arrow. Size of the polished section 30 mm.

5.3.4.2 Microscopic observations - Corrosion by liquid slag

The observed corrosion phenomena most characteristic for andalusite castables are described using the example of the reference castable RR at position 1 (see Figure 52) of the corrosion test. The polished section is shown in Figure 56. On the hot face of position 1, where the slag was deposited, a maximum temperature of approximately 1520 °C was measured. This position experienced the highest temperatures realised in the corrosion test. However, due to the thermal gradient within the specimen during the test, a temperature of approximately 1250 °C was measured at a position approximately 25 mm from the hot face. Therefore, a thermal gradient of approximately 10 K/mm must be considered in the polished section of RR at position 1 from the hot face with adhering slag to the opposite side of the polished section.

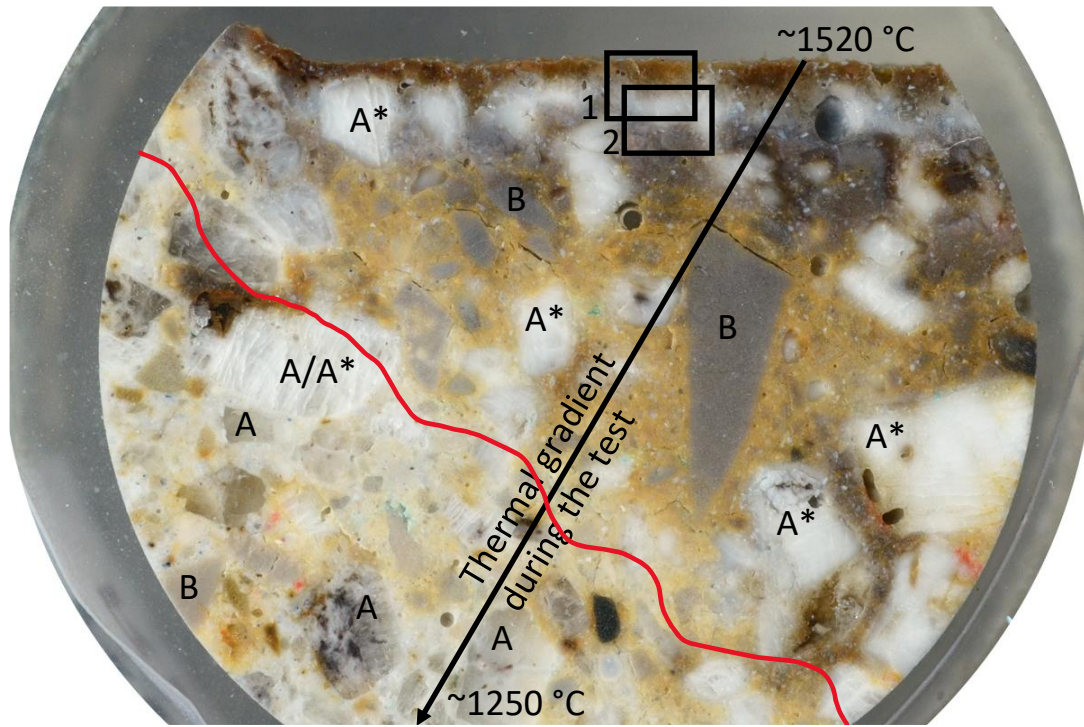


Figure 56: Polished section showing the polished section of RR at position 1 after the corrosion test. The two frames indicate the areas of SEM-images (

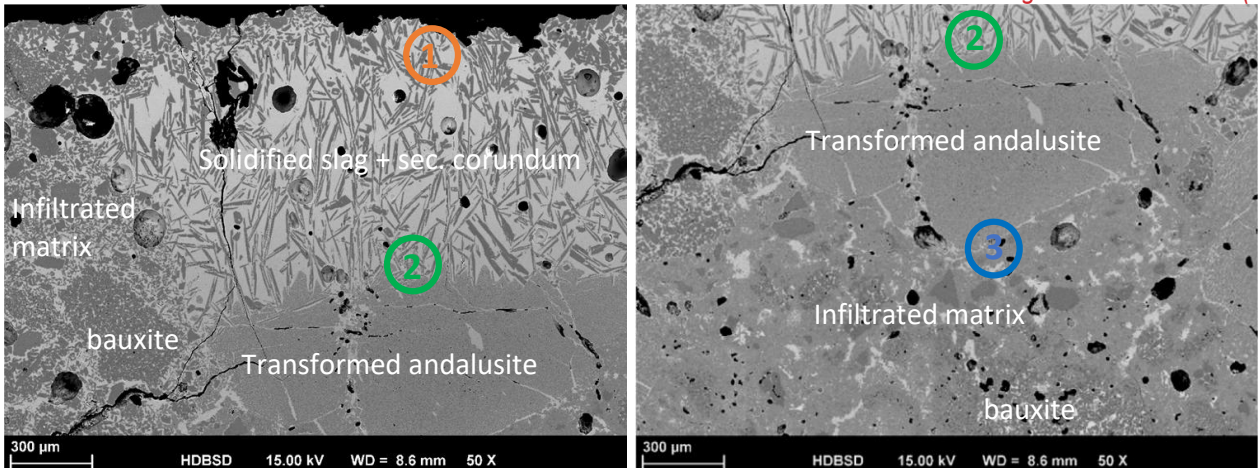


Figure 57. The red line approximates the gradually andalusite transformation limit. A = andalusite; A* = transformed andalusite; B = bauxite. Field of view: 30 mm.

In position 1, the slag interaction is also significant as slag particles were easily carried and deposited with the hot gases. In position 3 (slag bath) the slag interaction is more intense than in position 1, but the temperatures are lower and less well documented. In positions 2 and 4, both temperatures and slag intensities are lower.

At the contact between the refractory castable RR and the deposited, adhering slag layer (the surface to the channel), the andalusite grains were transformed due to the high temperatures during the test, probably facilitated by the presence of the molten slag. From the results of the stepwise heating experiments (chapter 5.3.3), it can be concluded that the degree of andalusite transformation observed in position 1 requires temperatures above 1500 °C.

In this area, the transformed andalusite grains (mullite + SiO₂) have been partially assimilated by deposited basic slag. The composition of the slag here is like that of slag 1 envisaged in Figure 58, containing approximately 40 wt.-% SiO₂, 33 wt.-% Al₂O₃ and 10 wt.-% CaO. The infiltration of

RR by the slag at position 1 preferentially followed the matrix of the castable and the infiltrated zone reaches a thickness of several mm, but not in the range of centimetres. The continued assimilation of mullite and SiO_2 at the contact and during infiltration saturated the slag with Al_2O_3 , leading to the crystallisation of secondary corundum in the form of thin idiomorphic platelets or idiomorphic overgrowths on irregularly shaped primary alumina grains.

With increasing depth of infiltration, the continued assimilation of mullite + silica also increased the silica content of the slag. At the same time, silica from the silica sol bonding system of the RR was dissolved. The composition of the slag here corresponds to that of slag 2 in Figure 58 and contains approximately 54 wt.-% SiO_2 , 31 wt.-% Al_2O_3 and 4 wt.-% CaO . When the silica in the slag is higher than about 58 wt.-%, it has been observed by SEM that mullite becomes stable. The increase in SiO_2 in the infiltrating melt eventually destabilises the primary corundum in this zone and mullite crystallises, forming coronitic rims around larger corundum grains. Smaller corundum particles are completely replaced by mullite. The composition of the slag here is like that of slag 3 in Figure 58 and includes approximately 62 wt.-% SiO_2 , 24 wt.-% Al_2O_3 , 1.5 wt.-% CaO . The alkali content of the melts also changes with depth of infiltration. While Na_2O is enriched in slag 2, K_2O is enriched in slag 3. It seems likely that alkali migration into the structure of the castable causes the formation of in situ melt which mixes with the infiltrating melt. Thus, the composition of the interstitial melt phase in the castable changes significantly with increasing distance from the contact. The composition of the original infiltrating basic slag changes due to assimilation of components of the castable, enhanced by alkali accumulation.

The infiltration depth of the modified slag is only a few mm. This can be explained by a decrease in the viscosity of the infiltrating slag due to the change in chemistry and the decrease in temperature along the thermal gradient. The Urbain model (Urbain 1987) can be used to estimate the temperature dependent viscosity of the three slag compositions within the relevant temperature interval at position 1. The results show that the viscosity increases as a result of the change in chemical composition, but the effect of the temperature drop along the thermal gradient (i.e. of the order of ~ 10 K/mm at position 1) is also significant. The dynamic viscosity of the slag therefore increases significantly with depth of infiltration.

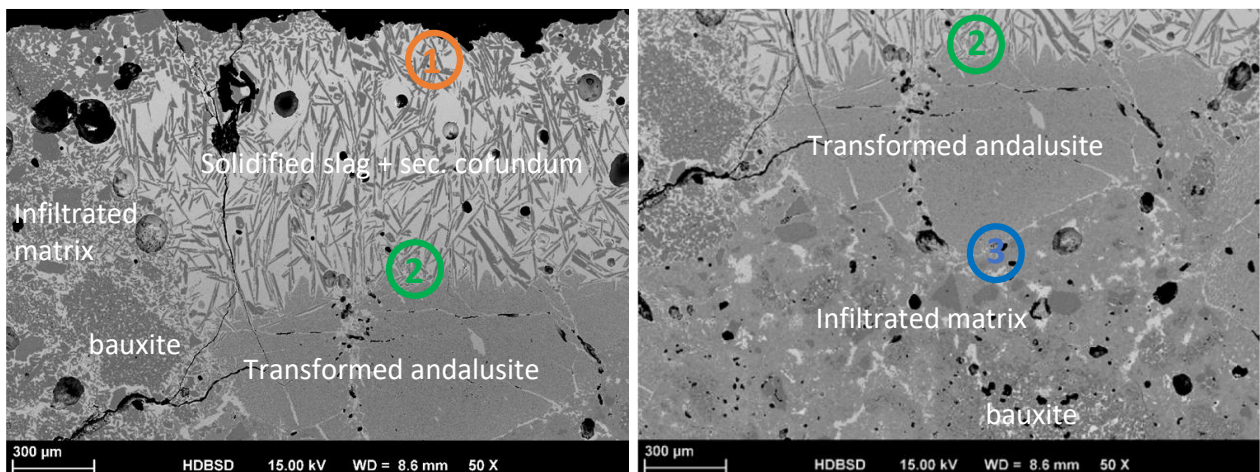


Figure 57: SEM images (BSE) of RR showing the areas as indicated in Figure 56, left micrograph Frame 1 and on the right frame 2. Within the circles with the numbers 1-3, the chemical composition of the solidified slag was measured by EDX. The solidified slag appears as bright, interstitial phase and the results are envisaged in Figure 58.

Oxide	slag 1	slag 2	slag 3
SiO ₂	40,7	53,6	61,8
TiO ₂	1,0	0,0	1,9
Al ₂ O ₃	33,1	30,6	23,8
Fe ₂ O ₃	4,0	0,8	2,0
CaO	10,3	3,9	1,6
MgO	3,9	0,8	1,0
MnO	0,7	0,3	0,0
Na ₂ O	2,4	7,0	1,9
K ₂ O	3,9	3,0	6,1
Sum	100,0	100,0	100,0

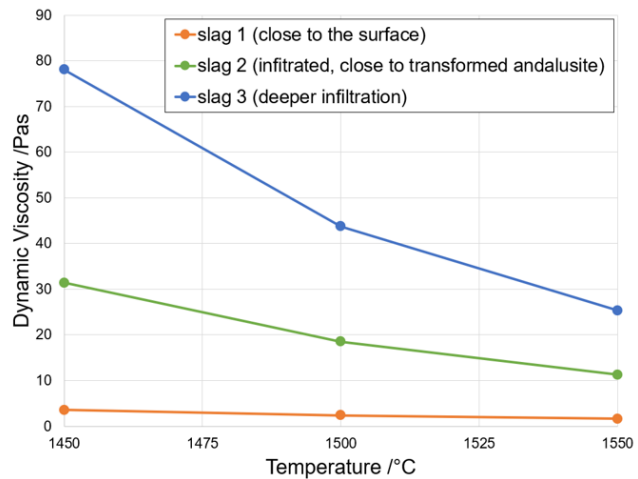


Figure 58: Compositions of the slags 1-3 (as indicated in

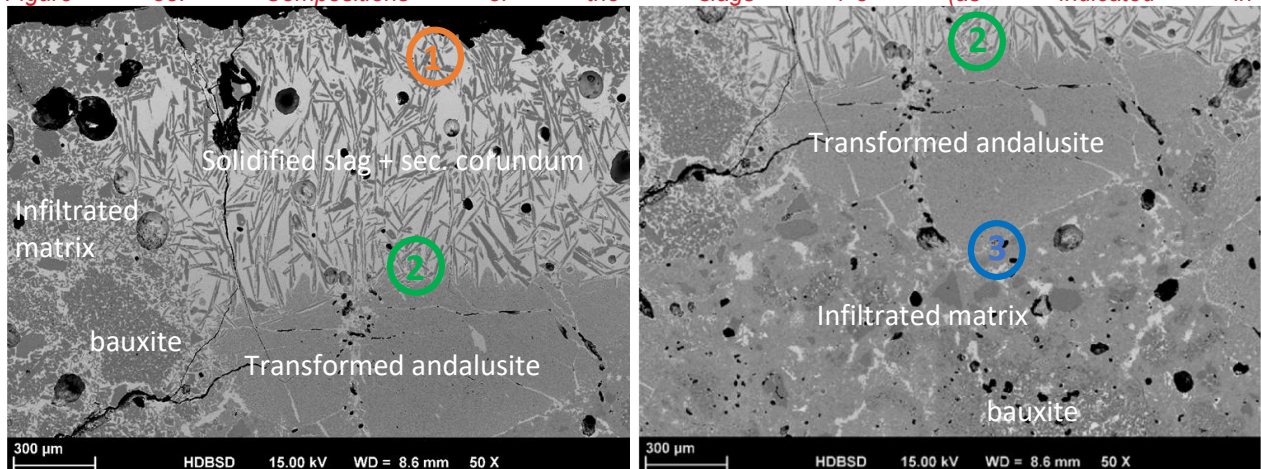


Figure 57, oxides in wt.-%) at different depths of infiltration and the corresponding calculated dynamic viscosities in the temperature range of relevance. The dynamic viscosity of the infiltrating slag 2 at the front side of a transformed andalusite grain is already about ten times higher compared with the more basic slag 1 at a position close to the surface, although the depth of infiltration of slag 2 is only about 1 mm. The slag 3 is situated behind the same transformed andalusite grain and the dynamic viscosity of slag 3 is further increased by the factor ~1,5. The black arrow in the diagram shows the estimated/schematic development of the slag viscosity during infiltration, influenced by changing chemical composition and cooling.

Figure 59 to Figure 72 summarize the results for the reference castables RE and RB. The corrosion phenomena found here are very similar to those previously described for RR. The only thing to consider here is that the cement adds CaO as an additional component of around 2.5 wt.-%. However, this does not fundamentally change the system, as CaO infiltrates through the slag into the castable in excess.

From the results of the corrosion test it can be concluded that the addition of andalusite increases the corrosion resistance of andalusite bearing castables by modifying the chemical composition of the infiltrating basic slag. The assimilation of andalusite (or transformed andalusite = mullite + SiO₂) increases the content of alumina and silica in the infiltrating slag, resulting in the crystallisation of corundum from the enriched, but still basic slag. In the course of infiltration and accompanied assimilation of andalusite, the silica content in the slag increases until mullite is formed by reaction with primary corundum from the castable. In addition, the increased silica content in the slag increases its viscosity. The formation of mullite and the increasing viscosity progressively obstruct the infiltration process. However, the migration of alkalis, especially K₂O, from the hot face into the castable is obvious and may be responsible for in-situ melting processes. In situ melt could mix up with infiltrating melt.

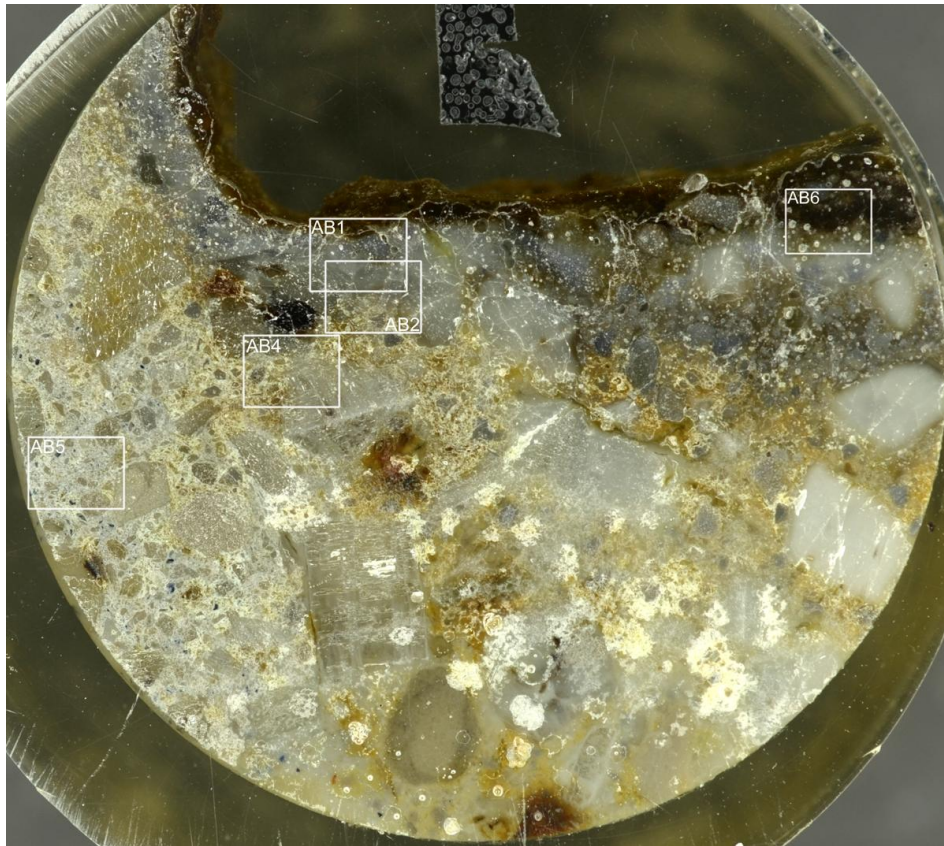


Figure 59: Polished section showing the polished section of RE at position 1 after the corrosion test. The 5 frames indicate the areas of SEM-images whereby AB1 and AB2 are envisaged in Figure 60 to Figure 66.

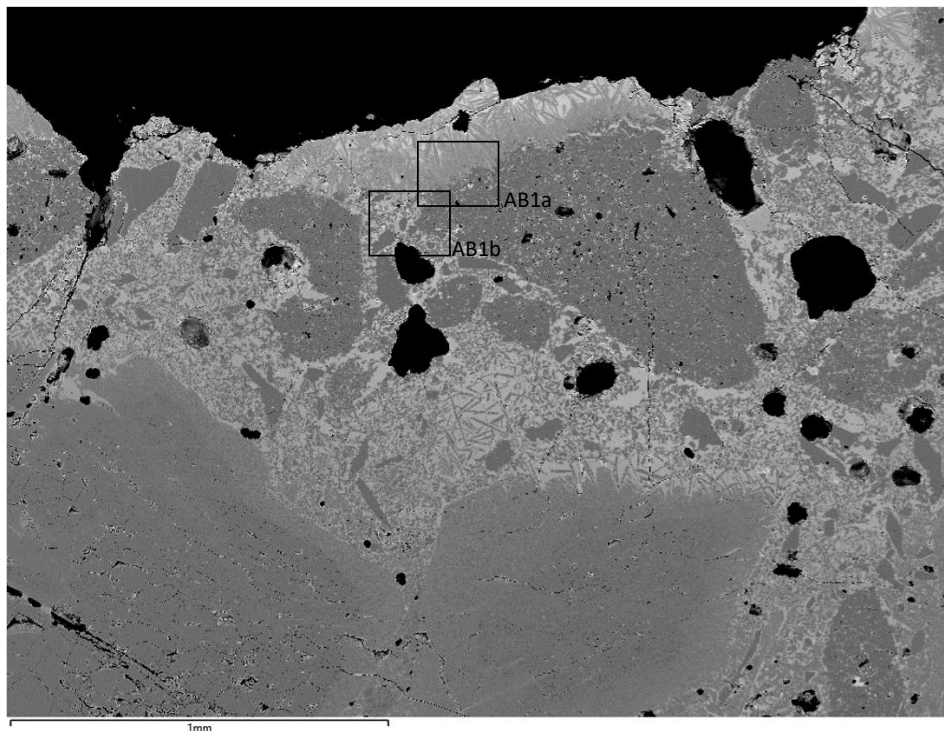


Figure 60: SEM image (BSE) of RE showing the area AB1 as indicated in Figure 59 (Magnification 25x).

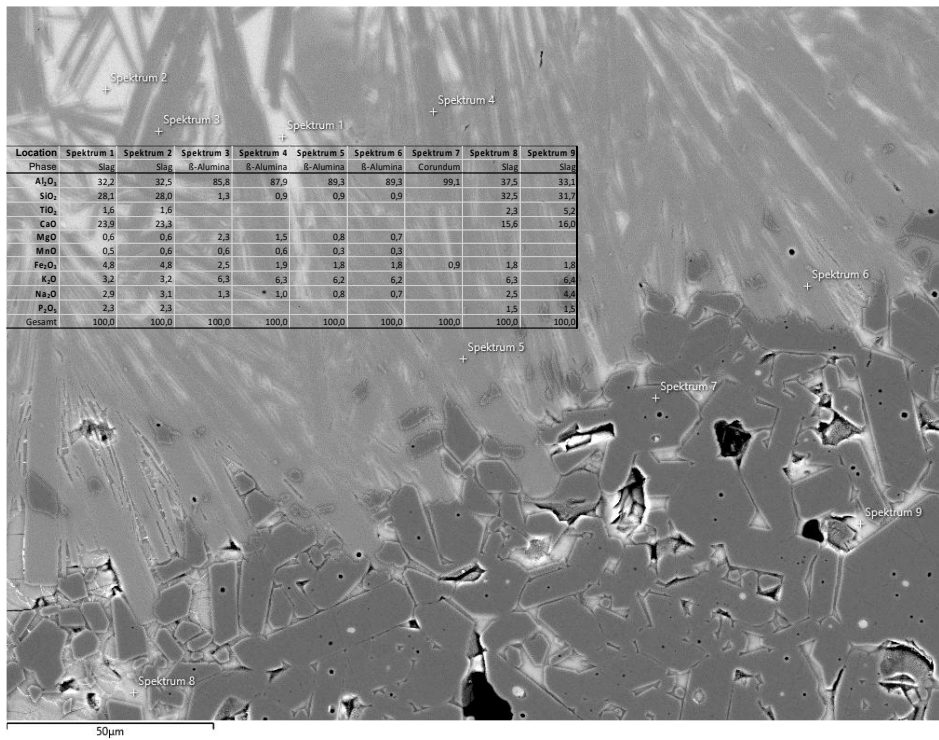


Figure 61: SEM image (BSE) of RE showing the areas AB1a as indicated in Figure 60 (Magnification 500x). At the contact: Bauxite (alumina) reacts with the basic slag under formation of diaoyudaite.

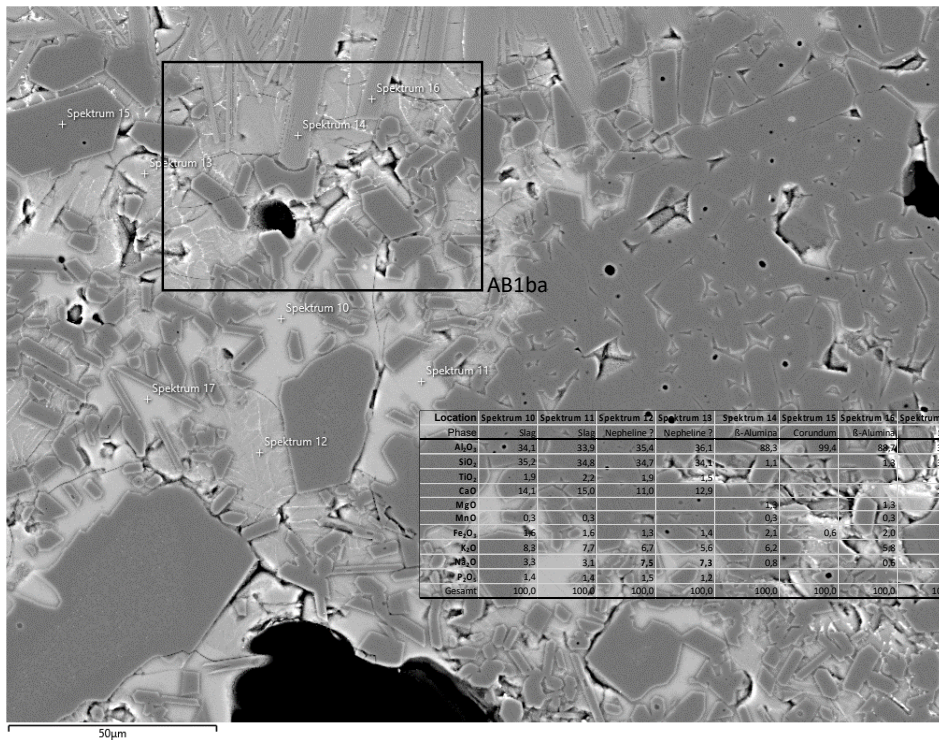


Figure 62: SEM image (BSE) of RE showing the areas AB1b as indicated in Figure 60 (Magnification 500x). Corundum is stable and forms euhedral crystals as well as diaoyudaite.

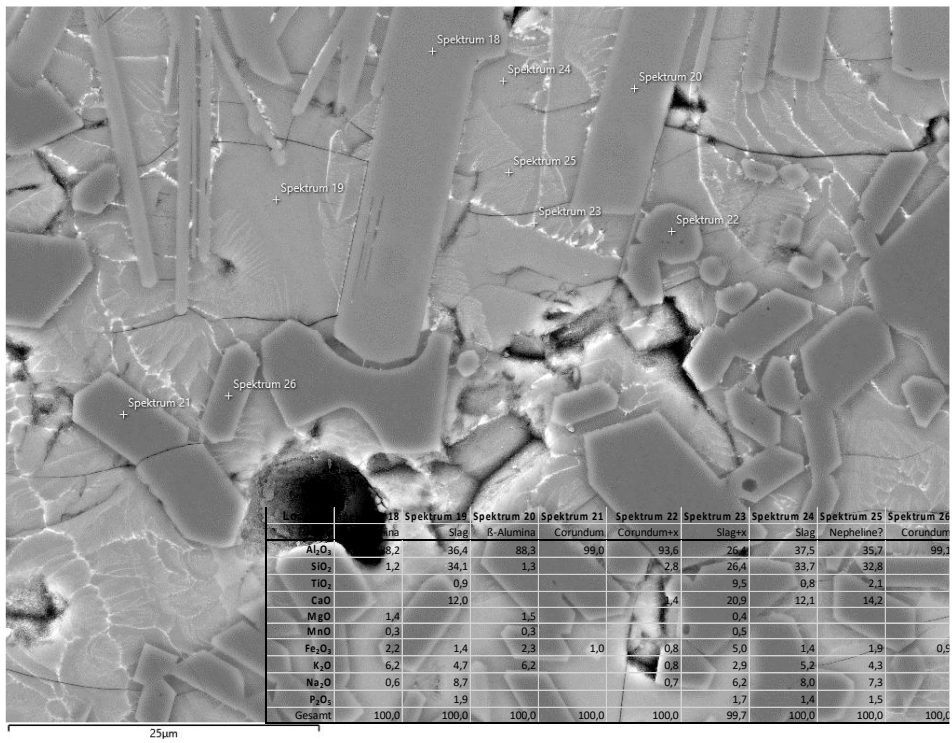


Figure 63: SEM image (BSE) of RE showing the areas AB1ba as indicated in Figure 62 (Magnification 1000x). Daoyudaoite replaces corundum if in direct contact.

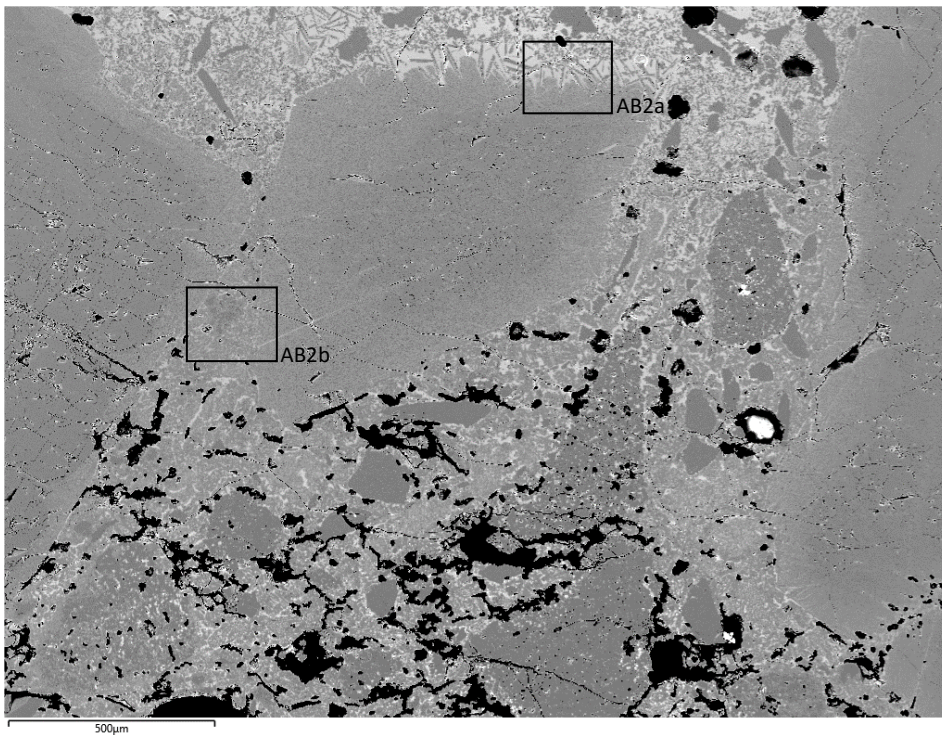


Figure 64: SEM image (BSE) of RE showing the areas AB2 as indicated in Figure 59 (Magnification 50x). The high contrast indicates the infiltrated slag.

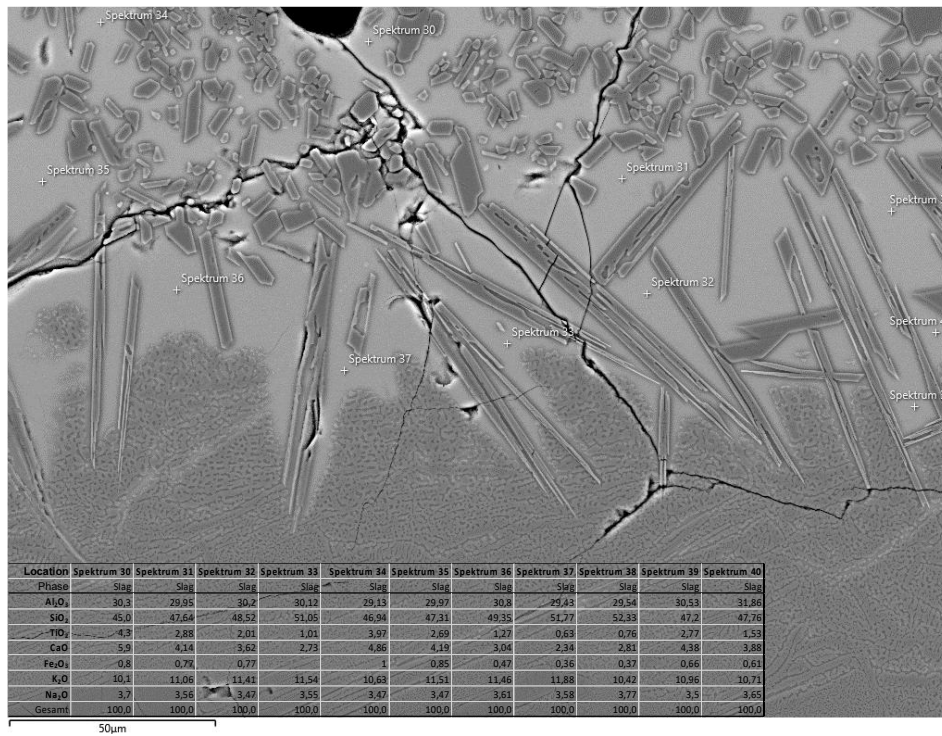


Figure 65: SEM image (BSE) of RE showing the areas AB2a as indicated in Figure 64 (Magnification 500x). At the bottom of the micrograph a large grain of decomposed andalusite is visible. In the slag that contains about 45 to 50 wt.-% SiO₂ corundum precipitates in euhedral thin platelets.

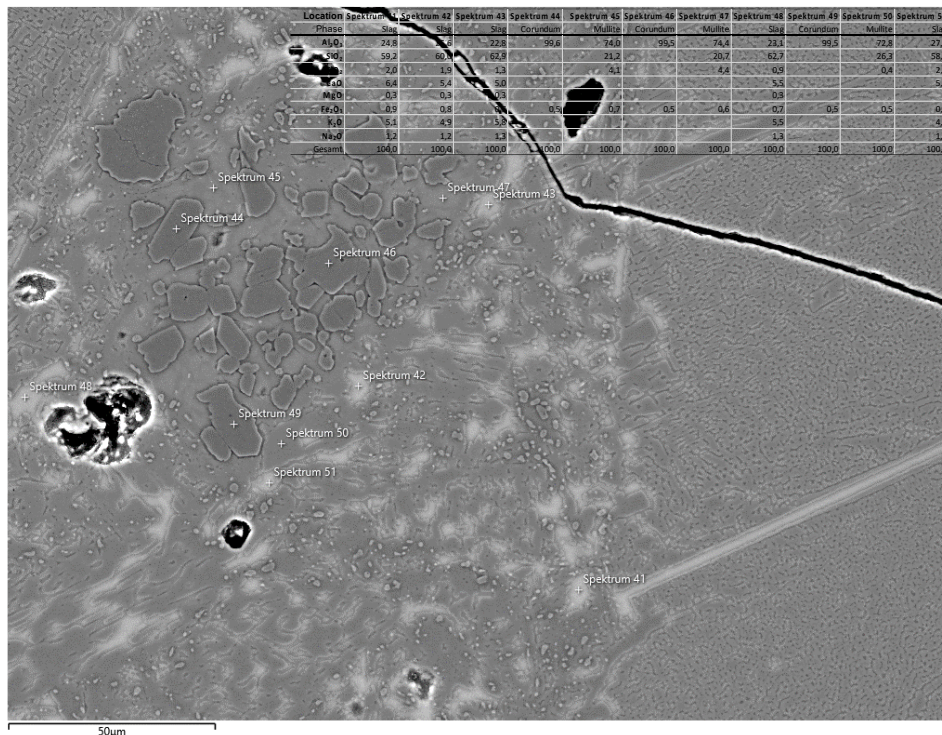


Figure 66: SEM image (BSE) of RE showing the areas AB2b as indicated in Figure 64 (Magnification 500x). On the left a large scaled decomposed andalusite grain is visible. The crystals on the left side with high relief are irregularly bounded and consist of corundum, which is no longer stable here because the slag is too acidic with over 60 wt.-% SiO₂. Mullite, which is precipitated from the melt, is stable in its place.

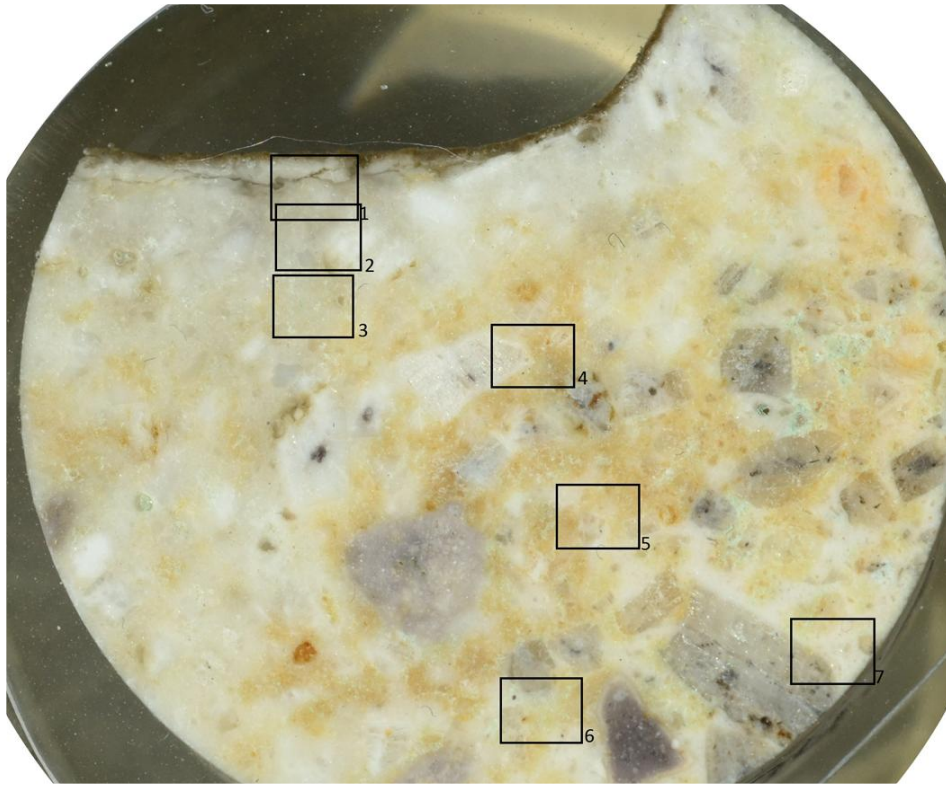


Figure 67: Polished section showing the polished section of RB at position 1 after the corrosion test. The 5 frames indicate the areas of SEM-images whereby AB1 and AB2 are envisaged in Figure 60 to Figure 66.

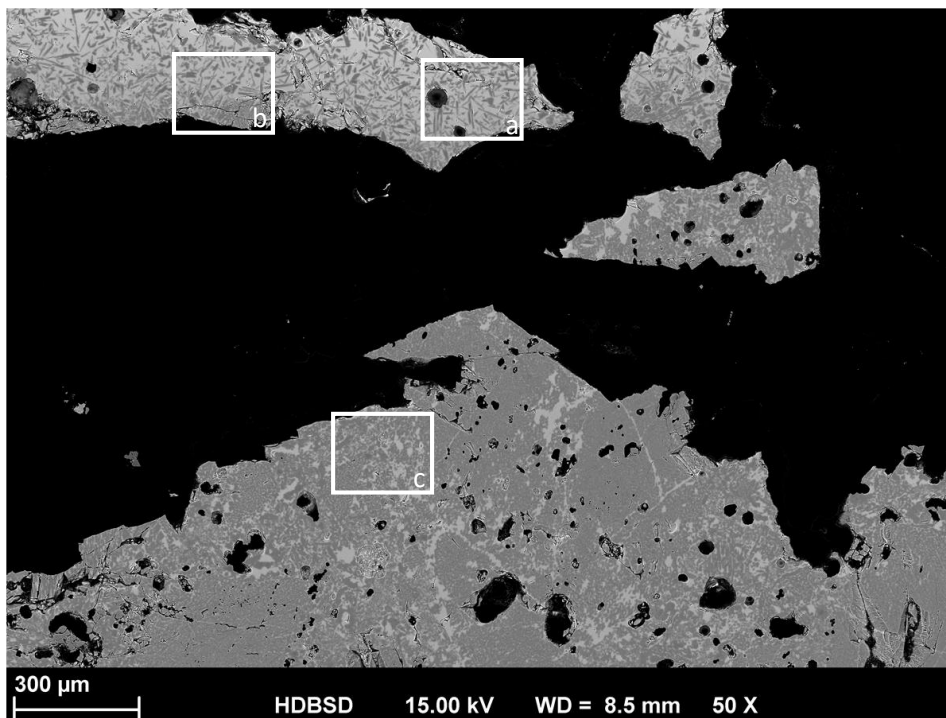


Figure 68: SEM image (BSE) of RB showing the area 1 as indicated in Figure 67 (Magnification 50x).

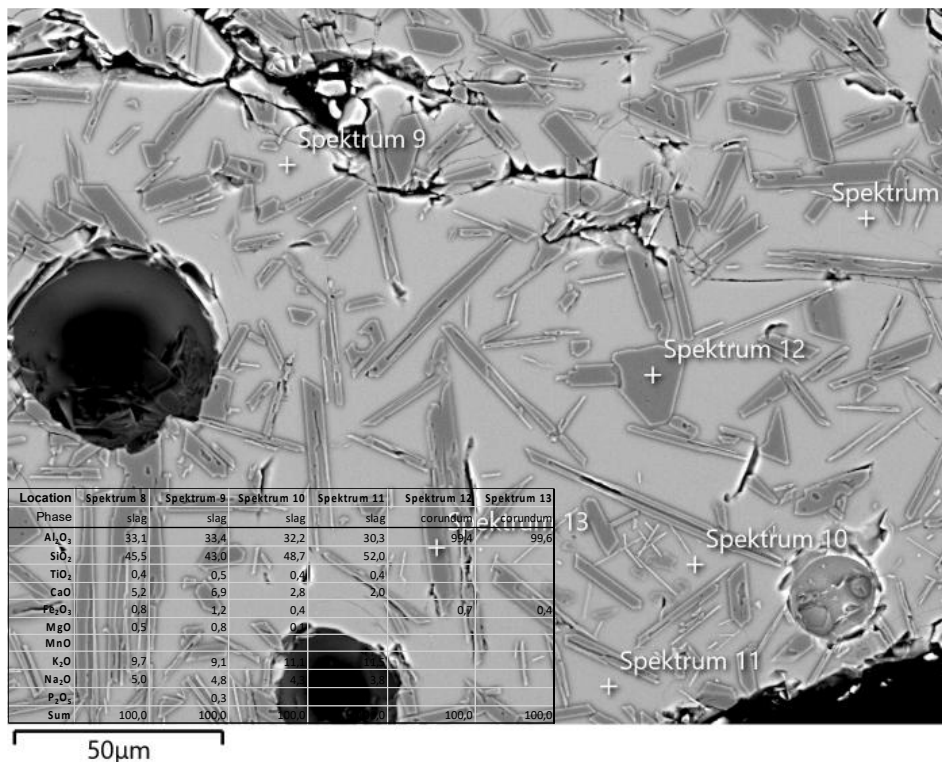


Figure 69: SEM image (BSE) of RB showing the area 1a as indicated in Figure 68 (Magnification 500x). Stable phase in the slag is corundum (euhedral crystals). In the slag, which has a low SiO₂ content of around 45 wt.-%, corundum is again precipitated as a stable phase as already shown in Figure 65.

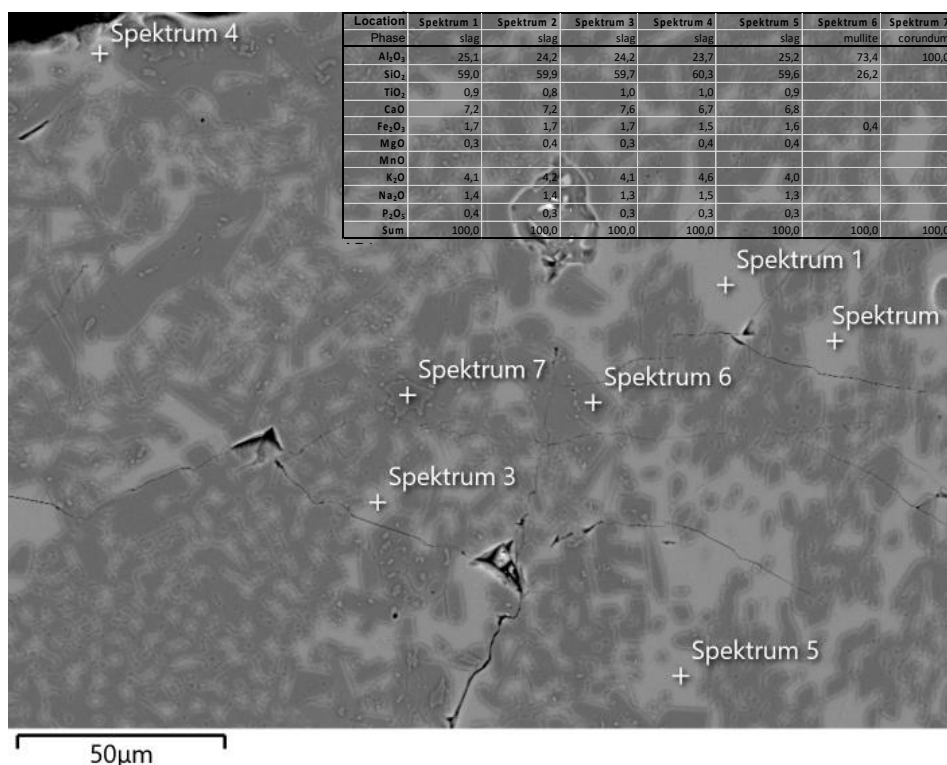


Figure 70: SEM image (BSE) of RB showing the area 1c as indicated in Figure 68 (Magnification 500x). An increase in the SiO₂ content of the slag in turn leads to mullite becoming a stable phase and displacing corundum as already envisaged in Figure 66.

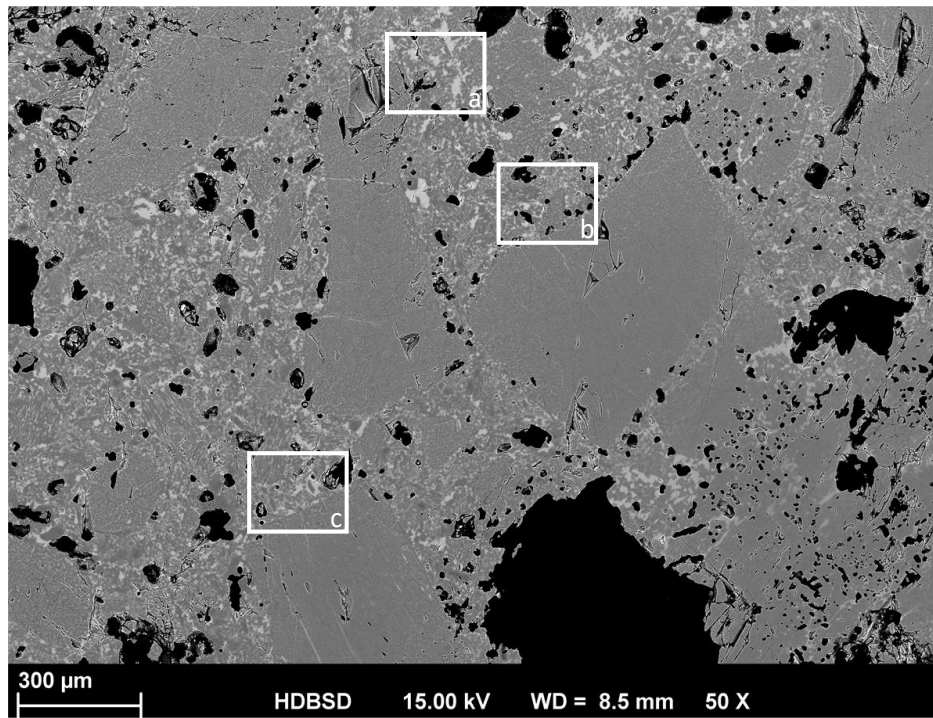


Figure 71: SEM image (BSE) of RB showing the areas 2 as indicated in Figure 67 (Magnification 50x).

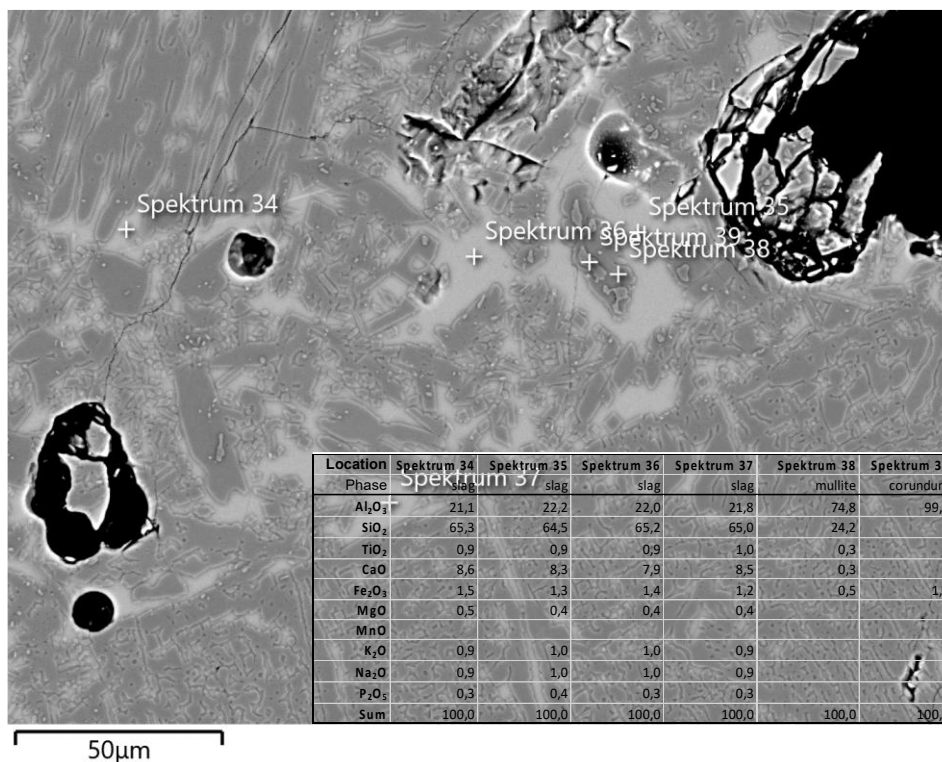


Figure 72: SEM image (BSE) of RE showing the area 2c as indicated in Figure 71 (Magnification 500x). With around 65 wt.-% SiO₂ in the slag, mullite is again the stable phase and forms euhedral crystals precipitating out of the slag.

5.3.4.3 Microscopic observations - Corrosion by volatile components

The decrease of temperature in the area of the chimney leads to a condensation of the volatile elements of the slag on the refractory materials of the chimneys. The lower third of the chimney was covered by a brownish layer (Figure 53). In the upper part, the layer turned from white to light blue. In the chimney, hematite Fe_2O_3 (brownish area in the chimney, see Figure 53), sulfides (thenardite Na_2SO_4 and blödite $\text{Na}_2\text{Mg}(\text{SO}_4)_2 \cdot 4\text{H}_2\text{O}$ and salts (sylvite KCl) were identified by Raman spectroscopy and SEM-EDX. The volatile elements of the slag formed layer of iron-rich btw. alkali-rich sulfides, depending on the temperature gradient in the chimney. An interaction between castable and these layers could not be detected which is most likely due to the low dwell time of four hours.

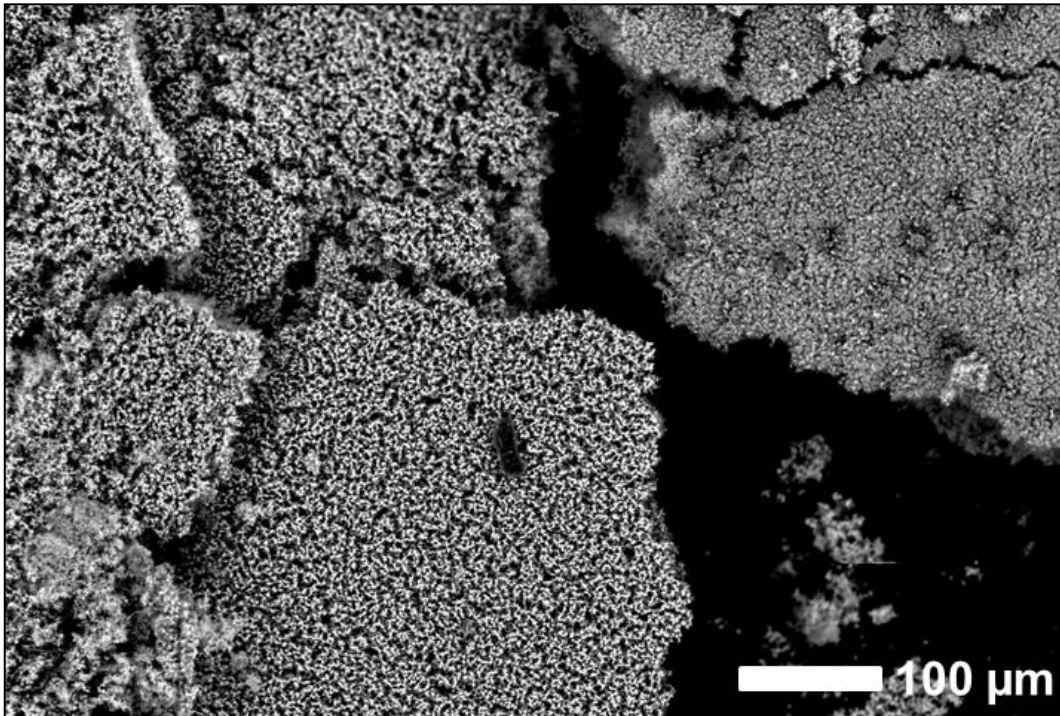


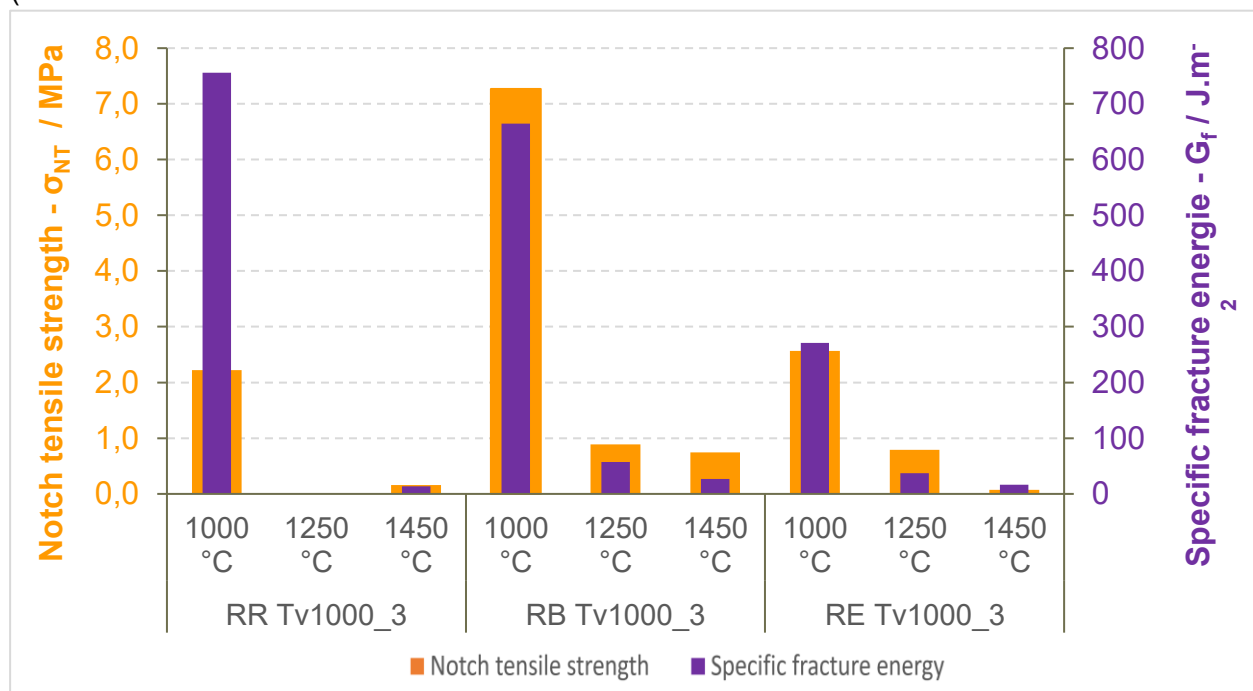
Figure 73: Flaky layer (potassium sulfate) from the upper light blue part of the chimney (red star in Figure 53).

5.4 Development of andalusite-free castables

In order to understand the behaviour of castables containing andalusite, the three reference castables were investigated in advance with regard to their thermal behaviour and corrosion properties. All three refractory castables were declared by the manufacturers to have outstanding thermal shock resistance, whereby the reference castables RR and RE are intended for application conditions between 1000 and 1700 °C and 1250 to 1600 °C respectively. For the reference castable RB, only an application temperature greater than 1200 °C is specified and is unlikely to come close to the two previously mentioned in terms of the application limit temperature, as the raw material selection was chosen to be less refractory in addition to andalusite. All products are preferably used in ferrous and non-ferrous metallurgy, in particular in discontinuously operating aggregates. Interacting corrosive media can be either basic or acidic.

The results presented so far show that melting phases are formed from 1300 °C and for RB from 1200 °C, which change the microstructure from a brittle to a ductile behaviour. The ductility can

also be easily recognised by the results of the creep under compression (creep) (Figure 50) and the notch tensile strength and specific fracture energy (



), which are barely measurable from around 1250 °C onwards. The NCC, RR, performs particularly poorly here, which is somewhat surprising as it is the only castable that forms mullite in the matrix instead of anorthite, which is generally expected to strengthen the microstructure. In general, the positive property of mullite formation and the high refractoriness derived from this should be critically reviewed based on the results presented here. In principle, it is unlikely that the materials can be used permanently at the intended application temperatures if they were used under isothermal conditions. This is also generally not the case, so that the high degree of melt formation in the castable only extends a few centimetres into the lining. It can be assumed here that this ductile layer acts like a protective layer and absorbs any thermal stresses introduced, which means that the stresses are not introduced into the still brittle area of the lining. It is well known that the high melting rate reported for all three castables under the specified working conditions also results in high shrinkage, which is counteracted using andalusite and kyanite, as these increase significantly in volume as they decompose. Any shrinkage cracks that occur are sealed. This initially creates the cosmetic impression of a well intact hot side, but also functionally prevents infiltration by process media. This also applies in particular to gaseous corrosive media, which cannot infiltrate, as the high degree of melting on the surface closes the open porosity of the lining like a glaze. Andalusite therefore acts as a shrinkage compensator during decomposition. The much-cited formation of an amorphous SiO₂ phase during the decomposition of andalusite is likely to play only a subordinate role here. In addition, it is also clear from the investigations presented here that andalusite fulfils the task of a shrinkage compensator better than kyanite, as the latter, as a high-pressure phase, decomposes with significantly higher reaction kinetics and the shrinkage compensation comes to a standstill earlier, causing the system to lose its function.

It can therefore be concluded that alternative raw material concepts must have similar functionality. On the one hand, the pronounced melt phase formation is inherent to the system in order to reduce thermally induced stress through ductile properties and to seal the surface, which significantly reduces the infiltration capacity. On the other hand, it is essential that the thermal

expansion of the andalusite is imitated by alternative systems, for example by the formation of new mineral phases that are more expansive than the reactants. This is where the decomposition of SiC under oxidising conditions comes in.

Model castables were developed that were intended to examine the mode of action of alternative raw materials and ultimately represent a feasibility study as to which raw materials lead to similar results as with andalusite-containing castables in a suitable combination and concentration.

To understand the thermal and kinetic behaviour of the substituting materials for andalusite in the matrix of high alumina refractory castables, the influence of fine andalusite with specific particle size and amount in high alumina low cement castable was investigated. A high alumina low cement castable was developed with adjusting the grain size distribution and additives in order to achieve castable with sufficient workability (flow and densification) and a sufficient strength evolution in green state. Furthermore, fine grain size of andalusite (Kerphalite) was added in constant amount (9 wt.-%) and specific grain size (0- 45 µm) as a part of the matrix components, while reactive alumina CTC20; RG4000 and cement forms the remained matrix components. The composition of the castable is presented in Table 15.

The mentioned offset variations were analysed with regard to their thermomechanical properties (creep and RUL) in order to make a further selection as to which offsets should be further processed. The backfills with kyanite, luting sand and SiC, whose thermal behaviour was investigated in depth, proved to be promising, whereby the focus here was on the description of the microstructure, the mineral phase analysis and MMH. While the latter provides an integral impression of the thermal behaviour, the samples for the former are thermally pre-treated.

Table 15: Andalusite-free model castable compositions. SiC, kyanite, luting sand, kaolinite and anorthite+kyanite replace tabular alumina in a suitable grain fraction by in total 9 wt.-%.

	MRC-S	MRC-K	MRC- L	MRC-KO	MRC-K/ANO
Component	wt.-%				
Tab. alumina (3-6 mm)	16.00	16.00	16.00	16.00	16.00
Tab. alumina (1-3 mm)	21.00	21.00	21.00	21.00	21.00
Tab. alumina (0.5-1 mm)	11.00	11.00	11.00	11.00	11.00
Tab. alumina (0.2-0.6 mm)	10.00	10.00	10.00	10.00	10.00
Tab. alumina (0-0.2 mm)	11.00	11.00	11.00	11.00	11.00
Tab. alumina (0-0.045 mm)		3.50		9.00	3.50
SiC	9.00				
Kyanite		9.00			6.00
Luting sand			9.00		
Kaoline				9.00	
Anorthite					3.00
CTC20	10.00	10.00	10.00	10.00	10.00
Microsilica	7.00	3.50	07.00	07.00	03.50
Secar 71	5.00	5.00	05.00	05.00	05.00

Sum	100.00	100.00	100.00	100.00	100.00
Water	5.00	5.00	6.60	09.00	05.70
Dispersing agent (FS20)	0.10	0.10	0.15	0.15	0.10

The primary objective of incorporating andalusite was to investigate its role in the castable matrix, analysing its thermal behaviour and mechanical properties. Based on these investigations, substitution materials were selected to replace the andalusite portion within the castable matrix. This allowed for further analysis and investigation of the thermal behaviour and mechanical properties of the model castables.

The model castables with andalusite or a substitution material were designed with a high alumina concentration, similar to andalusite (alumina > 65 wt. %). Tabular alumina with different grain sizes was introduced as aggregates. High alumina concentrations are necessary to achieve sufficient refractoriness between 1250 and 1500 °C to meet the requirements of the typical applications. The water content was set to 6 wt.-% to ensure sufficient workability and setting properties.

Model refractory castable with 9 wt.-% of the substitute; silicon carbide (MRC-S), kyanite (MRC-K), luting sand (MRC-L), kaolinite (MRC-KO), kyanite + anorthite (MRC- ANO /K) were produced.

5.4.1 Raw materials and recipes

The model castable contained different grades of tabular alumina (T60/64) sourced from Almatix GmbH in Ludwigshafen, Germany (Table 16 and Table 17). These grades were selected for their exceptional purity and expected uniformity. In addition, the binding phase for the cement-bound castables was provided by Kerneos GmbH of Oberhausen, Germany (Secar 71). Microsilica 971U was used from Elkem AS, Oslo, Norway. Dispersants for the castables were FS60 and FS20 from BASF SE, Ludwigshafen, Germany.

As an alternative to andalusite, the following materials from Germany were used: Silicon carbide from ESK-SiC GmbH in Frechen, kyanite from Refratechnik Steel GmbH in Bendorf, anorthite from Franz Mandt GmbH und Co. KG in Wunsiedel, kaolin (R125) from Hans Wolbring GmbH and luting sand from EKW GmbH.

Table 18, Table 19, and Table 20 show the chemical analysis of the selected substitutes for andalusite. All these materials expected to have the ability to provide SiO₂ for a highly viscous silica melt phase and for the formation of mullite.

Table 16: Reactive alumina CTC20, RG 4000 and cement Secar 71 used and classified by specific surface area, particle size, particle size distribution, and chemical analysis, manufacturer's specifications.

Properties / methods		CTC20	RG 4000	Secar 71
Particle size distribution		Typ.	Typ.	Typ.
Specific surface area / BET	m ² /g	2.10	7.2	
Particle size / d50-Cilas	µm	1.8	0.6	8-63
Chemical analysis				
Al ₂ O ₃	%	99.7	99.8	68.7-70.5
MgO	%	-	-	< 0.5
Na ₂ O	%	0.12	0.08	< 0.5
Fe ₂ O ₃	%	0.03	0.02	0.10 – 0.3
SiO ₂	%	0.03	0.03	0.2 – 0.6
CaO	%	0.02	0.03	28.5 – 30.5

Table 17: Fine grain tabular alumina raw materials used, classified by grain size, grain size distribution and chemical analysis, manufacturer specifications.

Properties / methods	T60 0 - 0, 045		T60 0 – 0,2		T60 0,2 – 0,6		T60 0,5 - 1		T60 1,0 – 3,0		T60 3,0 – 6,0			
	typ.	max.	typ.	max.	typ.	max.	typ.	max.	typ.	max.	typ.	max.		
Particle size	mm		0.045		0.2		0.60		1,00		3.00		6.00	
Chemical analysis			-		-				-		-			
Al ₂ O ₃	%	99.10	99,50	-	99,50	-	99.50		99,50	-	99,50	-		
MgO	%	-	-	-	-	-	-		-	-	-	-		
Na ₂ O	%	-	0.60	-	0.40	-	0.40	-	0.40	-	0.40	-	0.40	
Fe ₂ O ₃	%	-	0.03	-	0.02	-	0.02	-	0.20	-	0.02	-	0.02	
SiO ₂	%	-	0.12	-	0.09	-	0.09	-	0.90	-	0.09	-	0.09	

Table 18: Kaolin and Anorthite as substituting raw materials classified after chemical analysis, producer's specification.

Material	Al ₂ O ₃	SiO ₂	Fe ₂ O ₃	TiO ₂	CaO	MgO	Na ₂ O	K ₂ O	P ₂ O ₅	V ₂ O ₅	LOI (loss on ignition)
	wt.-%										
Anorthite	26.50	57.60	0.54	0.00	7.13	0.34	5.98	1.22	-	-	0.3
Kaolin R125	34.3	50.4	0.5	0.4	-	-	0.2	1.9	-	-	11.5 (1000 °C)
Kyanite	56.99	40.94	0.51	1.17	0.01	0.01	0.01	0.05	0.10	0.06	0.21

Table 19: Silicon carbide raw material classified after chemical analysis, producer's specification.

Description (substance)	SiC	C _{free}	Si _{free}	Al ₂ O _{3 free}	CaO _{free}	Fe ₂ O ₃	Fe _{ferro}
Fractions (Wt.-%)	98	0.3	0.7	0.2	0.1	0.1	0,1

Table 20: Luting sand raw material classified with XRD mineralogical analysis.

Quartz	84 wt.-%
Kaolinite	16 wt.-%

5.4.2 Castable preparation and mixing design

In the formulation of the model castables with selected substitutes, a graded tabular alumina was used as the refractory aggregate with the following weight percentages 16 wt.-% (3-6 mm), 21 wt.-% (1-3 mm), 11 wt.-% (0.5-1 mm), 10 wt.-% (0.2-0.6 mm) and 11 wt.-% (0-0.2 mm). In order to investigate the thermal and kinetic behaviour of the selected replacement materials within the castables, the fine andalusite fraction in the matrix of the model castable with andalusite addition (Table 15) was replaced by a constant amount of the new materials (SiC, luting sand, kaolin, anorthite and kyanite) at 9 % by weight and with a particle size range of 0-0.045 mm (Table 15). In addition, the fifth castable was formulated by combining anorthite and kyanite in a ratio of 1:2, allowing the combined effect of the two materials in the matrix to be studied. Fine reactive CTC20 alumina and microsilica were added to improve the properties of the castables. The binding phase was achieved using cement (Secar 71), while FS60 and FS20 were used as dispersants. All castables were prepared with an appropriate amount of deionised water to ensure good flowability. This should be emphasised in particular for the variation with kaolinite, as here the water content had to be increased from 5 to 9 wt.-%.

The castables were dry mixed in an intensive mixer with stick agitator and simultaneous rotation for mixes ≤ 4 kg and star agitator and counter rotation for mixes ≥ 4 kg for one minute at the lowest speed. Immediately after water addition, the speed was increased to 450 rpm and wet mixing continued for a further 4 minutes. All test-pieces for the different methods of analysis (RUL, creep, wedge splitting, MMH and channel slag test) were cast in moulds with the same

dimensions as the reference castables as described in Chapter **Fehler! Verweisquelle konnte nicht gefunden werden.** The test-pieces were kept in a climatic cabinet for 48 hours at 20 °C and 95% relative humidity. The test-pieces were then dried to constant mass at 110 °C in a heating cabinet.

5.4.3 Thermal and mechanical behaviour of andalusite-free model castables

To establish a correlation between the signals in the MMH-curves and discrete phase changes, we subjected samples to a controlled heating process, with the same rate used in MMH, up to specific predefined temperatures. Subsequently, we conducted a cooling process. This approach enables a direct comparison of the Refractoriness under load (RUL) with phase changes detected by MMH at distinct temperatures (Figure 77). Additionally, Table 21 presents the main thermo-mechanical properties (D_{max} , T_{Dmax} , $T_{0.5}$, T_1 , T_2 and T_5) of the model castables that obtained from RUL results. Subsequently, XRD and SEM analyses were conducted on the samples to elucidate modifications in their mineralogical and microstructural properties.

Table 21: Main thermo-mechanical properties of the model castable derived from Refractoriness under Load (RuL) measurements according to DIN EN ISO 1893.

		MRC-S	MRC-L	MRC-K	MRC-ANO/K	MRC-KO
D_{max}	%	0.987	0.835	1.11	0.748	0.62
T_{Dmax}	°C	1255	1237	1284	1084	1033
$T_{0.5}$	°C	1325	>1700	1465	1310	1161
T_1	°C	1375	>1700	1485	1425	1425
T_2	°C	1595	>1700	1500	1443	1578
T_5	°C	1685	>1700	1535	1468	1636

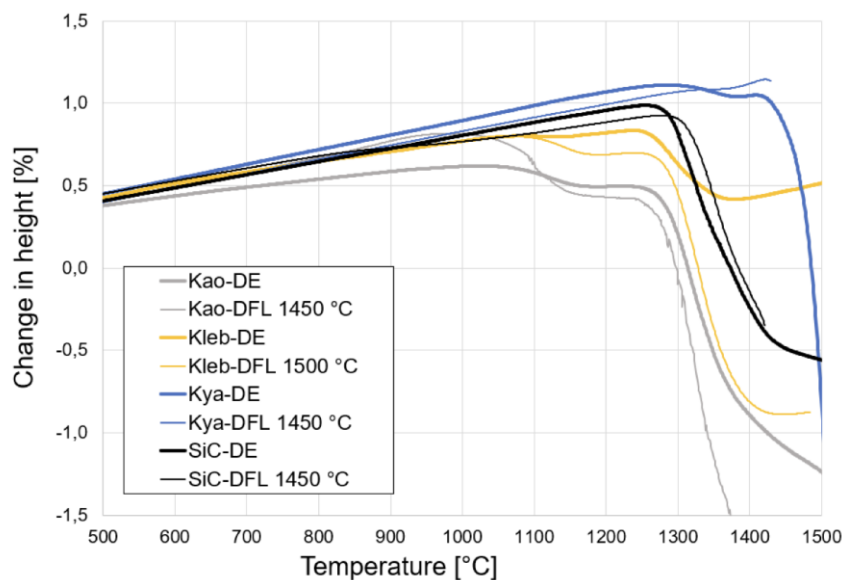


Figure 74: Refractoriness under load (RUL) measured for the model castables, kaoline, luting sand, kyanite and SiC. The samples were pre-fired for 1 h at 1000 °C.

Figure 75 shows that the reference castables exhibit significantly better volume stability, at least at first glance. However, it can also be seen that the model castable containing SiC in particular has the lowest creep and that luting sand and kyanite flow in a similar order of magnitude. At the test temperature of 1450 °C, the model castable with anorthite proved to be thermally unstable and was therefore no longer pursued.

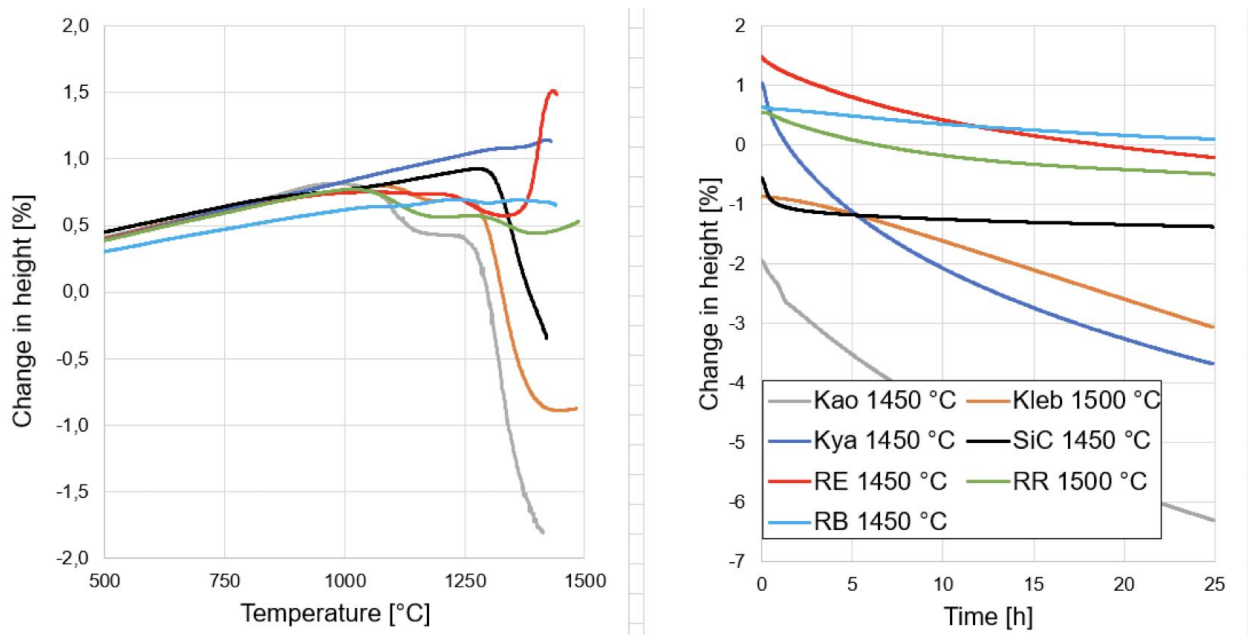


Figure 75: Refractoriness under load (RUL) measured for the model castables, kaoline, luting sand, kyanite and SiC. The samples were pre-fired for 1 h at 1000 °C. Creep was performed at a temperature of 1450 °C. In addition, the diagrams depict the results obtained for the reference castables as already envisaged in Figure 26.

5.4.3.1 Model refractory castable with luting sand addition (MRC-L)

At 1100 °C, the presence of ceramic bonding in MRC-L was observed, accompanied by the formation of shrinkage cracks in the matrix (Figure 76). Upon reaching 1200 °C, melting occurred, resulting in the rounding of pores, and the presence of cement grains identified as calcium aluminate (CA) and CA₂. The temperature increased to 1300 °C, intensifying the formation of a melt phase. The first signs of mullite formation, anorthite, and remnants of cement grains (CA₂) were also detected. Subsequently, at 1400 °C, significant melt formation was observed, accompanied by the corrosion of corundum and the formation of mullite. Localized growth of corundum was evident in the lower right region of the sample. By 1500 °C, corundum remnants, mullite, anorthite, and solidified residual melt were present, with the cement grains being fully assimilated. Quartz grains transformed into cristobalite, while intensive mullite formation (medium grey) occurred at the expense of corundum (prominent), overlapped by the crystallization of anorthite (light grey ribs), which likely occurred during the cooling process.

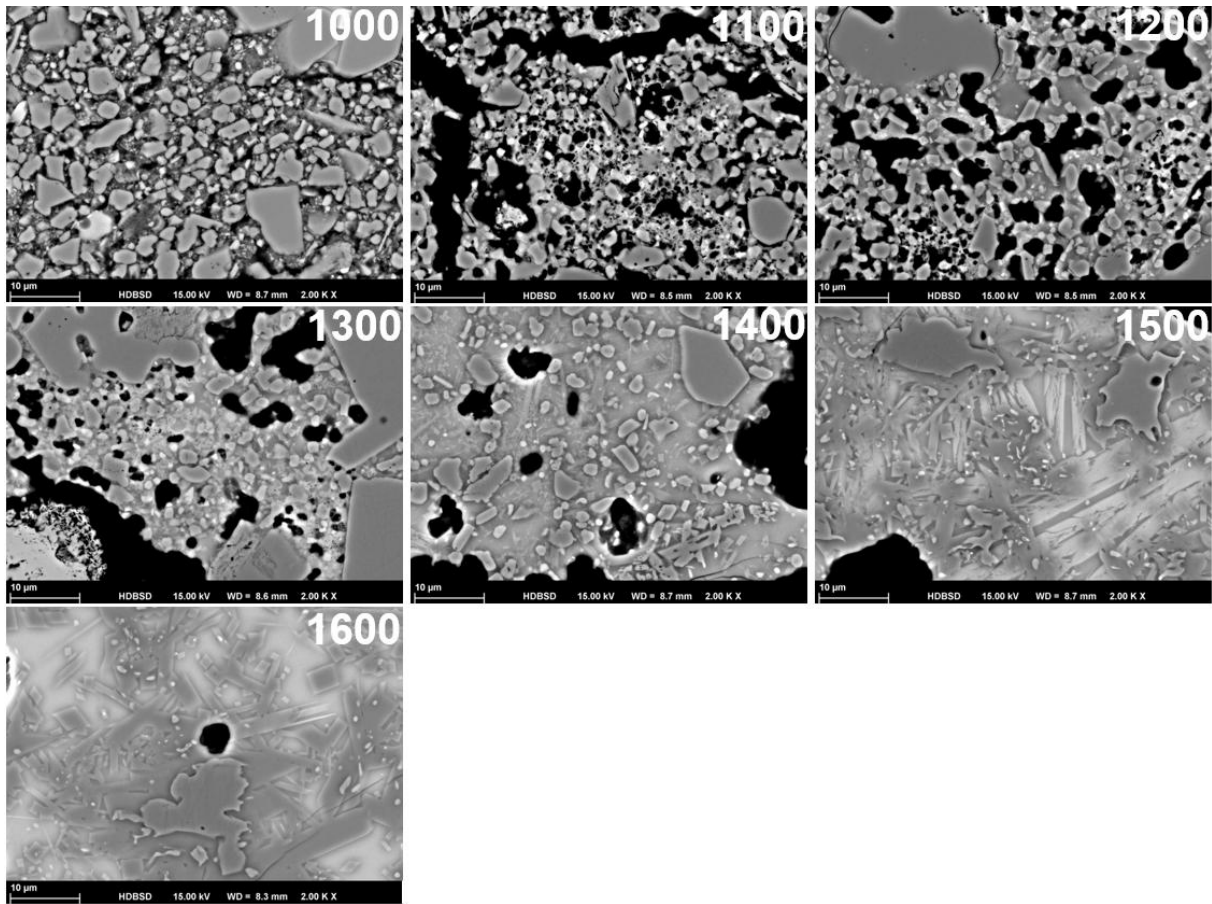


Figure 76: Evolution of the microstructure of the model castable MRC-L with luting sand depending on the temperature of the thermal treatment. The matrix of MRC-L is significantly finer grained due to the small grain size of the luting sand than the other model castables.

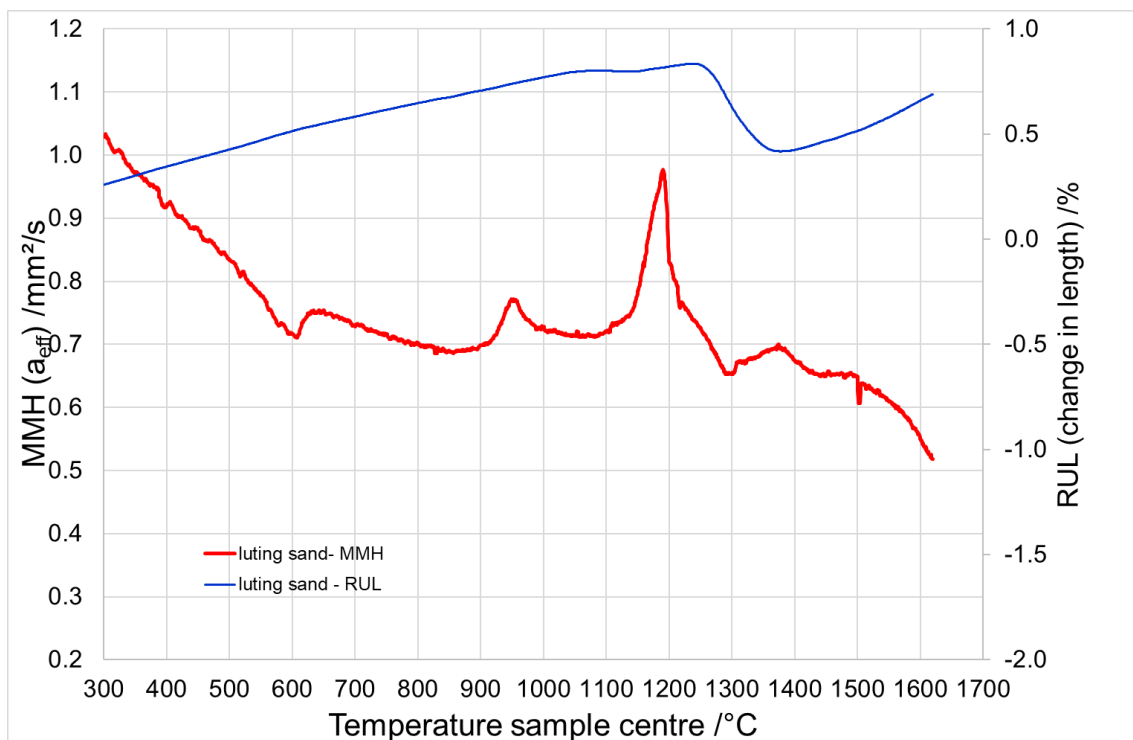


Figure 77: Results of MMH (red curve) and RUL (blue curve) obtained for the low cement model castable with Luting sand addition. The test-pieces for RUL were pre-fired at 1000 °C for 1 h before the test.

In the model castable with addition of luting sand, MRC-L, the thermal analysis revealed noteworthy reactions within specific temperature ranges. Between 500 and 600 °C, the MMH-curve displayed an endothermic peak which indicated the presence of reaction. The literature reveals that within this temperature range, kaolinite undergoes a process of dehydration and dehydroxylation, resulting in the formation of amorphous meta-kaolinite through an endothermic reaction.

Between 900 and 1200 °C, significant exothermic reactions were observed in the MMH curve (Figure 77) that could be attributed to the sintering process. Mineralogical and microstructural analysis revealed that mullite crystals began to emerge with the gradual elevation of the castables firing temperature (Figure 76 und Figure 78).

At 1300 °C, the MMH curve displayed another rising segment, coinciding with an expansion in the RUL curve beyond 1300 °C. The comparison of this expansion in RUL with the rise in the MMH curve around 1300 °C suggests that significant mullitisation began at approximately 1300 °C. Simultaneously, XRD analysis indicated an increase in the quantity of mullite around this temperature, along with a decrease in corundum content (Figure 78), which could be attributed to mullite formation in the castable. Moreover, the emergence of anorthite crystallization was observed in SEM photos, most likely as a consequence of the material cooling down.

As the heating process progressed, there was an increase in the liquid phase which attacked mullite and decreased its stability, consequently leading to anorthite and corundum crystallization during the cooling process of the castable as observed in SEM. The decline observed in the MMH curve above 1400 °C aligns with these observations.

Additionally, a decrease in the refractoriness (RUL) curve, indicating softening, occurred around 1200 °C and could be associated with the formation of a molten phase within the castable. Beyond 1400 °C, the refractoriness was re-established, mainly due to mullite formation from the components SiO₂ and Al₂O₃ in the matrix. This was evident in the increased values of T_{0.5}, T₁, T₂, and T₅, which extended beyond 1700 °C. These observations correlated with XRD results, showing an increase in mullite content and a decrease in corundum content above 1400 °C.

Figure 78 also shows, however, that the reactions mentioned are still kinetically inhibited at the temperatures indicated. Thus, after a thermal pre-treatment time of 8 hours, the mullite increase at 1400 °C is 13 wt.-% higher than without a holding time and the maximum yield in the latter case is not reached at 1500 but only at 1600 °C. After thermal pre-treatment, it becomes clearer that the formation of mullite also consumes corundum. The content is reduced from 86 to 76 wt.-% after 8 hours at a pre-treatment temperature, which is around 8 percentage points less than after pre-treatment at 1630 °C without holding time. In the presence of SiO₂, introduced by the luting sand, diaoyudaoite is not stable and begins to decompose at 1000 °C. Na₂O is absorbed here into an early melting phase, which is already recognisable from Figure 76 at 1100 °C.

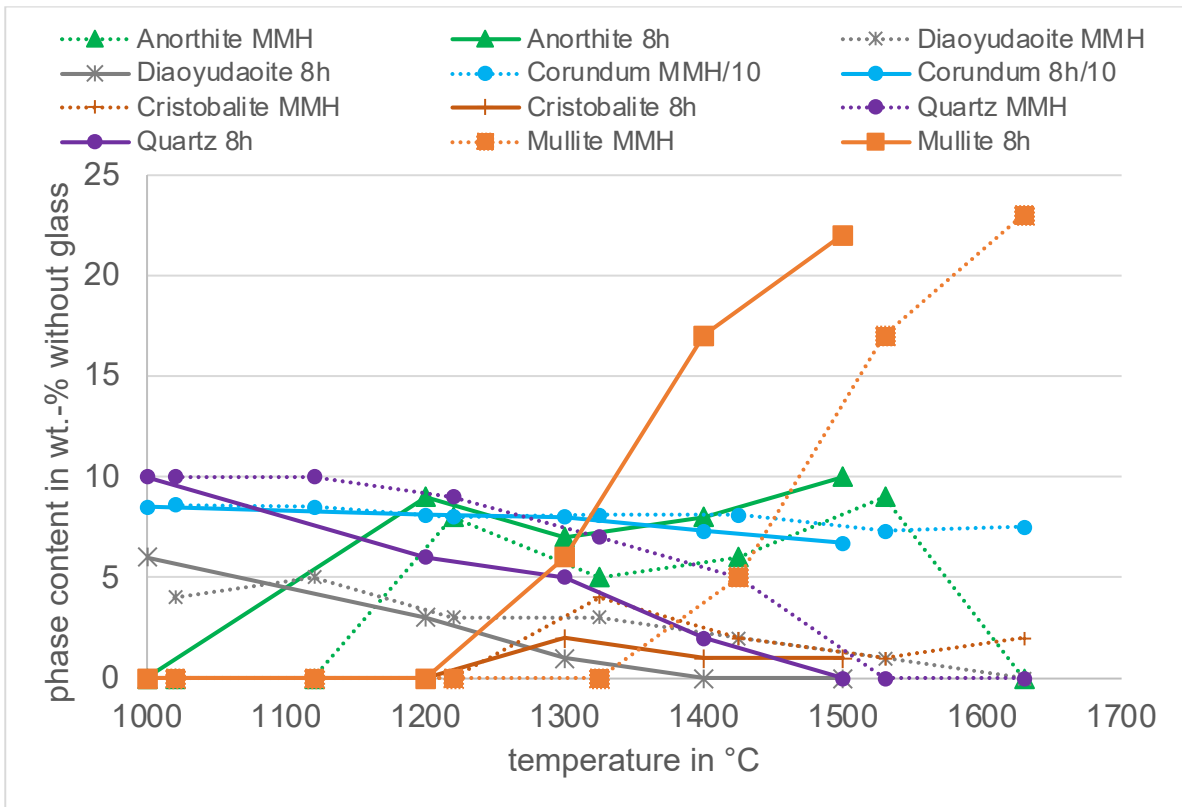


Figure 78: Rietveld analysis of phase content in model castable, luting sand. The results were calculated without considering the glass content, which increases considerably with temperature. The diagram shows the results for model castable, luting sand, treated for 8 hours at 1000, 1200, 1300, 1400 and 1500 °C (solid lines) and with no holding time simulating MMH. The corundum concentration is given by a value divided by 10 to keep the diagram clear and to better visualise smaller concentrations.

5.4.3.2 Model refractory castable with SiC addition

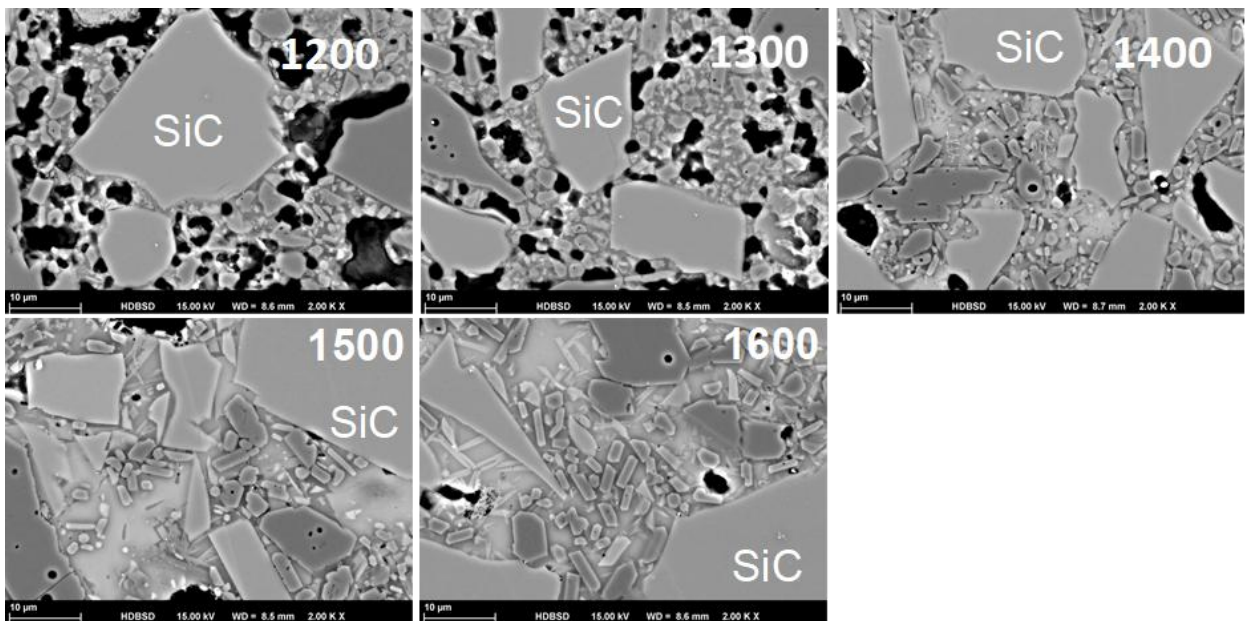


Figure 79: Evolution of the microstructure of the model castable MRC-S with SiC depending on the temperature of the thermal treatment.

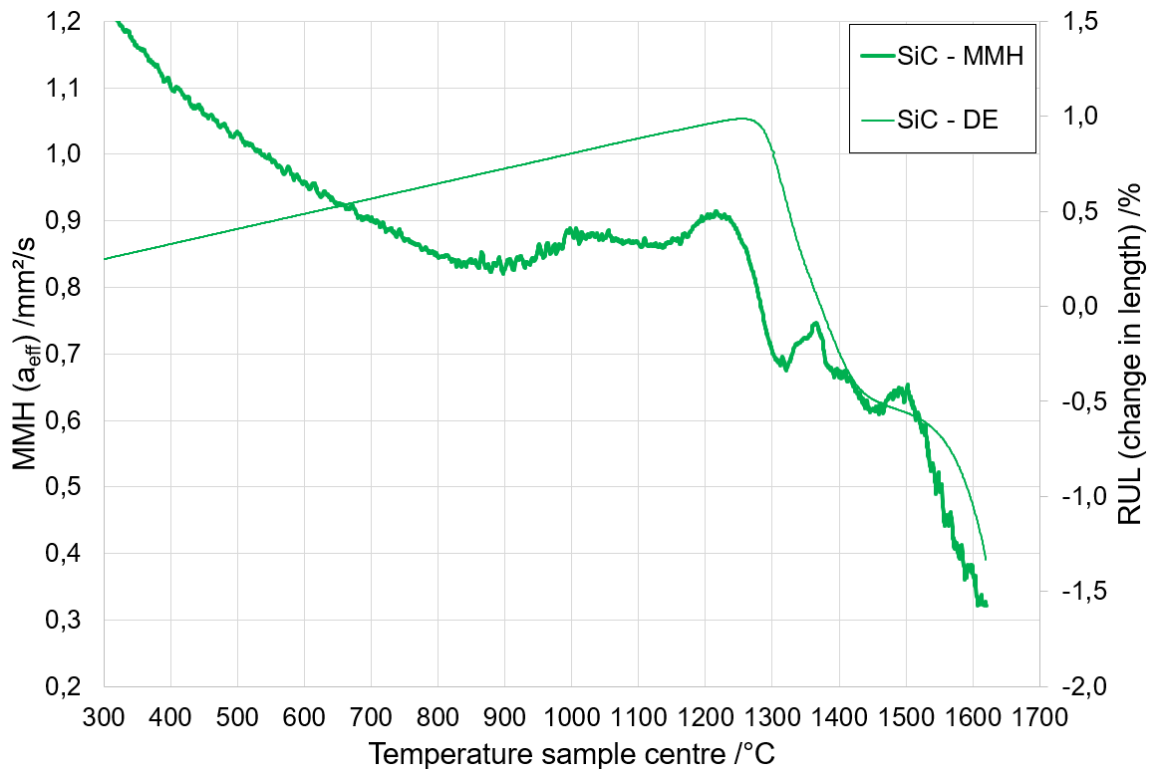


Figure 80: Results of MMH and RUL obtained for MRC-S. The test-pieces for RUL were pre-fired at 1000 °C for 1 h before the test.

According to the MMH curve in Figure 80, no noticeable changes were observed in the model refractory castable contained SiC (MRC-S) until reaching 1100 °C. However, the XRD analysis (Figure 81) revealed a slight decrease in corundum content and the formation of anorthite crystals within the matrix between 1100 °C and 1200 °C. These XRD findings indicate that reactions might have occurred between the cement and the alumina-silica components in the matrix, resulting in the formation of a melt phase. Subsequently, anorthite crystals likely crystallized from the melt during the cooling process. The SEM observations at 1200 °C showed that corundum particles are enveloped by a molten phase, resulting in rounded pores. In contrast, the SiC grains did not exhibit significant transformation and still show flat surfaces as typical for this raw material. An exothermic peak appeared in the MMH curve between 1150 °C and 1250 °C, suggesting the existence of a second reaction during this temperature range. Nevertheless, the XRD results did not reveal significant alterations within the same range. This discrepancy could potentially be ascribed to specific reactions happening within the material and the creation of ceramic bonds. The SEM results (Figure 79) lend further support to these findings.

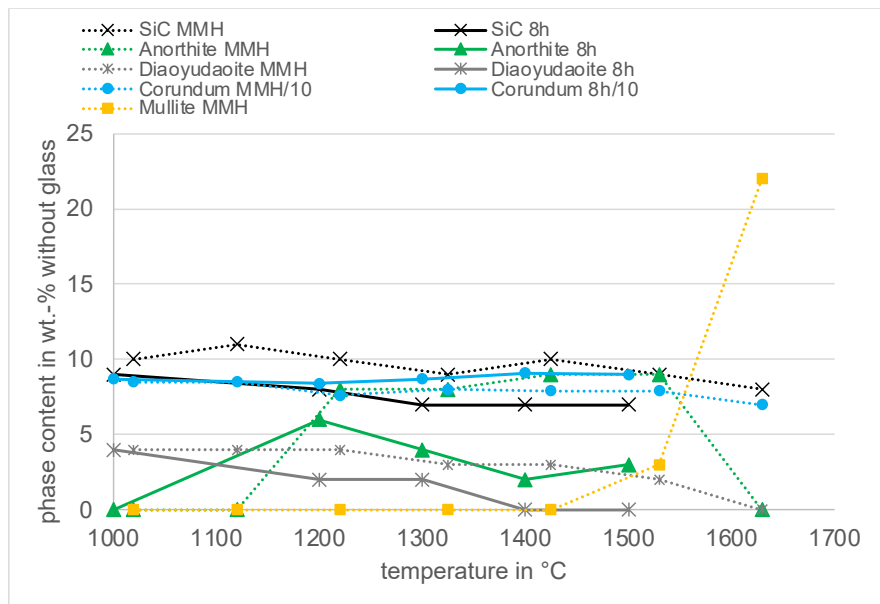


Figure 81: Crystalline phase content of the model castable with SiC determined by Rietveldt. The results were calculated without considering the glass content, which increases considerably with temperature. The diagram shows the results for model castable, SiC, treated for 8 hours at 1000, 1200, 1300, 1400 and 1500 °C (solid lines) and with no holding time simulating MMH. The corundum concentration is given by a value divided by 10 to keep the diagram clear and to better visualise smaller concentrations.

As the heating temperature was raised to 1400 °C, there was an increase in the quantity of the melt phase present in the castable. This was accompanied by the absence mullite formation which acts as ceramic bonding, within the matrix, as illustrated in Figure 79. XRD analysis revealed that a small quantity of mullite began to develop at temperatures exceeding 1400 °C. Nevertheless, it became apparent that as the temperature increased further, the substantial presence of the melting phase adversely affected mullite, leading to a reduction in its concentration. This phenomenon is evident in the XRD results of the castables after an 8-hour dwell time, as mullite's presence was not discernible as the dwell time of the castable extended. Consequently, this resulted in a considerable weakening of the matrix, as evidenced by the results of the (RUL) test. The RUL test indicated a decrease in the temperature at which the castable exhibited 0.5 % deformation (referred to as $T_{0.5}$), which was measured to be 1325 °C as shown in Table 21. This value was lower compared to the reference andalusite castables. As the temperature continued to rise, it was observed that the formation of anorthite appeared to dissolve (see Figure 81), resulting in an increase in the quantity of melt phase and corundum grains.

It should also be mentioned that diaoyudaoite is no longer stable between 1000 and 1200 °C and releases sodium into the melt phase. The process is completed at 1400 °C if the model castables are thermally treated for 8 hours. If heated according to MMH (20 K/minute), the decomposition of the diaoyudaoite is not completed until 1630 °C has been reached.

5.4.3.3 Model refractory castable with kyanite addition MRC-K

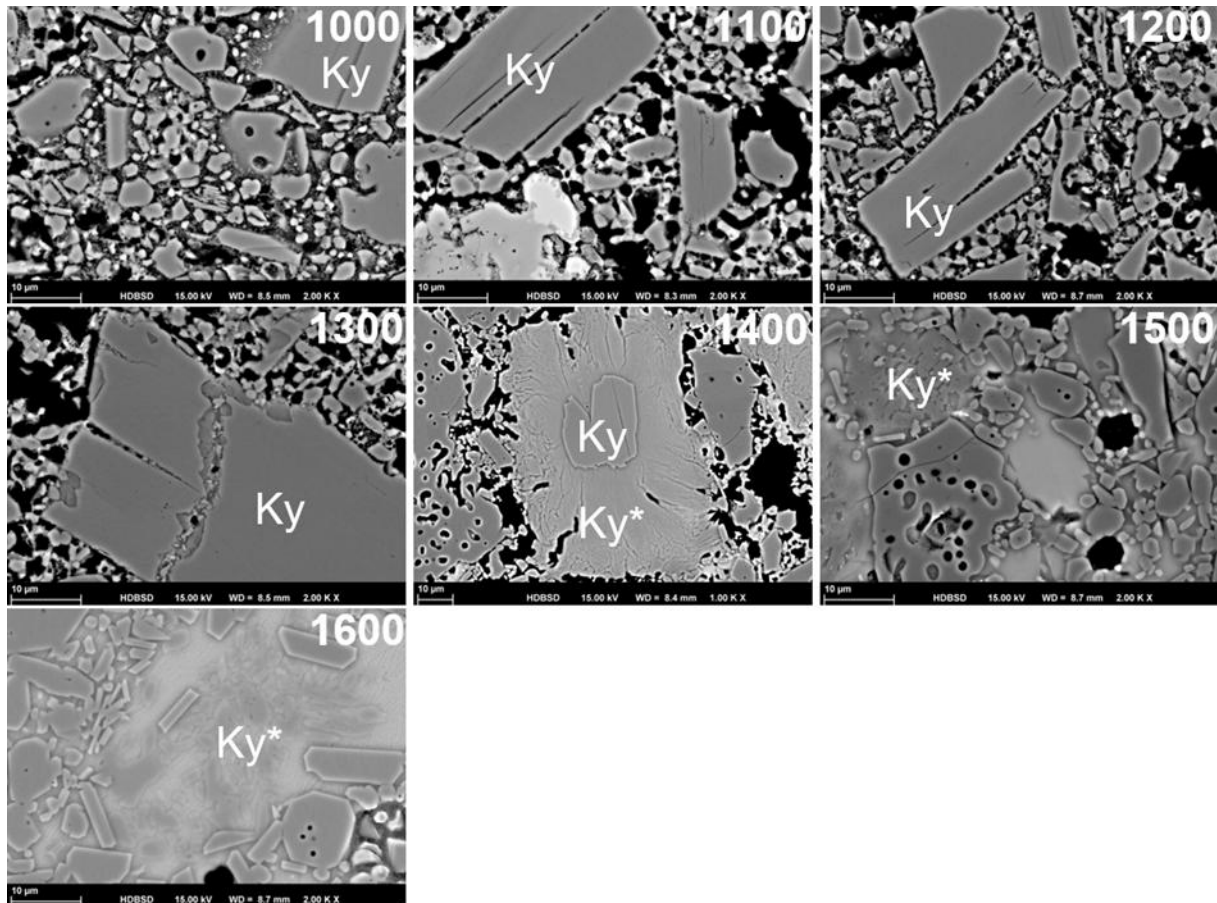


Figure 82: At 1100°C and 1200°C, the kyanite remained stable in the presence of calcium aluminate (CA) and CA₂, which were formed during the cement hydration process. At 1300°C, the transformation of kyanite started to transform to mullite, marked by noticeable changes in the microstructure. At 1600 °C kyanite is fully transformed.

The transformation of kyanite in the model castable was investigated through microstructural analysis (Figure 82). At 1100 and 1200 °C, the kyanite remained stable in the presence of calcium aluminate (CA) and CA₂. However, at 1300 °C, the decomposition of kyanite started to transform to mullite, marked by noticeable changes in the microstructure (Figure 82). The transformation of kyanite in the studied castables was accompanied by a significant volume expansion, as evidenced by the results of the refractoriness under load (RUL) tests (Figure 84). The maximum expansion observed ($D_{\max} = 1.11\%$) was found to be the highest among the model castables, indicating the pronounced expansion associated with the kyanite transformation. By 1400 °C, the transformation of kyanite persisted, accompanied by the formation of cracks and an increase in pore size due to the transformation reaction (Figure 83 b). At 1500 °C, while mullite remained in the region of transformed kyanite, it seemed not stable in the region of cement grains, since anorthite displaced mullite in the influence zone of former cement grains, either through the presence of anorthite melt or the subsequent cooling and solidification into anorthite and residual melt (Figure 83 a). As the temperature reached 1600 °C, the amount of molten phase in the structure increased which attacked mullite reduced its amount in the castable.

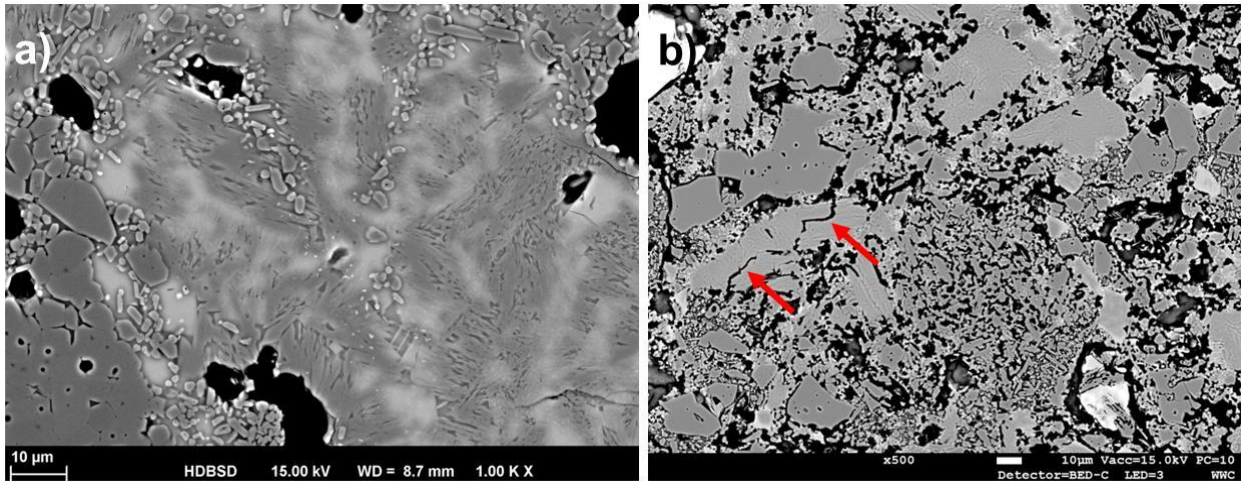


Figure 83: a) MRC-K at 1500°C, Transformed kyanite. Mullite+SiO₂ partially displaced by Ca-rich phase (presumably Anorthite). b) SEM of MRC-K matrix after firing at 1300 °C with 8 h dwell time showing microcracks in the matrix as result of kyanite transformation.

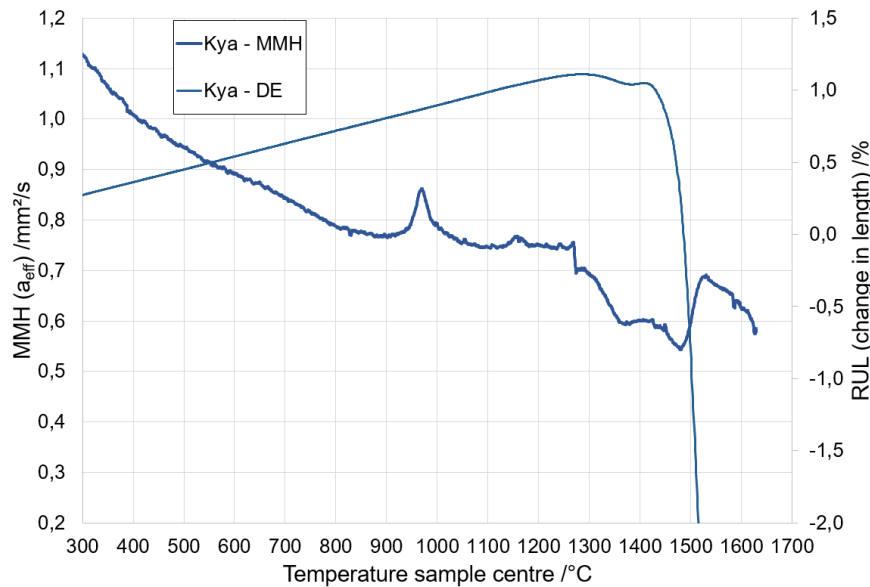


Figure 84: Results of MMH and RUL obtained for MRC-K. The test-pieces for RUL were prefired at 1000 °C for 1 h before the test.

In a temperature range between 900 and 1000 °C, the first reaction in the MMH curve (Figure 84) became apparent, which could be attributed to the sintering process. Whereas the curve demonstrated a stable stage with minimal changes until reaching 1250 °C. The transformation of kyanite occurred between 1200 °C and 1300 °C associated with an endothermic reaction. During this transformation, the breaking of existing bonds in kyanite and the formation of new bonds in mullite required heat energy. Consequently, the reaction absorbed heat from the surroundings, resulting in an endothermic process. The XRD analysis revealed a gradual decrease in kyanite starting from 1200 °C and continuing until 1500 °C, indicating a temperature range associated with kyanite transformation. Simultaneously, there was an increase in the amount of mullite observed, demonstrating a correlation between the decrease in kyanite and the formation of mullite. The expansion observed in the RUL curve provided confirmation of the transformation of kyanite within the temperature range of 1200 to 1300 °C. This was evident from the TD_{max} (Temperature of Maximum Expansion) occurring at 1284 °C the table 8, with a peak expansion of 1.11 %. The

formation of mullite in the castable matrix contributes to an increase in its refractoriness, as evidenced by the higher $T_{0.5}$ value of 1465 °C. In contrast, the absence of ceramic bonding, such as mullite, in the MRC-S (model refractory castable with SiC addition) leads to a decrease in its $T_{0.5}$ value to 1325 °C. Between the temperatures of 1350 and 1450 °C, another minor peak was observed in the MMH curve. The XRD results depicted in Figure 85 indicate the presence of anorthite within this temperature range. It appears that as the temperature increased and the cement phases in the matrix dissolved, the cement reacted with Al_2O_3 and SiO_2 present in the matrix, leading to the formation of anorthite. Above 1500 °C, the anorthite attacked the mullite, causing its dissolution and resulting in an increase in the amount of melt phase and corundum as clearly evident in the SEM analysis (Figure 82). The decrease observed in the RUL curve around 1400 °C provides confirmation of the formation of a melt phase and anorthite.

Diaoyudaoite is again not a stable phase above 1000 °C in the presence of SiO_2 , which is released during the decomposition of kyanite, and is completely resorbed above 1400 °C, whereby Na_2O is absorbed into the melt phase and has an additional melting point lowering effect. The initially stabilising anorthite is also absorbed into the melting phase from around 1550 °C.

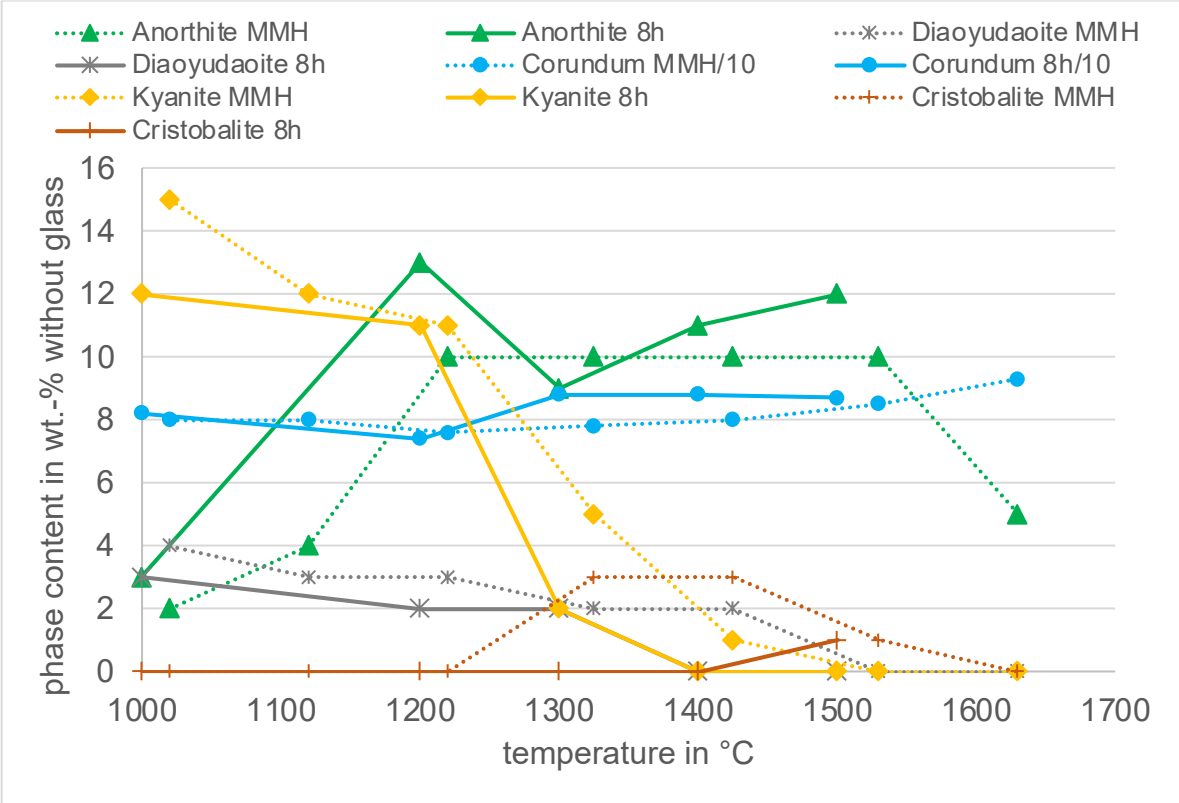


Figure 85: Crystalline phase content of the model castable with kyanite determined by Rietveldt. The results were calculated without considering the glass content, which increases considerably with temperature. The diagram shows the results for model castable, kyanite, treated for 8 hours at 1000, 1200, 1300, 1400 and 1500 °C (solid lines) and with no holding time simulating MMH. The corundum concentration is given by a value divided by 10 to keep the diagram clear and to better visualise smaller concentrations.

5.4.4 Corrosion resistance of the andalusite-free model castables

The corrosion resistance of the three reference castables RR, RE and RB against high-alkali ash is high. The main corrosion mechanism was the dissolution of aluminium-silicate phases within the basic slag at the contact. This corrosion mechanism was most pronounced in the RR and

least pronounced in the RB castable. The limited infiltration of basic melt even in RR and the glassy state of the solidified slag in this domain can be explained with the high viscosity of the silica-rich “compound” melt (= infiltrated original basic slag + assimilated refractory components + K_2O). Obviously, the highly viscous, silica rich melt densifies the microstructure of the castable in the contact zone and prevents intensive infiltration of basic slag. Decreasing temperatures along the thermal gradient further increases the viscosity of the melt.

The enrichment of SiO_2 in the infiltrating slag can be enabled by alternative SiO_2 -donators by the substitution material for andalusite for example SiC or kaolin.

5.4.4.1 Macroscopic observations

Samples were taken for the preparation of microsections at positions P1 and P3, the exact position of which can be seen in Figure 52. Accordingly, the model castable reacted with the liquid slag at P3 and P1 only received slag splashes but experienced the highest temperatures from the burner flame. Figure 87 shows photos of the microsections at P3. All materials show a thick slag coat, the contact to the refractory material is sharp but irregularly limited, which means that the decomposition of the model castables takes place via the always weaker matrix. MRC-K (kyanite) has obviously reacted particularly little with molten slag. MRC-ANO (anorthite) reacted most strongly, so that larger grains of the castable were already incorporated into the slag. In the case of MRC-KO (kaolinite), a stress crack can be recognised at the corner, which presumably originated retrogradely and indicates the high degree of vitrification of the model castable. SiC-containing model castables, with and without the addition of iron, also show the inclusion of tabular alumina in the slag, which also indicates progressive wear.

If these results are compared with those that can be obtained at P1 (Figure 88), i.e. at the hottest point in the slag channel test, a white contact zone to the interior of the slag channel test becomes apparent in the SiC-containing materials, which indicates the burn-off of SiC. Iron does not lead to an expected higher degree of glazing here and does not differ from the low-iron variant. The high temperatures of around 1530 °C have ensured that the model castable with anorthite has undergone a high degree of melting, which in turn can be recognised by the craquelure-like shrinkage crack texture. The interaction with the corrosive media is also particularly pronounced here. The addition of kaolin, luting sand or kyanite does not lead to any visible interaction here. However, the anorthite-containing castable also shows a stress crack here, which indicates a clear degree of melting of the model castable, which in turn correlates with the softening behaviour of this model castable (Figure 74).

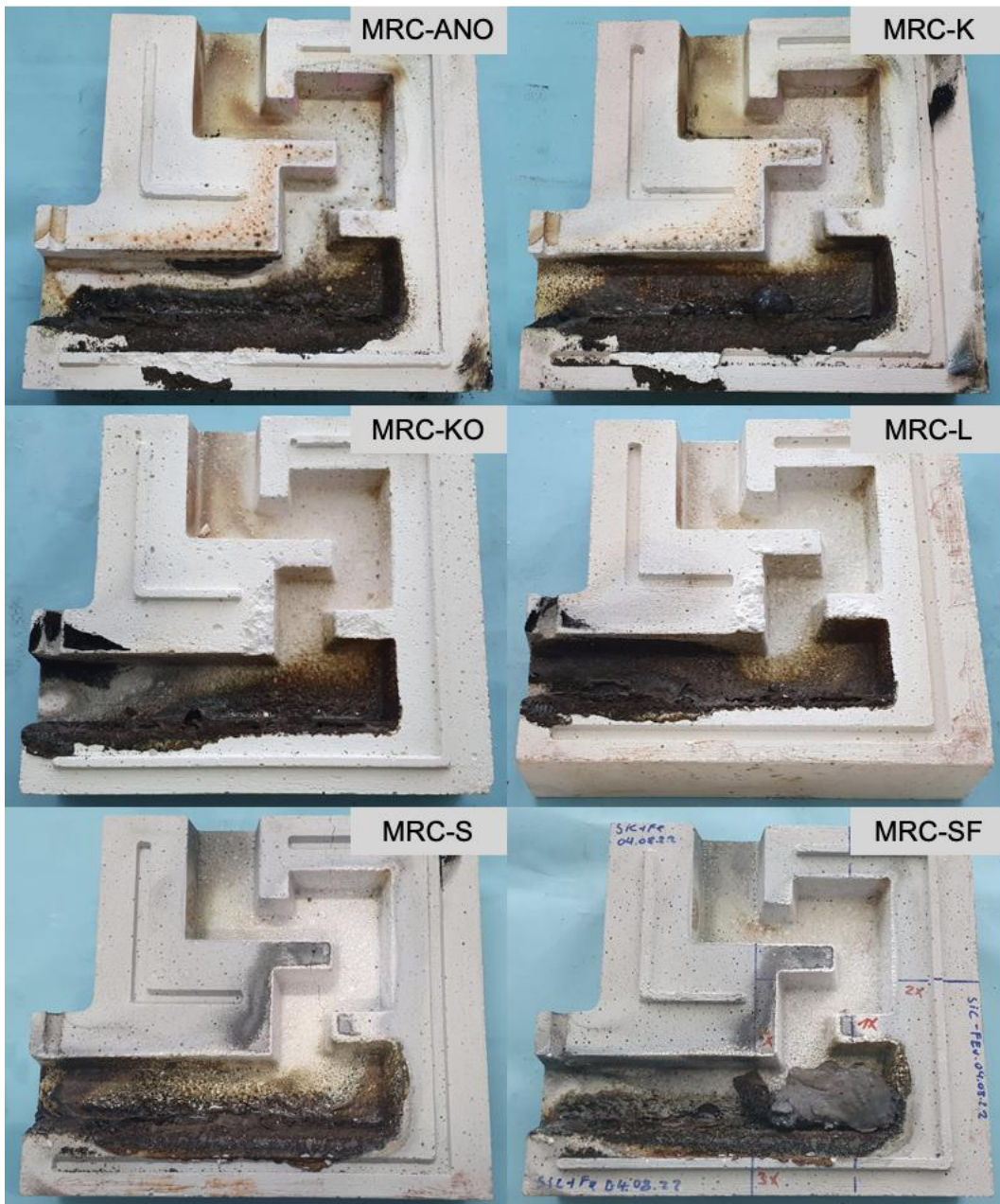


Figure 86: Half shells of the model castables after the channel slag test. (MRC-ANO...anorthite, MRC-K...kyanite, MRC-KO...kaolinite, MRS-L...luting sand, MRC-S...SiC, MRC-SF...SiC+hematite) The results are shown after 4 hours of exposure to the basic slag presented in Table 5. The test temperature varies depending on the position, so that temperatures at the inlet are 1520 °C and drop to 1250 °C towards the outlet.

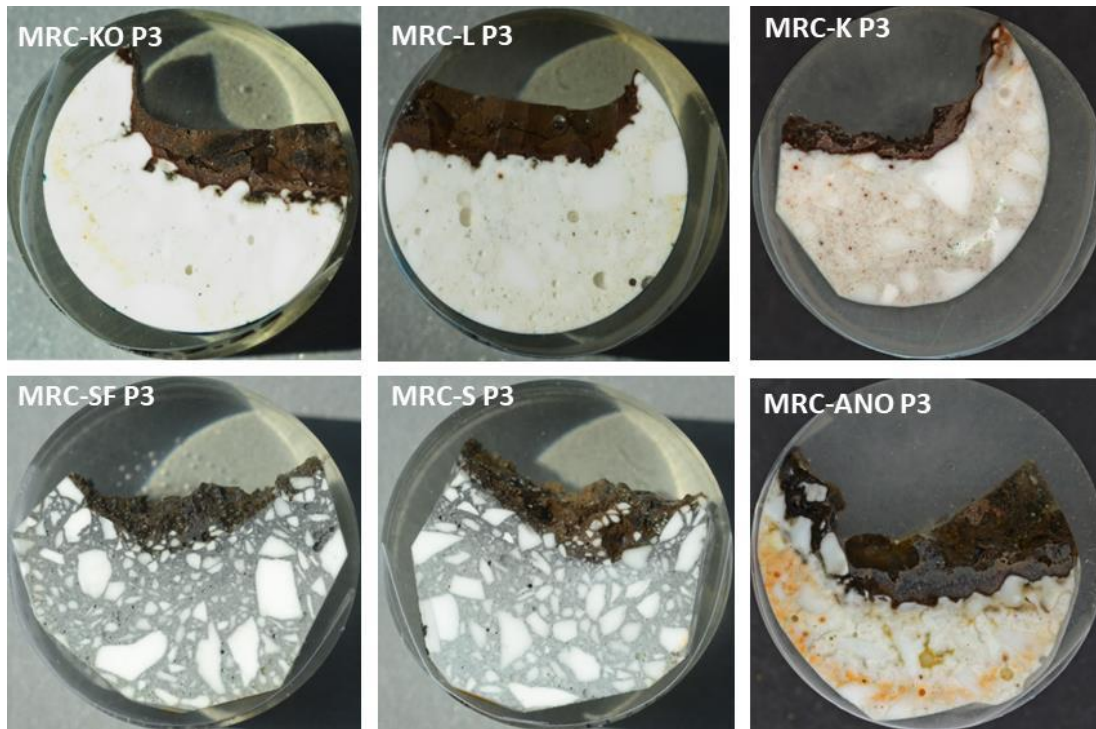


Figure 87: A thick layer of brownish slag adheres on the surface on the test specimen of the andalusite-free model castables (Position 3). Size of the polished section 30 mm (MRC-ANO...anorthite, MRC-K...kyanite, MRC-KO...kaolinite, MRS-L...luting sand, MRC-S...SiC, MRC-SF...SiC+hematite).

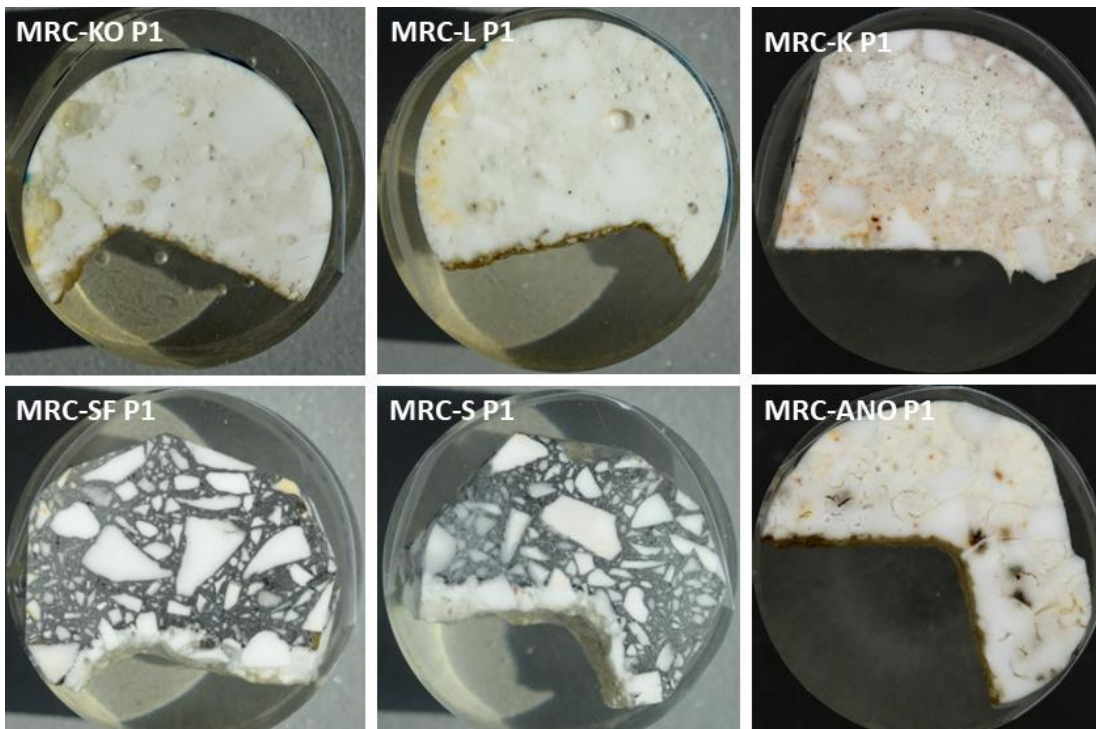


Figure 88: A thin layer of brownish slag adheres on the surface on the test-pieces of the andalusite-free model castables MRC-KO, MRC-L, MRC-ANO (Position 1). A thick white glassy layer was formed, covering the model castable containing SiC (MRC-SF and MRC-S). The temperature gradient ranges from approximately 1520 °C to 1240 °C. Size of the polished section 30 mm (MRC-ANO...anorthite, MRC-K...kyanite, MRC-KO...kaolinite, MRS-L...luting sand, MRC-S...SiC, MRC-SF...SiC+hematite).

5.4.4.2 Slag interaction in the microstructure

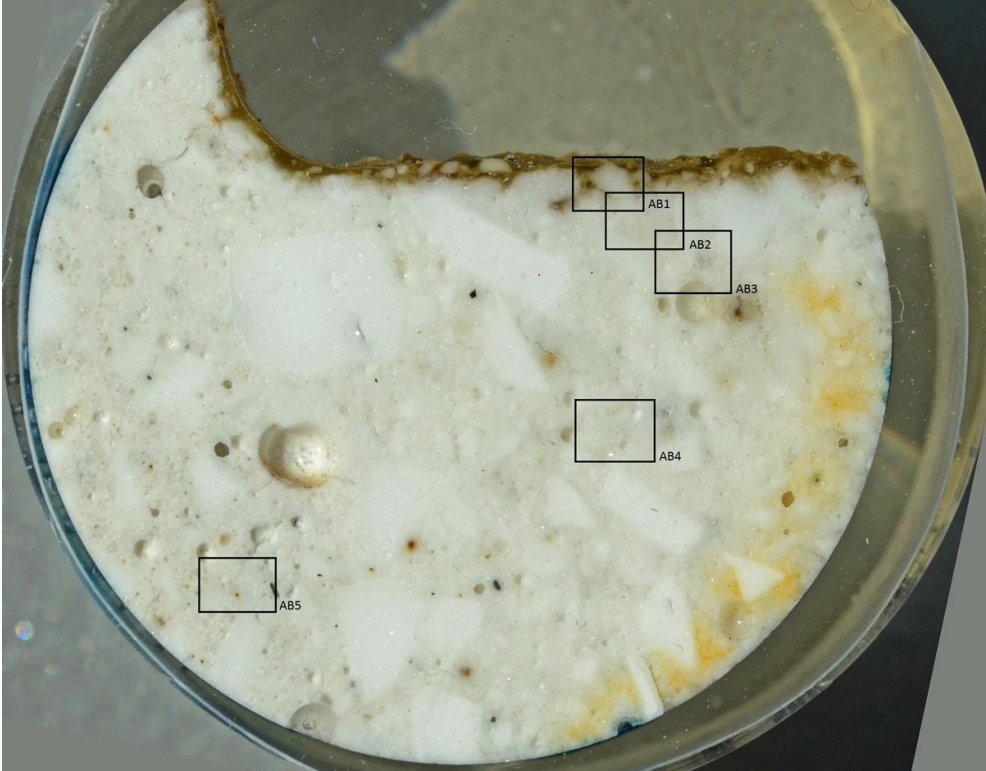


Figure 89: A thin layer of brownish slag adheres on the surface on the test-pieces of the andalusite-free model castables MRC-L (luting sand) at position, P1 of the slag channel test. The black squares refer to the positions of SEM microanalysis.

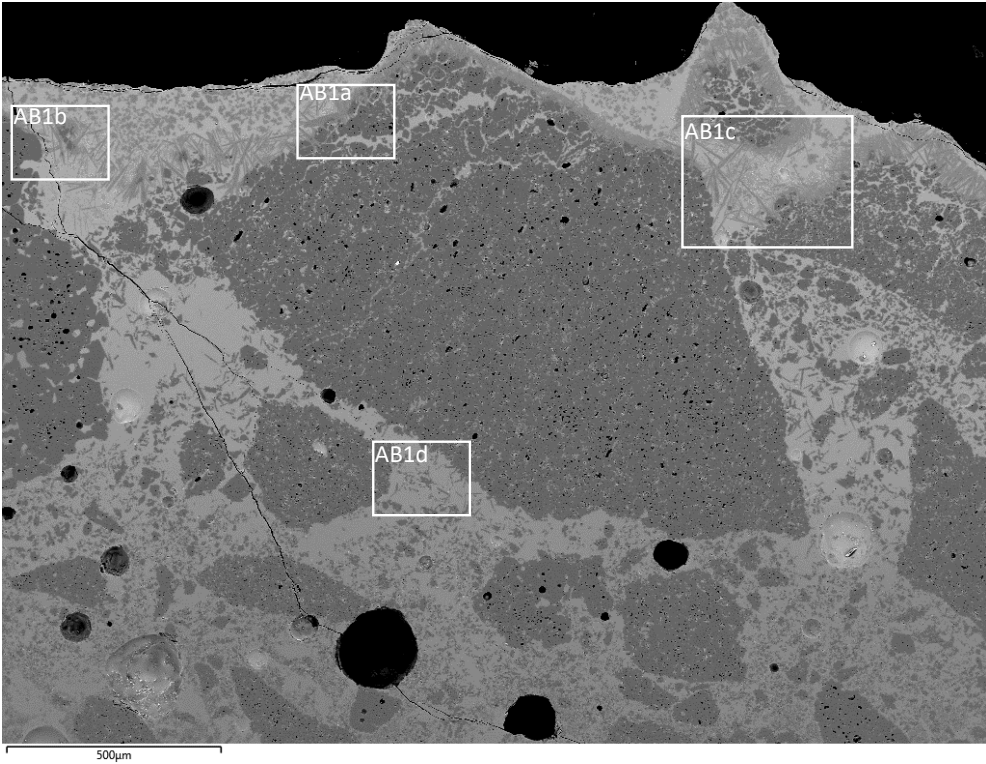


Figure 90: SEM image (BSE) of MRC-L showing the area AB1 as indicated in Figure 89 (Magnification 50x). The infiltrating slag stands out clearly from the castable due to the high contrast and infiltrates even into the open porosity of coarse tabular alumina grains.

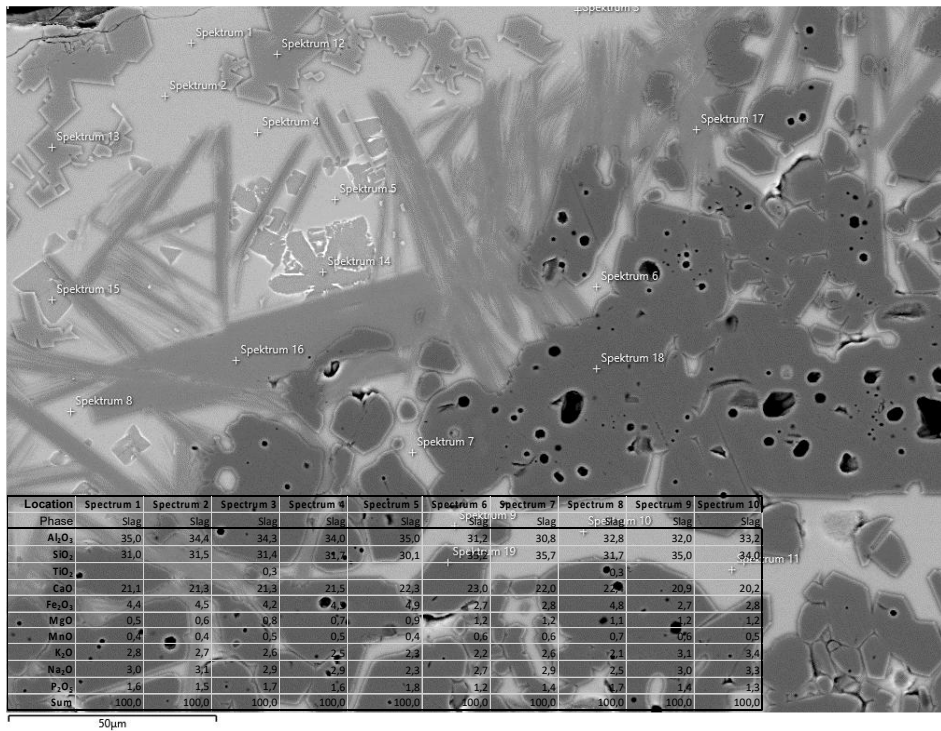


Figure 91: SEM image (BSE) of MRC-L showing the area AB1a as indicated in Figure 89 (Magnification 500x). The image section diagonally divides an infiltrated tabular alumina coarse grain (bottom right) and the adhering slag, in which diopydauite forms at the expense of the corundum, which is no longer stable. The formations, which look like ice crystals, can be recognised as nepheline.

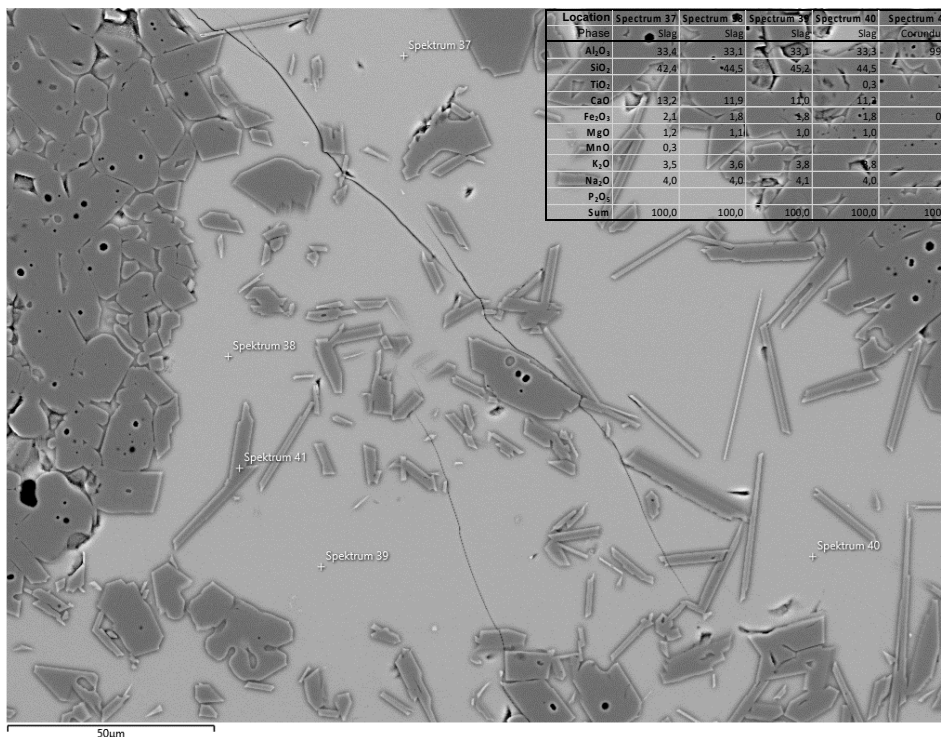


Figure 92: SEM image (BSE) of MRC-L showing the area AB1d as indicated in Figure 89 (Magnification 500x). The image is dominated by slag, which was liquid during the corrosion test (bright contrast). Coarse grains of tabular alumina can be recognised at the edges. The slag has an SiO₂ content of approx. 45 wt.-% and is therefore basic, whereby corundum crystallises as a stable phase in a thin tabular form.

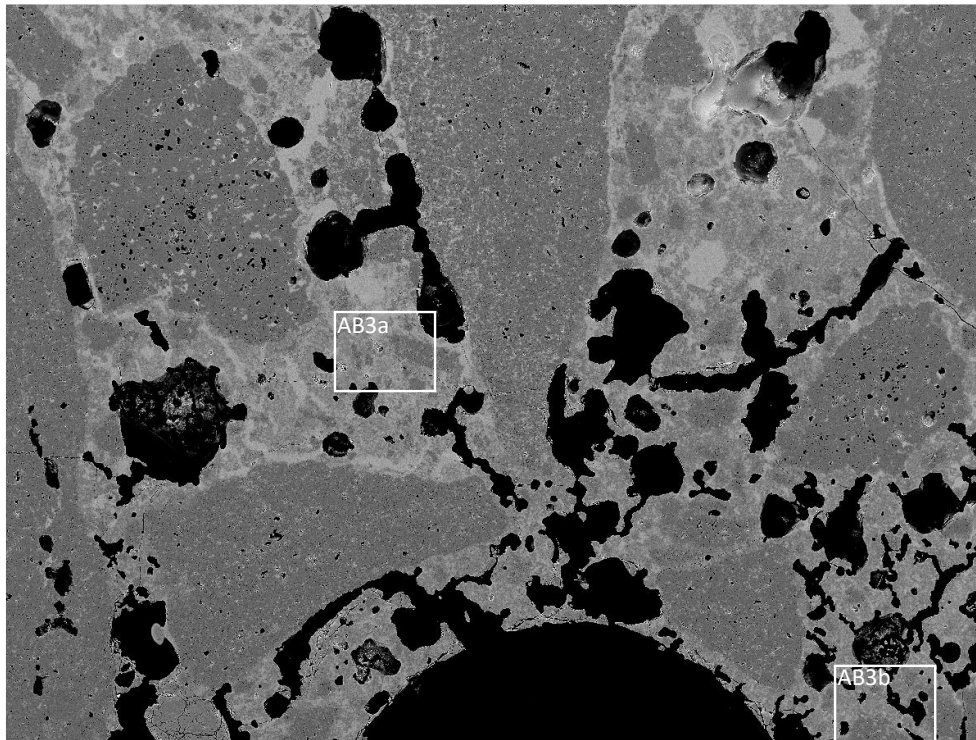


Figure 93: SEM image (BSE) of MRC-L showing the area AB3 as indicated in Figure 89 (Magnification 50x). Even at this depth, the slag can still be recognised by the high contrast. The round pores (black) here indicate a significant degree of melting.

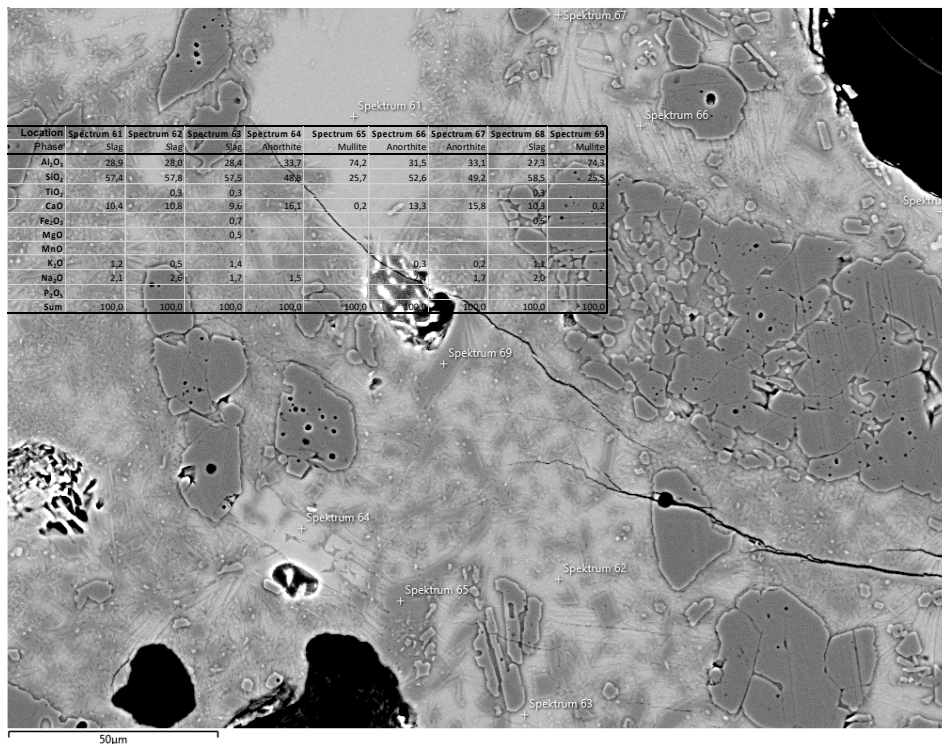


Figure 94: SEM image (BSE) of MRC-L showing the area AB3a as indicated in Figure 93 (Magnification 500x). The image is dominated by slag, which was liquid during the corrosion test (bright contrast). Coarse grains of tabular alumina can be recognised to be unstable in the presence of a slag that contains approximately 57 wt.-% SiO₂. Instead of corundum, mullite is a stable phase that is precipitated euhedral in the slag that is in liquid state during the corrosion test.

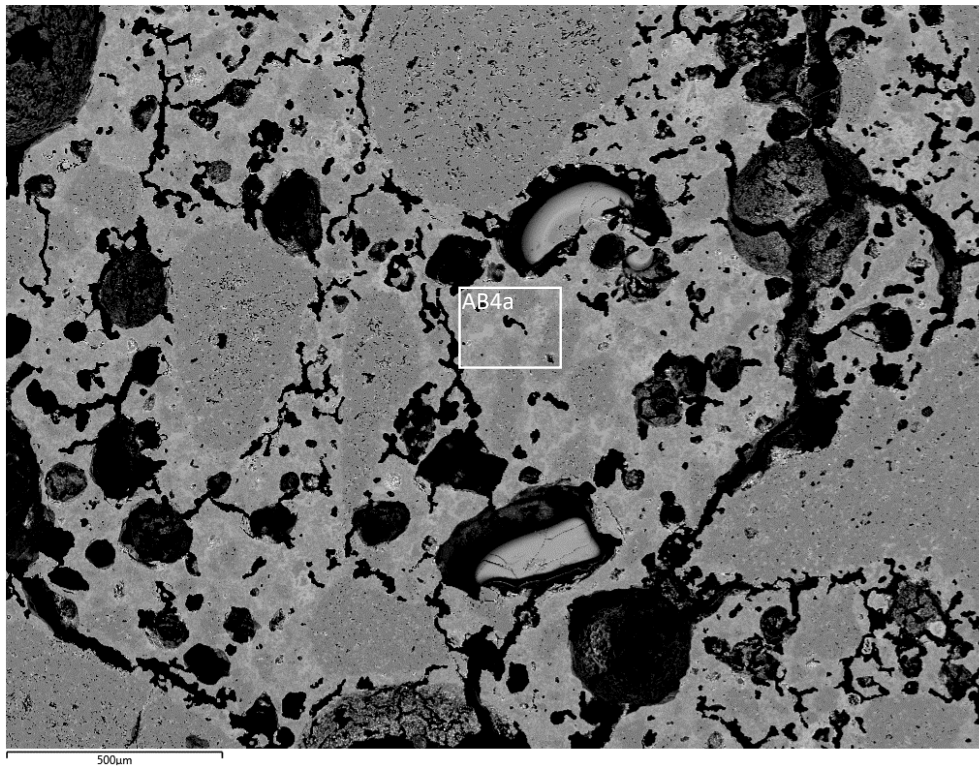


Figure 95: SEM image (BSE) of MRC-L showing the area AB4 as indicated in Figure 89 (Magnification 50x). In this depth of the section (Figure 89) infiltration is still visible by the high contrast in the matrix but is less intense than visible in the prior micrographs.

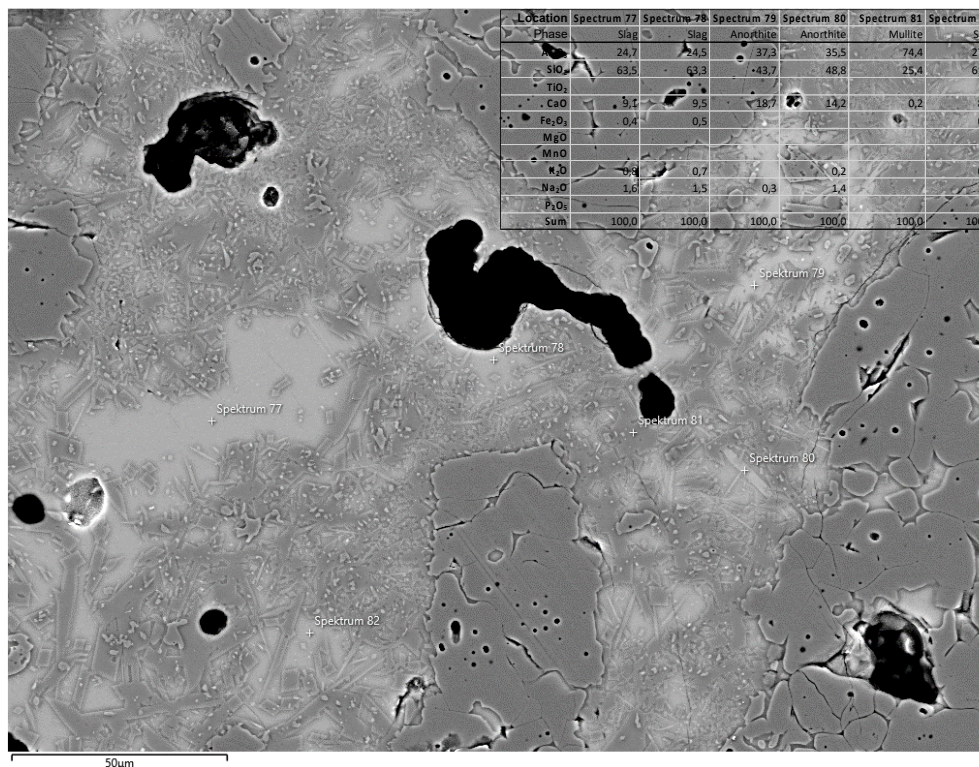


Figure 96: SEM image (BSE) of MRC-L showing the area AB3a as indicated in Figure 95 (Magnification 500x). The image is dominated by slag, which was liquid during the corrosion test (bright contrast). Coarse grains of tabular alumina can be recognised to be unstable in the presence of a slag that contains approximately 62 wt.-% SiO₂. Instead of corundum, mullite is a stable phase that is precipitated euhedral in the slag that is in liquid state during the corrosion test.

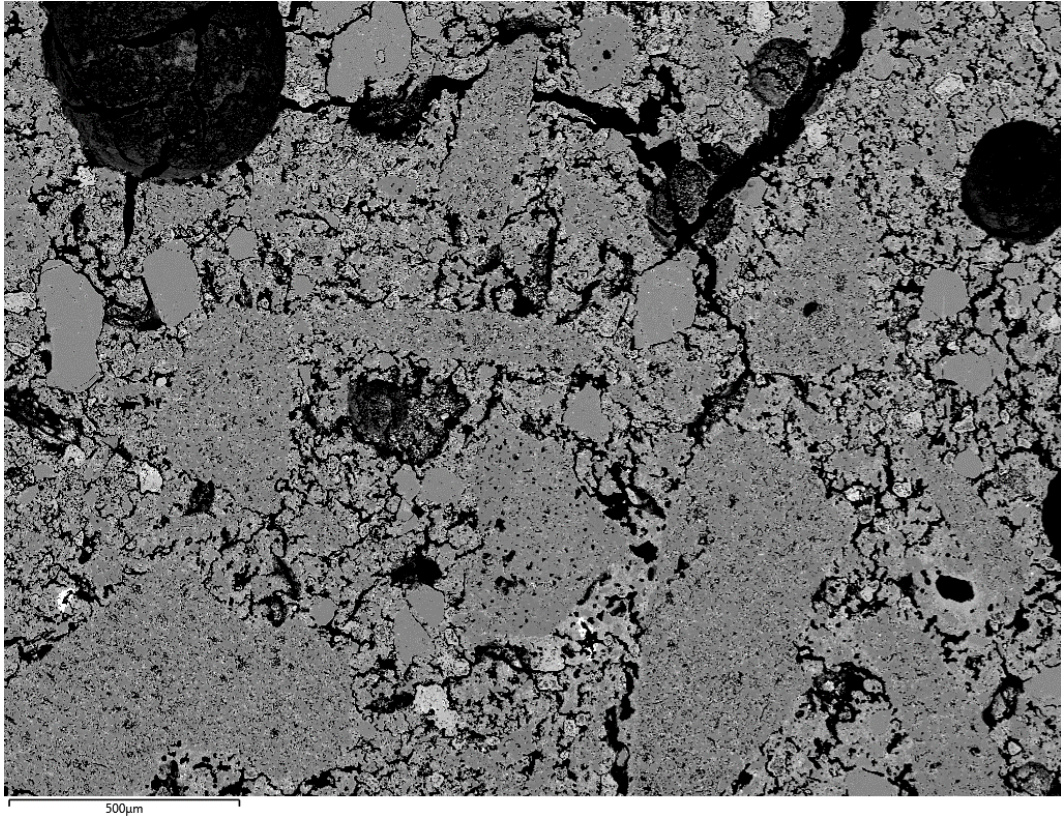


Figure 97: SEM image (BSE) of MRC-L showing the area AB5 as indicated in Figure 89 (Magnification 50x). The micrograph indicates the unchanged structure of the castable containing luting sand. Cracks that are visible starting from the round pores are indicating a shrinkage of the matrix due to sintering.

The model castable containing luting sand showed similar corrosion behaviour to the reference castables. However, the slag penetrated deeper here, which is due to insufficient post-expansion, as no andalusite was used here. However, closer to the contact with the hot side, especially where temperatures above 1400 °C are to be expected, the formation of cristobalite from deep quartz, a component of the luting sand, appears to re-densify the microstructure. Mineralogically, it can again be observed that the SiO₂ concentration in the slag determines whether corundum or mullite is stable. As has already been worked out for the reference castables, the critical SiO₂ concentration is around 58 wt.-%.

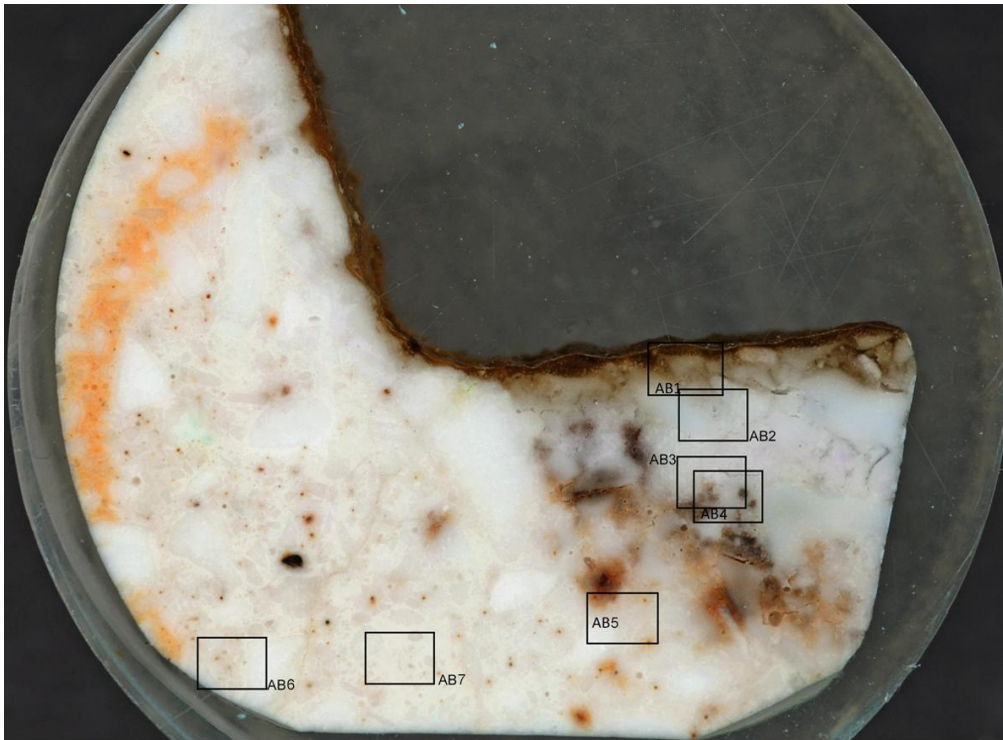


Figure 98: A thin layer of brownish slag adheres on the surface on the test-pieces of the andalusite-free model castables MRC-K (kyanite) at position, P1 of the slag channel test. The brownish colour in indicates a more pronounced infiltration by the slag. The black squares refer to the positions of SEM microanalysis.

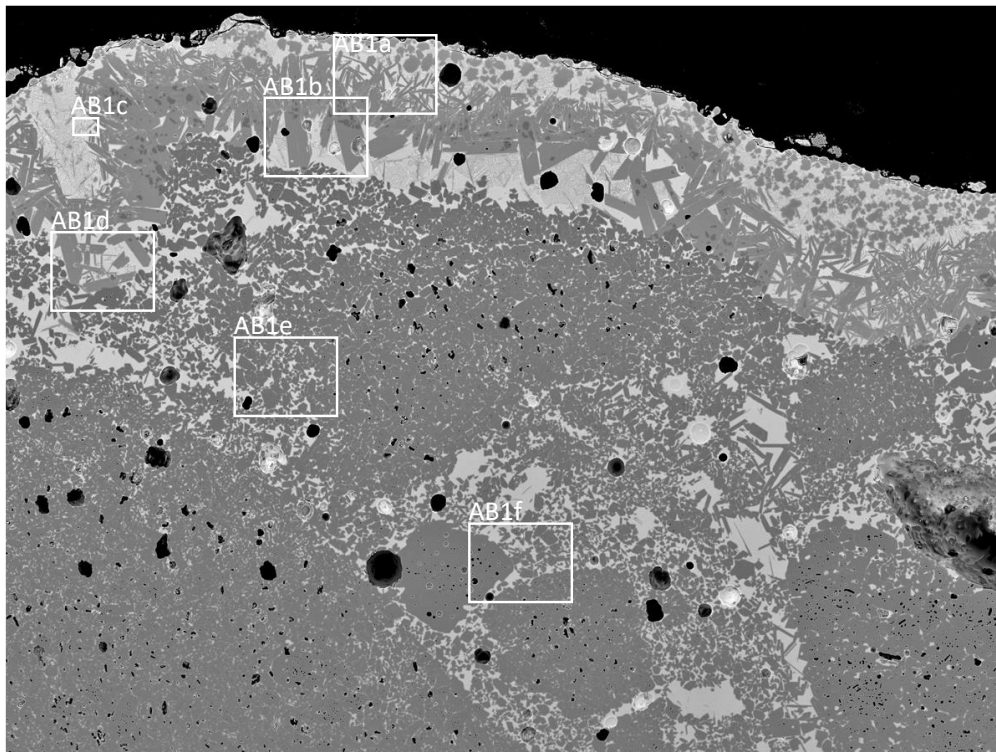
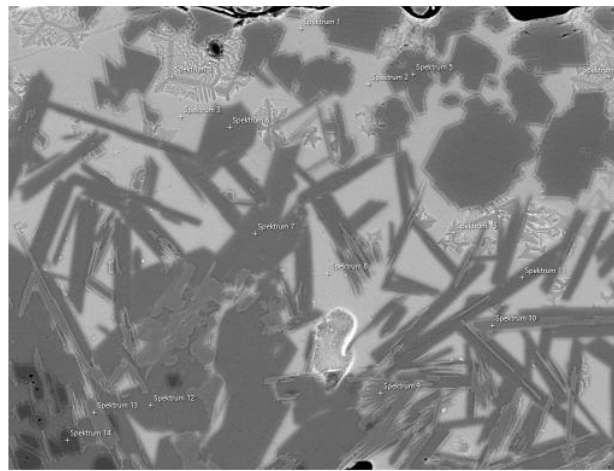


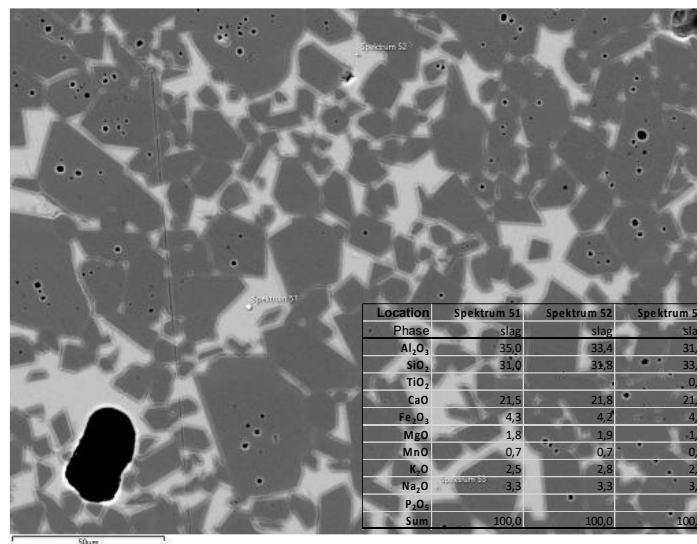
Figure 99: SEM image (BSE) of MRC-K (kyanite) showing the area AB1 as indicated in Figure 98 (Magnification 50x). The image is dominated by slag, which was liquid during the corrosion test (bright contrast). Coarse grains of tabular alumina can be recognised to be unstable in the presence of a slag that contains at the contact to the channel approximately 30 wt.-% SiO_2 . Large euhedral crystals at the hot face (top of the micrograph) can be predominantly addressed as hibonite. Euhedral crystals with isomorphic appearance seem to be diaoyudaoite according to the chemical analyses. This appearance is not very common for this phase as it prefers tabular shapes like that visible for hibonite.



Location	Spektrum 1	Spektrum 2	Spektrum 3	Spektrum 4	Spektrum 5	Spektrum 6	Spektrum 7	Spektrum 8
Phase	slag	slag	slag	nepheline-Ca	spinel	β -alumina	β -alumina	slag
Al ₂ O ₃	39,2	38,3	38,2	41,2	72,1	86,1	85,7	34,3
SiO ₂	28,6	29,7	28,8	28,4		1,1	1,4	31,6
TiO ₂								
CaO	23,0	22,9	23,4	20,4		1,7	1,6	24,0
Fe ₂ O ₃	3,8	3,8	4,6	3,7	7,5	2,9	2,8	4,6
MgO	0,5	0,5	0,6		18,8	3,1	3,2	1,2
MnO	0,3	0,3	0,5		1,6	0,3	0,3	0,6
K ₂ O	2,1	2,2	1,7	2,1		3,5	3,5	1,5
Na ₂ O	2,6	2,3	2,2	4,4		1,4	1,5	2,2
P ₂ O ₅								
Sum	100,0	100,0	100,0	100,0	100,0	100,0	100,0	100,0

Location	Spektrum 9	Spektrum 10	Spektrum 11	Spektrum 12	Spektrum 13	Spektrum 14	Spektrum 15	Spektrum 16
Phase	hibonite	hibonite	β -alumina	β -alumina	hibonite	corundum	nepheline-Ca	nepheline-Ca
Al ₂ O ₃	86,2	87,1	85,8	86,7	85,8	99,9	39,8	42,0
SiO ₂	1,2	1,0	1,4	1,0	1,6		30,7	28,0
TiO ₂	0,3							
CaO	8,2	8,2	1,6	1,8	8,2	0,1	18,8	20,0
Fe ₂ O ₃	3,4	3,0	2,8	2,5	3,3		3,3	3,3
MgO	0,8	0,7	3,2	2,7	0,9		0,5	
MnO			0,4	0,3	0,2			
K ₂ O			3,5	3,5			2,0	2,6
Na ₂ O			1,3	1,6			5,0	4,1
P ₂ O ₅								
Sum	100,0	100,0	100,0	100,0	100,0	100,0	100,0	100,0

Figure 100: SEM image (BSE) of MRC-K (kyanite) showing the area AB1a as indicated in Figure 99 (Magnification 500x). The micrograph indicates the slag zone of the kyanite model castable at position, P1. Beside the already under Figure 99 described newly formed euhedral crystals, ice crystal shaped, were formed retrogradely and the skeletal appearance indicates a high cooling rate. Said crystals can be addressed as a Ca-rich Nepheline.



Location	Spektrum 51	Spektrum 52	Spektrum 53
Phase	slag	slag	slag
Al ₂ O ₃	35,0	33,4	31,4
SiO ₂	31,0	31,8	33,7
TiO ₂			0,3
CaO	21,5	21,8	21,8
Fe ₂ O ₃	4,3	4,2	4,1
MgO	1,8	1,9	1,9
MnO	0,7	0,7	0,8
K ₂ O	2,5	2,8	2,7
Na ₂ O	3,3	3,3	3,4
P ₂ O ₅			
Sum	100,0	100,0	100,0

Figure 101: SEM image (BSE) of MRC-K (kyanite) showing the area AB1e as indicated in Figure 99 (Magnification 500x). The micrograph indicates the slag zone of the kyanite model castable at position, P1. The slag is poor in SiO₂ (approx. 35 wt.-%) that makes corundum to a stable phase which recrystallizes euhedral in the slag (bright contrast).

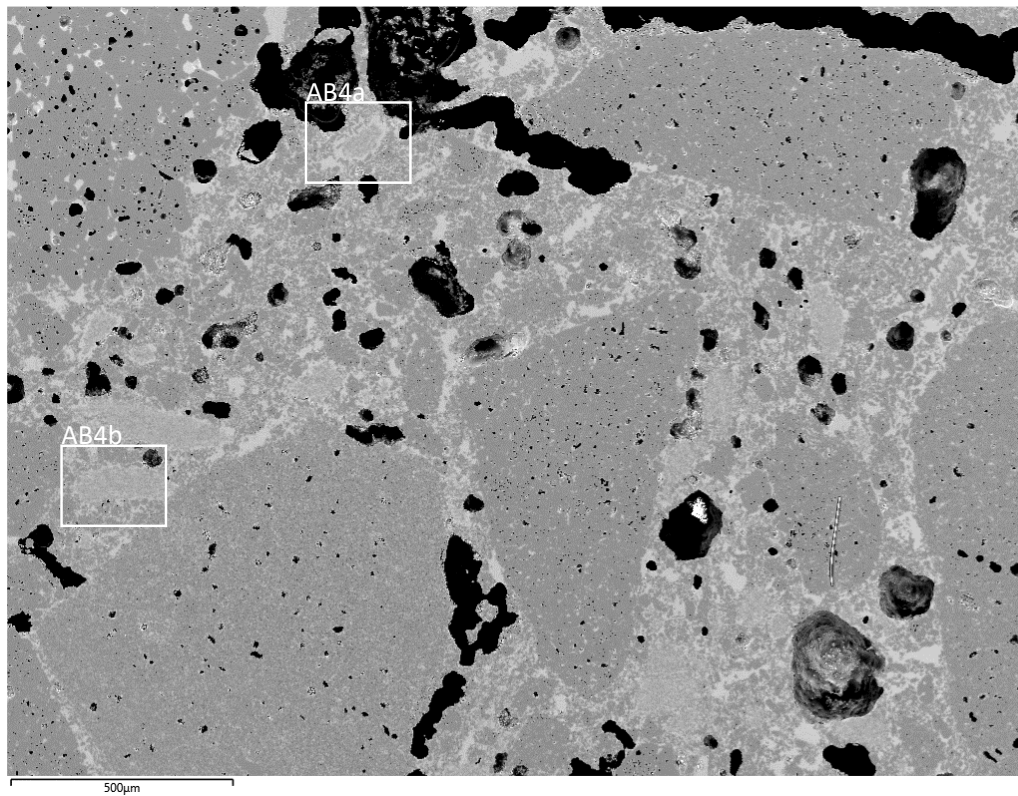


Figure 102: SEM image (BSE) of MRC-K (kyanite) showing the area AB4 as indicated in Figure 98 (Magnification 50x). The image still shows the typical structure of a refractory castable even if the high contrast is indicating that the slag has already infiltrated the matrix.

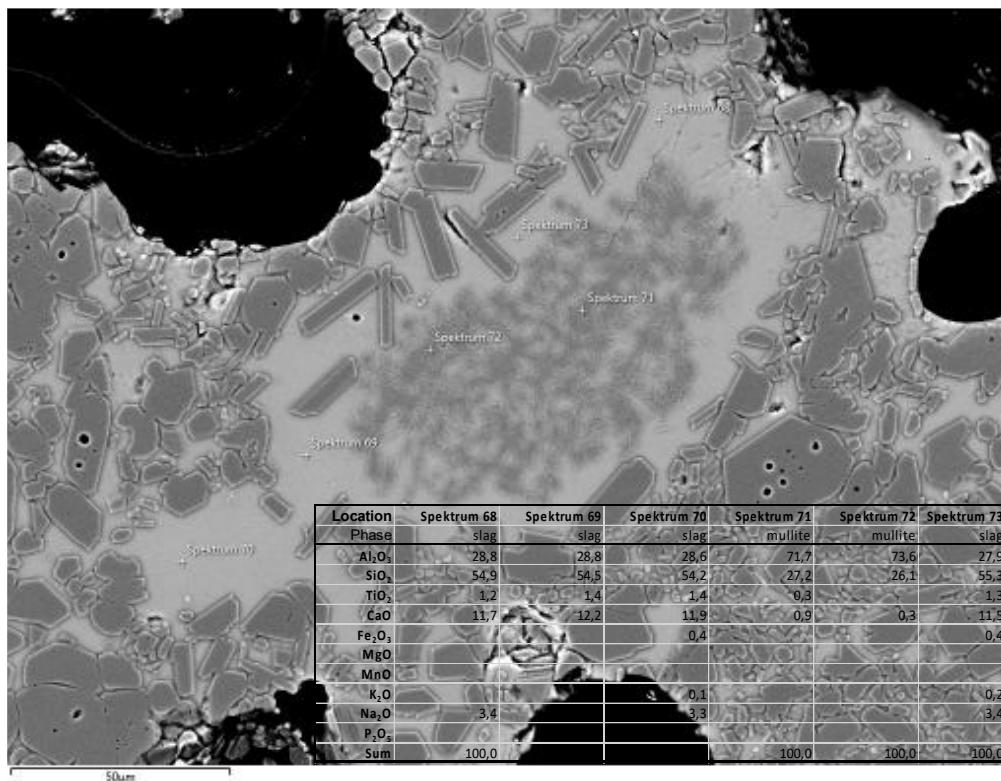


Figure 103: SEM image (BSE) of MRC-K (kyanite) showing the area AB4a as indicated in Figure 99 (magnification 500x). The micrograph indicates the slag zone of the kyanite model castable at position, P1. The slag is rich in SiO₂ (approx. 55 wt.-%) that makes mullite to a stable phase which recrystallizes euhedral in the slag (bright contrast).

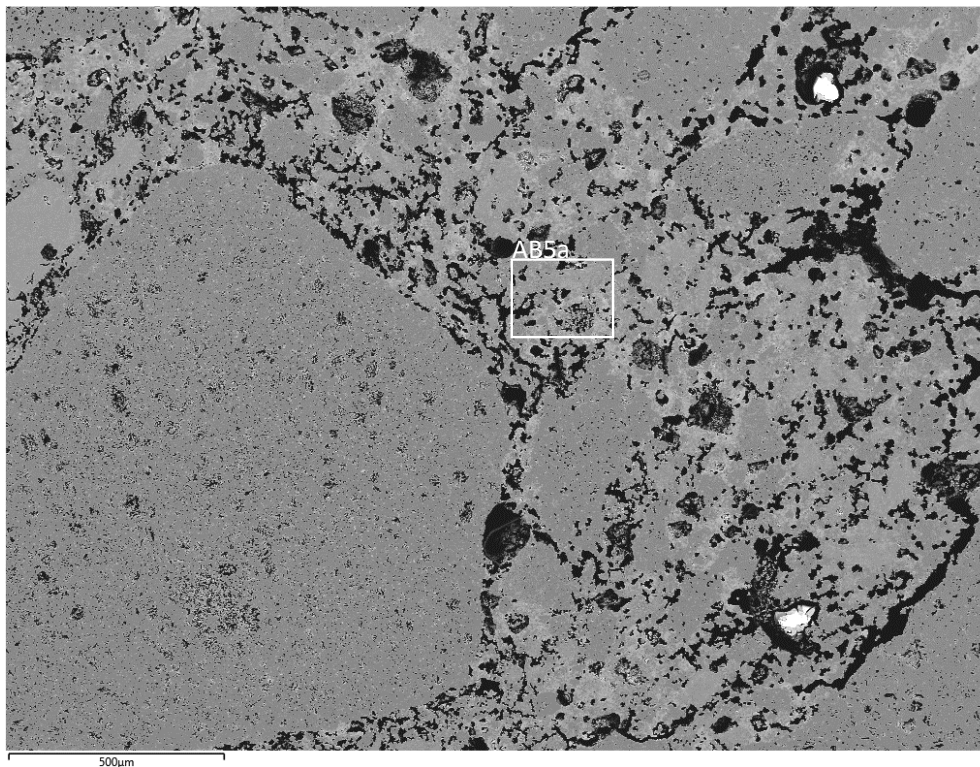


Figure 104: SEM image (BSE) of MRC-K (kyanite) showing the area AB5 as indicated in Figure 98 (magnification 50x). The image shows at the first glance an almost unchanged material. Particles with highest contrast can be addressed as residual cement grains.

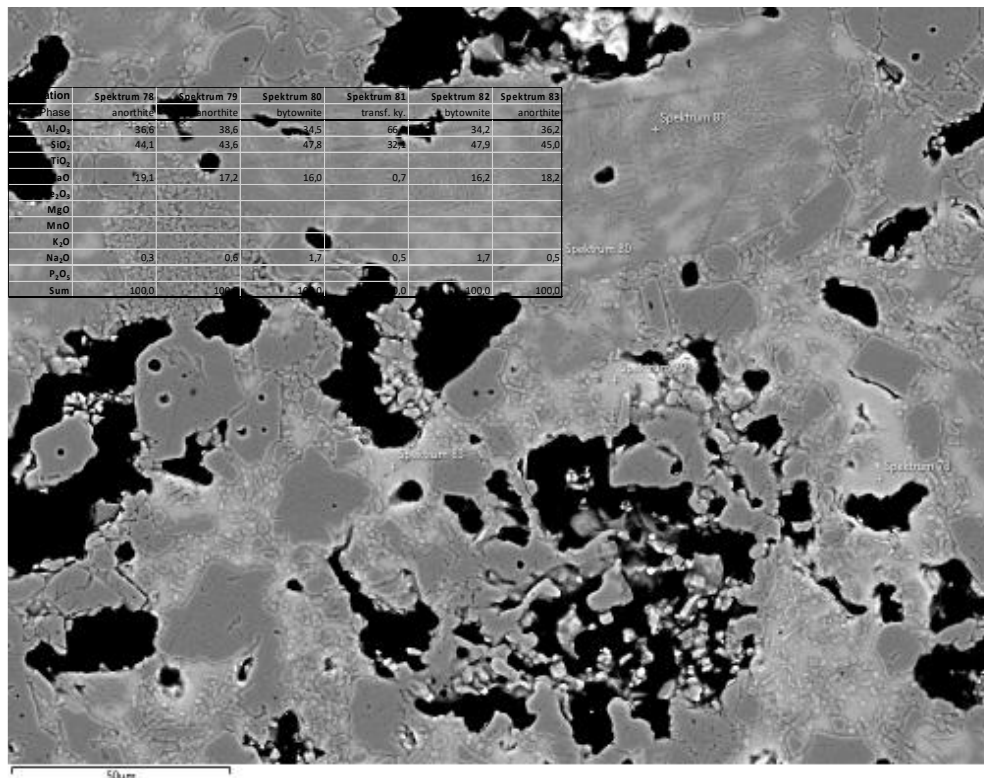


Figure 105: SEM image (BSE) of MRC-K (kyanite) showing the area AB5a as indicated in Figure 104 (magnification 500x). The micrograph indicates the slag zone of the kyanite model castable at position, P1. The degree of chemical alteration by the slag is negligible. Ca derived from the cement is responsible for the high contrast and reacts with kyanite to anorthite that could appear Ca-rich, containing up to 2 wt.-% Na₂O. This is the typical thermal decomposition of kyanite in the presence of Ca derived from the cement and was already reported for the reference castables.

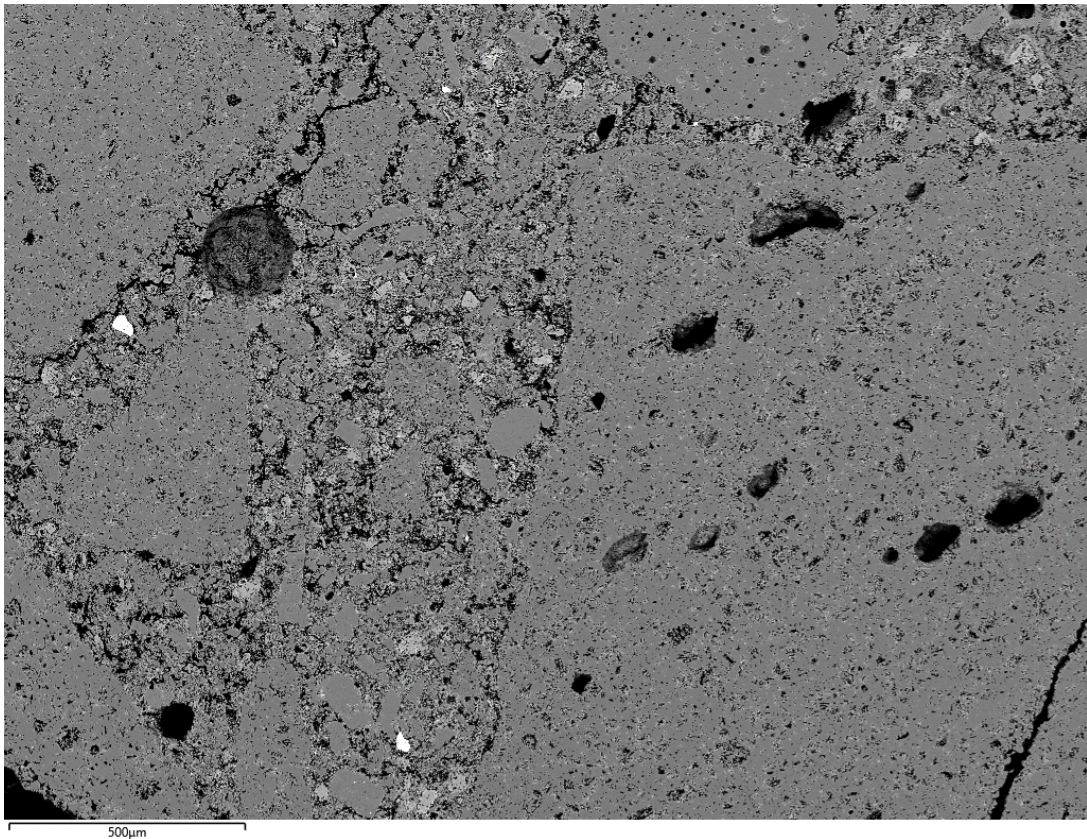


Figure 106: SEM image (BSE) of MRC-K showing the area AB6 as indicated in Figure 98 (magnification 50x). The image shows an almost unchanged material. Particles with highest contrast can be addressed as residual cement grains. In the upper left corner, a prominent crack is visible that could be attributed to the expansion of the castable induced by the decomposition of kyanite. The crack also indicates that the castable behaves still brittle at position AB6 (approx. 1200 °C)

The model castable containing kyanite showed a quite similar thermal behaviour as the reference castable, which is not surprising since kyanite as the high-pressure modification of the Al_2SiO_5 polymorphs is also thermally decomposed. In contrast to andalusite, however, thematically altered kyanites show a kind of dissolution from the edge of the crystals, whereby the dense mullite structure is not formed, as is recognisable for andalusite (Figure 82). In the presence of basic slag (Table 5), however, similar dissolution phenomena are observed, which are essentially based on the same chemical composition of the polymorphs. The reaction of the kyanite with the cement added as a binder is induced purely thermally and leads retrogradely to the formation of anorthite, which in turn contains up to 1.5 wt.-% Na_2O , i.e. albite components. The SiO_2 content is apparently not sufficient for higher albite concentrations, as the incorporation of Na instead of Ca in the crystals needs more SiO_2 in the crystal lattice. Albite incorporates around 25 wt.-% more SiO_2 into the crystal lattice (Albite: $\text{Na}[\text{AlSi}_3\text{O}_8]$: Anorthite: $\text{Ca}[\text{Al}_2\text{Si}_2\text{O}_8]$). Of the 11 wt.-% Na_2O offered by the slag, a large proportion is already bound to diaoyudaoite on the hot side, which crystallises at the expense of the corundum. Figure 82 also shows, however, that the kyanite decomposes as expected at lower temperatures than andalusite, which means that the positive effect of post-expansion comes to an end earlier and thus acts less well as a shrinkage compensator. The thermal decomposition of kyanite in the slag channel test, in the sharp temperature gradient described in chapter 4.4.13 (see also Figure 56), also shows another weakness of the decomposition of kyanite, which always starts at lower temperatures. As can be seen from Figure 106, the elongation caused by the decomposition of the kyanite begins at a time when the microstructure of the kyanite model castables is still brittle. This results in the formation of expansion cracks in

the otherwise unaffected microstructure. It is difficult to judge to what extent this is detrimental to the actual use of these materials in later applications. It can be assumed, however, that this area is structurally stressed during use in such a way that the structure is pushed tightly instead of forming cracks. However, this behaviour can also be observed with the reference castables and here in particular with the cement-free RR, which still exhibits brittle behaviour at 1450 °C (Figure 40), as it does not form an anorthitic melt at this temperature (lack of Ca), but the decomposition of the andalusite has already led to significant elongation. The result is a crack structure that leads to the loss of the bonding of the coarse grains.

Irrespective of the elongation behaviour of the kyanite-containing model castables, the chemical reactivity with the basic slag is comparable to the andalusite reference castables. The basic slag infiltrates the castable surface, whereby the SiO₂-rich matrix becomes basic with less than 35 wt.-% (Figure 101). As a result, corundum becomes stable and forms euhedral crystals in a molten environment. With increasing depth, the influence of the slag decreases, so that from an SiO₂ content of around 55 wt.-%, mullite is established as a stable phase, which also crystallises euhedral at the expense of the corundum from the melt.

The importance of a SiO₂-rich melt has already been described in previous chapters whereby the SiO₂ content has a positive effect on the viscosity in such a way that the melts become increasingly viscous and thus stabilise the microstructure, despite high degrees of melting.

5.4.5 Wedge Splitting Tests

The fracture behaviour of the model castables containing kyanite (MRC-K) and luting sand (MRC-L) were characterised using the wedge splitting method (Figure 107). Both model castables displayed higher fracture mechanical parameters (notch tensile strength and specific fracture energy) than the previously investigated industrial ones. However, the very high strength measured for the model castable containing kyanite is not matched by a significantly higher specific fracture energy, which indicated to a very brittle behaviour at least until 1250 °C as long as kyanite stay stable. Above 1250 °C and because of the decomposition of kyanite into mullite, and especially, a melt phase, no fracture mechanical parameters could be assessed as the test pieces were too weakened by the presence of the melt phase to enable investigation. Either splitting spontaneously before reaching the testing temperature (1450 °C) or by the testing temperature under the weight of the loading column. In contrast, the model castable containing luting sand (MRC-L) displayed a much more favourable ratio of specific fracture energy to notch tensile strength, indicating a rather ductile behaviour already at a temperature of 1000 °C. Despite a significant weakening of the model castable at the temperature of 1250 °C, a strengthening at is observed at 1450 °C while maintaining a certain ductility. The massive formation of mullite at this temperature and above may explain this particularly interesting and positive behaviour.

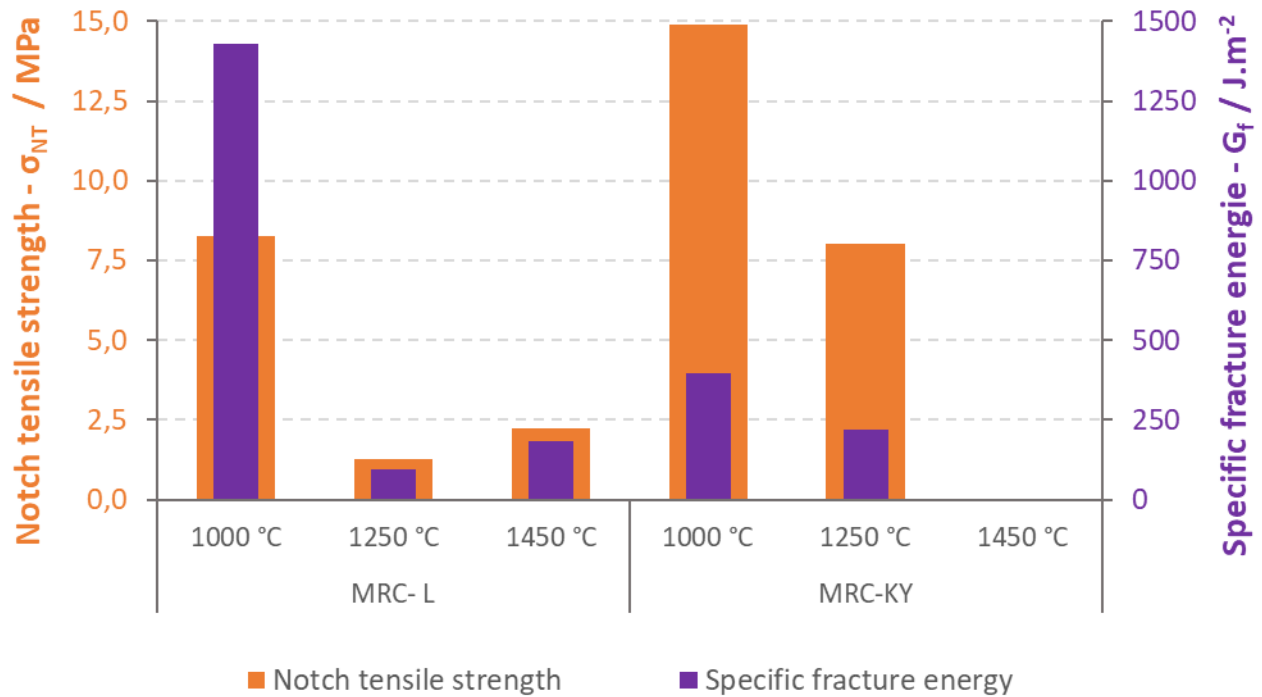


Figure 107: Results for the wedge splitting tests on the model castables MRC-KY and MRC-L performed by 1000 °C, 1250 °C and 1450 °C.

5.5 Conclusion

Andalusite based refractories are generally used for applications where a superior high-temperature volume stability, high thermal shock resistance and corrosion resistance against alkali rich slags and atmospheres is necessary. Depending on the exact requirements of the respective application, high-temperature volume stability, for example, may be more important than corrosion resistance and the material must be adapted accordingly.

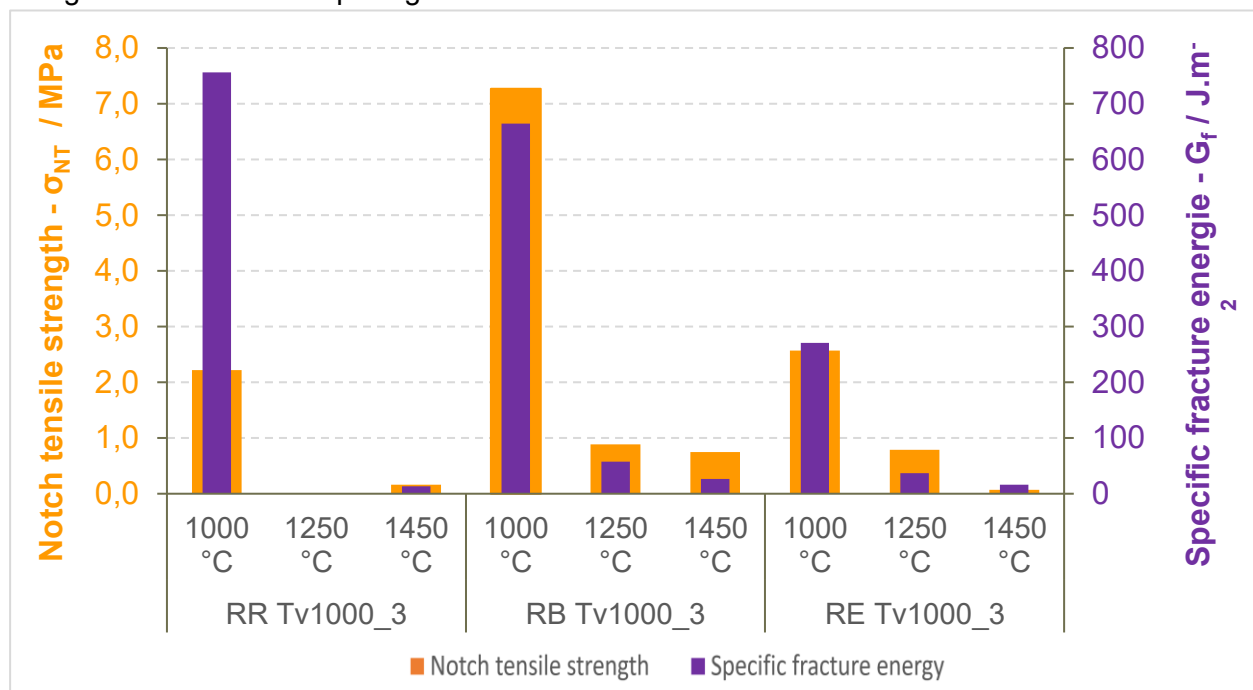
The role of andalusite in andalusite based castables depends on the grain size, because the reaction is strongly kinetically hampered. Due to the small surface to volume ratio, the andalusite coarse grain decomposes at higher firing temperatures than the small andalusite grains in the fine matrix. Therefore, the major temperature interval of the andalusite transformation in RR, obtained from the results of XRD is between 1400 and 1500 °C, whereas the andalusite decomposition in RE already starts at 1200 °C and significantly at 1300 °C (compare Figure 27 and Figure 28). The influence of the dwell time is also represented by the temperature difference for the andalusite decomposition from the firing without dwell time and the firing for 8 hours, respectively. Without dwell time, the andalusite decomposition in RR starts in the test-piece fired to 1400 °C, whereas it already starts in the test-pieces fired to 1300 °C for 8 hours.

The superior high-temperature volume stability of andalusite based refractories is claimed to be the result of skeletal mullite crystals with interstitial amorphous silica, sometimes designated as “felted mullite” aggregates originated from slowly converting andalusite. The microstructure of the fired andalusite based reference castables (between 1000 and 1500 °C) showed no interaction between the andalusite coarse grain and the matrix that could be the due for the high-temperature volume stability. The volume expansion of 4-5 % that is related to the andalusite decomposition has a positive influence on the volume stability. The volume expansion has a counteracting effect

to the shrinkage due to ceramic sintering. The slow decomposition of andalusite is particularly favourable in a refractory material that is exposed to a thermal gradient. In the first millimetres of the hot side of the lining, the andalusite transforms, while it is still stable on the cold side. The andalusite based castables demonstrated high creep resistance during the first 25 h, while the model castables containing andalusite, kyanite and luting sand exhibited lower creep resistance. Only the model castable containing SiC exhibits superior volume stability. A superior high-temperature volume stability of andalusite based refractories could also be achieved using the modelled castable with kyanite.

In the matrix of the andalusite based castables no mullite was found after thermal treatment. The mullite and interstitial amorphous silica that was formed within the andalusite decomposition has formed a phase of anorthitic composition with the existing CaO from the matrix, which was probably liquid at peak temperature, but anorthite crystals formed on cooling. The melt formation leads to a plastic behaviour at application temperature of a refractory castable and therefore prevents the spread of cracks induced by thermal shock.

The high degree of melting of the reference castables also becomes clear when the results of the wedge splitting test are used.



clearly shows that significant proportions of melting phase must already be present from 1250 °C, as neither the notch tensile strength nor the specific fracture energy hardly show any strength. In the context of this work, however, it can be shown that the strengths for the model castables also collapse at 1250 °C but are better than for the reference castables (*Figure 107*). The three investigated andalusite based castables have a good corrosion resistance against alkali rich slags and atmospheres.

Anorthite could facilitate melt phase formation in high alumina low cement castable. Kyanite on the other hand as explained before produces mullite during its transformation. A combination of kyanite and anorthite in the model castable were incorporated. The aim here was to examine their interactions with other matrix components and to observe the resulting phase formations and to determine if this combination could serve as a viable substitute for andalusite in refractory castables, providing valuable insights into its potential suitability.

In principle, it can therefore be said that the current opinion on andalusite-containing castables must be questioned. In the reference castables analysed, it could not be proven that the formation of mullite during the decomposition of the andalusite causes a solidification of the structure, which results in the much-described refractory stability. In general, it should be noted here that this statement is based on the results of RuL and Creep. It must be taken into account here that in both cases the loss in height of the test specimens is compensated for by the increase in volume caused by the decomposition of the andalusite and kyanite, and ultimately an apparently high refractoriness is measured. Andalusite therefore appears to act primarily as a shrinkage compensator, which acts in the refractory lining to inhibit the formation of cracks on the hot side, although a high melt phase content is already demonstrably present. The melt phase on the hot side, in turn, seals the surface by significantly reducing the open porosity as in a glaze, which, unlike glazes, is in the liquid phase at operating temperature and thus greatly hinders the infiltration of volatile corrosive media. This may be the reason for the high corrosion resistance that is commonly attributed to andalusite castables. Despite the verified high melt phase content, andalusite castables are described as extremely resistant to thermal shock, although the thermomechanical strength (wedge splitting test) is no longer present from around 1250 °C. However, the melt phase in turn opens up the possibility of reacting ductile to thermal stresses, which means that thermo-mechanically induced cracks can no longer be initiated and consequently no spalling occurs.

An alternative must therefore be found for a target-oriented substitution of andalusite that is capable of expansion on the one hand and forms a dedicated amount of smelt phase on the other. The development of the model castables was aimed at this with a useful result, but the composition must be further adapted in all cases. In particular, additions with luting sand appear to be a highly interesting solution here, as the kaolinite forms melt on the one hand and the deep quartz expands strongly during the transformation to cristobalite on the other. Unfortunately, the post-expansion only sets in at around 1400 °C, which is actually too late to inhibit shrinkage induced cracks. The targeted use of small quantities of kyanite as an additional component could be helpful here.

6. Literature

- | | |
|---------------------|---|
| Bowen et al. 2017 | Bowen, L., He, M., Wang, H. „Phase Transformation of Andalusite-Mullite and Its Roles in the Microstructure and Sinterability of Refractory Ceramic“, <i>Metallurgical and Materials Transactions A</i> , pp. 3188-3192, July 2017. |
| Cölle 2013 | Cölle, D. “Alumosilicate “Made in Germany”: High-temperature Raw Material with Excellent Innovation Potential”, <i>Refractories Worldforum</i> , 2013. |
| Dannert et al. 2000 | Dannert C, Durschang B, Raether F: Optimizing of sintering processes for porcellain using in-situ measuring methods. <i>Mat. Week and Materialica</i> , Proceedings, 2000. |
| Dubreuil 1999 | Dubreuil, P., Sobolev, V.M. (1999). Andalusite: A promising material for manufac- |

- turing high-quality refractories. *Refractories and Industrial Ceramics*, 40 (3-4).
- Fangbao et al. 2004 Fangbao Y., Rigaud, M., Liu, X., Zhong, X. „High temperature mechanical properties of bauxite-based SiC-containing castables“, *Ceramics International* 30, p. 801–805, 2004.
- Fouzia et al. 2018 Fouzia C., Hamidouche, M., Belhouchet, H., Jorand, Y., Rachida, D., Fantozzi, G. „Mullite fabrication from natural kaolin and aluminium slag“, *Boletín de la Sociedad Española de Cerámica y Vidrio* 57, p. 69–177, 2018.
- Frulli et al. 2018 Frulli, D., Heever, D.V.D., Ahouanto, F., Parr, C. „Andalusite based raw materials for Refractory Castable: properties and application“. *Materials Science* 2018
- Ildefonse et al. 1997 Ildefonse, J. P., Gabis, V., Cesbron, F. (1997). Mullitization of andalusite in refractory bricks. *Key Engineering Materials*, (136 PART 3), 1798-1801.
- Kakroudi et al. 2008 Kakroudi, M.G., Yeugo-Fogaing, E., Gault, C., Huger, M., Chotard, T. (2008). Effect of thermal treatment on damage mechanical behaviour of refractory castables: Comparison between bauxite and andalusite aggregates. *Journal of the European Ceramic Society*, 28 (13), 2471-2478.
- Liao et al. 2005 Liao, G., Xu, G. et al (2005). Effects of firing temperature and soaking time on sintering property of andalusite based refractories. *Naihuo Cailiao*, 39 (4), 255-258.
- Litowski 1982 Litovsky E. *Thermal Physical Properties of Refractories in the Wide Range of Temperature and Gas Pressure*, Dr. of Sc. Thesis, IVTAN of USSR Ac. Of Sc., Moscow, 1982.
- Maglic et al. 1989 Maglic KD, Cezairlina A, Peletsky VE. *Compendium of Thermo-physical Properties Measurement Methods. Recommended Measurement Techniques and Practices*, V 1-2, Plenum Press, New York and London, (1989).
- Mavahebi et al. 2019 Mavahebi, S., Bavand, M., Nemat, A. „SiC fines effects on the microstructure and properties of bauxite-based low cement refractory castables“, *Ceramics International*, p. 16338–16346, 2019.
- McCracken 2014 McCracken, W. H., De Ferrari, C. A. (2014). Andalusite, an underutilized refractory raw material with undeveloped high potential. *Proceedings of the Unified International Technical Conference on Refractories, UNITECR 2013*, 1129-1134.
- Namiranian & Kalantar 2011 Namiranian A. and Kalantar, M. „Mullite synthesis and formation from kyanite concentrations in different conditions of heat treatment and particle size“, *Iranian Journal of Materials Science & Engineering*, pp. 29-36, 9 2011.

- Nyoka et al. 2013 Nyoka, M., Brazier, D., Courtney, T., Parry, R. A. (2013). Merits of using andalusite-based refractories compared to bauxite-based refractories. *Journal of the Southern African Institute of Mining and Metallurgy*, 113 (8), 647-650.
- Poirier et al. 2009 Poirier, J., Bouchetou, M.L., Colombel, L. Hubert, P. „Andalusite: An Attractive Raw Material for its Excellent Thermal Shock Resistance“, *Refractories Worldforum*, pp. 93-102, 2009.
- Rebouillat and Rigaud 2002 Rebouillat, L. and Rigaud, M. Andalusite-based high-alumina Castables *Journal of the American Ceramic Society* 85 (2) 373-378, 2002.
- Report IGF project 17764 N Verbesserung der thermomechanischen Eigenschaften von feuerfesten Erzeugnissen bei Einsatztemperaturen zwischen 1000 bis 1550 °C durch gezielte Schmelzphasenbildung im keramischen Gefüge. IGF-Forschungsvorhaben no 17764 N, final report
- Ren et al. 2018 Ren, B., Li, Y., Nath, M., Wang, Q., Xu, Y. (2018). Enhanced alkali vapor attack resistance of bauxite-SiC refractories for the working lining of cement rotary kilns via incorporation of andalusite. *Ceramics International*, 44 (18), 22113-22120.
- Schneider 1997 Schneider, H. Thermal Expansion of Andalusite. *Journal of American Ceramic Society* 62 (5), 1979.
- Scheider and Majdic 1981 Schneider H, Majdic, A. Preliminary investigation on the kinetics of high temperature transformation of sillimanite to 3/2 mullite plus silica acid comparison with the behaviour of andalusite and kyanite, *Sci. Ceram.*, 11, 191-196, 1981
- Urbain 1987 Urbain, G. Viscosity Estimation of Slags, *Steel Res.*, 58 [3] 111-116 (1987).
- Walaan et al. 2014 Walaan, T., Psiuka, B., Kubackib, J., Steca, K., Podwórn, J. Multitization process of andalusite concentrates – Role of natural inclusions. *Ceramics International* 40,5129–5136, 2014.
- Zawrah & Khalil 2005 Zawrah, M., Khalil, N. M. „High alumina castables reinforced with SiC“, *Advances in Applied Ceramics*, pp. 312-317, 2005.